

Technical University Delft
Faculty of Civil Engineering and Geosciences

PLASTICITY Ct 4150

The plastic behaviour and the calculation of beams and frames subjected to bending

Prof. ir. A.C.W.M. Vrouwenvelder

March 2003

Preface

Course CT4150 is a Civil Engineering Masters Course in the field of Structural Plasticity for building types of structures. The course covers both plane frames and plates.

Although most students will already be familiar with the basic concepts of plasticity, it has been decided to start the lecture notes on frames from the very beginning. Use has been made of rather dated but still valuable course material by Prof. J. Stark and Prof. J. Witteveen. After the first introductory sections the notes go into more advanced topics like the proof of the upper and lower bound theorems, the normality rule and rotation capacity requirements. The last chapters are devoted to the effects of normal forces and shear forces on the load carrying capacity, both for steel and for reinforced concrete frames. The concrete shear section is primarily based on the work by Prof. P. Nielsen from Lyngby and his co-workers.

The lecture notes on plate structures are mainly devoted to the yield line theory for reinforced concrete slabs on the basis of the approach by K. W. Johansen. Additionally also consideration is given to general upper and lower bound solutions, both for steel and concrete, and the role plasticity may play in practical design. From the theoretical point of view there is ample attention for the correctness and limitations of yield line theory for reinforced concrete plates on the one side and von Mises and Tresca type of materials on the other side. This, however, is not intended for examination.

I would like to thank ir Cox Sitters for his translation of the original Dutch text into English as well as for his many suggestions for improvements.

A. Vrouwenvelder
Delft, 2003

Table of Contents

Preface

1	Introduction	4
1.1	Computational models in structural mechanics	4
1.2	Modelling of the material behaviour	5
1.3	The elastic-plastic behaviour of simple bar structures	7
1.4	Elasticity versus plasticity approach	10
1.5	Historical overview	11
2	The elastic-plastic calculation	13
2.1	The moment-curvature distribution for the rectangular cross-section	13
2.2	Arbitrary cross-sections.....	17
2.3	The moment-curvature distribution of reinforced concrete	21
2.4	The elastic-plastic behaviour of a statically indeterminate beam	23
2.5	The elastic-plastic behaviour of a frame	26
3	Plastic limit state analysis	29
3.1	Introduction	29
3.2	Upper-bound theorem	29
3.2.1	Systematic application.....	32
3.2.2	Special cases.....	35
3.2.3	Uniformly distributed load	36
3.2.4	Proof of the upper-bound theorem	37
3.3	Lower-bound theorem	38
3.3.1	Application	38
3.3.2	Uniformly distributed load	40
3.3.3	Proof of the lower-bound theorem	41
3.4	Combination of upper- and lower-bound theorems	41
3.5	Some consequences of the lower- and upper-bound theorems	43
4	Rotation capacity.....	44
4.1	Introduction	44
4.2	Restrained steel beams	44
4.3	Experiments by Stüssi and Kollbrunner.....	48
4.4	Reinforced concrete.....	49
5	The yield contour	52
5.1	Plane truss	52
5.2	Yield contour of a portal frame	54
5.3	Normality	57
5.4	Plastic potential, convexity	59
6	Yield criteria.....	63
6.1	Introduction	63
6.2	The yield criterion of Tresca (steel)	63
6.3	The yield criterion of von Mises (steel)	65
6.4	The yield criterion of Mohr-Coulomb (concrete, rock / soil)	67

7	Effects of normal forces on plastic frame behaviour	70
7.1	The influence of the normal force on the fully plastic moment.....	70
7.1.1	Introduction	70
7.1.2	Rectangular cross-section.....	70
7.1.3	Arbitrary double-symmetric cross-section.....	72
7.2	The moment-curvature diagram in the presence of a normal force	76
7.2.1	Rectangular cross-sections	76
7.2.2	I-shaped cross-sections.....	78
7.3	Reinforced concrete cross-section.....	79
7.4	Yield function and normality	84
8	The influence of the transverse force on the full-plastic moment.....	98
8.1	Steel cross-sections	98
8.1.1	Rectangular cross-sections	99
8.1.2	I-sections	103
8.2	Reinforced concrete cross-sections	105
8.2.1	Introduction	105
8.2.2	Yield lines	106
8.2.3	Beam with stirrup reinforcement / upper-bound calculation	109
8.2.4	Beam with stirrup reinforcement / lower-bound calculation	112
	Reading list.....	118

1 Introduction

1.1 Computational models in structural mechanics

In structural mechanics the following basic quantities appear:

- Displacements: u_x, u_y, u_z
- Strains: $\epsilon_{xx}, \epsilon_{yy}, \epsilon_{zz}, \epsilon_{xy}, \epsilon_{yz}, \epsilon_{xz}$
- Stresses: $\sigma_{xx}, \sigma_{yy}, \sigma_{zz}, \sigma_{xy}, \sigma_{yz}, \sigma_{xz}$
- Forces: f_x, f_y, f_z .

For static situations the relations between these quantities are given by three sets of equations:

- 1) Kinematical equations
- 2) Constitutive equations
- 3) Equilibrium equations

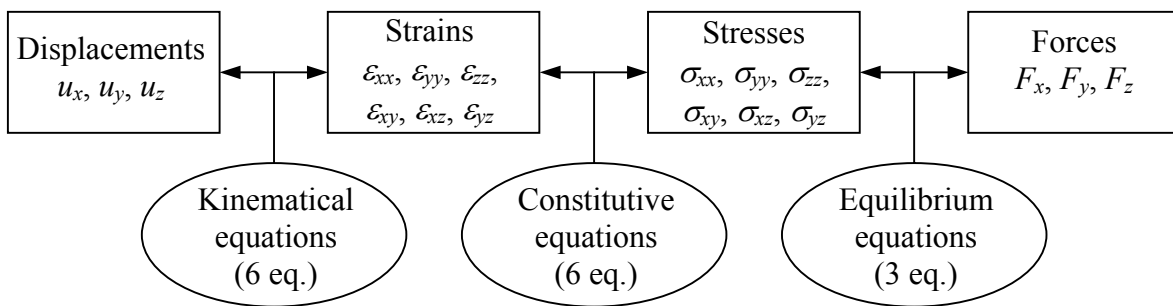


Fig. 1.1: Relations between the basic quantities in structural mechanics.

As indicated in Figure 1.1, the kinematical equations relate the strain components to the displacements and the stress components are related to internal and external forces by the equilibrium equations. These equations are of a purely geometric nature and independent of the material behaviour. The influence of the material is expressed in a third set of equations, the constitutive equations. For elastic materials six constitutive equations exist, which couple the six stress components to the six strain components. This set is known as Hooke's law. However, in many structural mechanical elements the number of basic variables is much smaller. For a beam, for instance, often only the stress component σ_{xx} is of importance.

A further classification of applied mechanics depends on the fact that each of the sets of equations can be linear or non-linear. One distinguishes:

1. *Geometrically linear and non-linear models*
2. *Physically linear and non-linear models*

The first item refers to the linearity or non-linearity of the kinematical and/or equilibrium equations. According to the exact theory, the equations are non-linear, but under certain conditions linear approximations may give useful results. The second item refers to the

constitutive equations, which may be linear (elastic) or non-linear (non-linear elastic, elastic-plastic, plastic, fracture). A computational strategy for a certain type of structure is a combination of both items and leads to 4 possibilities.

This course covers primarily computational methods for structures of one-dimensional elements (beams, frames) with geometrical linear and physical non-linear behaviour. The material behaviour is characterised by “plasticity”. Distinction is made between methods that describe the behaviour for an incremental increase of the external load and methods that only are able to obtain the load at failure. The use of incremental methods is required for accurate stability calculations on reinforced concrete and steel. For many structures in the common building practice, it is sufficient to know the ultimate load bearing capacity. The corresponding computational method is called *plastic collapse analysis*. This course specially focuses on this aspect.

1.2 Modelling of the material behaviour

It is the strength of the continuum mechanics to describe relations between stresses and strains on a macroscopic scale on basis of a limited number of phenomenological constants, without paying attention to the processes occurring on an atomic scale. Under the restriction of time-independent material behaviour, the mechanical behaviour of polycrystalline material (for example steel) under increasing load is controlled by successively two mechanisms:

- *Elasticity*

For an elastic material, a unique relation between stresses and strains exists. When after loading the stresses are reduced to zero, the deformed body gets back its original shape. In the classical theory of elasticity, the strains are small and the six constitutive equations are linear. Isotropic materials contain two independent material constants (for example the modulus of elasticity E and Poisson’s ratio ν).

- *Plasticity*

A plastic material is characterised by permanent plastic deformations when after loading the stresses are reduced to zero. The total strain in any point of a plastic material is the sum of the reversible elastic and the irreversible plastic strain. The constitutive relations in that case are given by the so-called yield functions combined with flow rules.

Experiments, especially tensile tests, provide the necessary basic information about the material behaviour. Fig. 1.2a shows the relation between the conventional stress (force divided by original cross-sectional area) and the axial strain (elongation divided by an original reference length) of annealed mild steel in tension. Until the *upper yield point* is reached at point a , the stress-strain relation is linear. After that, the stress suddenly drops to the *lower yield point* a' and remains constant up to point b . The stretch $a'b$ is called *plastic yield* or *plastic flow*. After point b the stress increases with increasing strain. This phenomenon is called “*hardening*”. Finally, the maximum conventional stress is reached at point c , after which the stress reduces because of *necking* of the test piece, until fracture occurs at d .

The yield stress of mild steel is in the order of 200-400 N/mm², the ultimate stress is about 400-600 N/mm² and the strain at fracture is 30%-50%. A material capable of sustaining large strains is called “*ductile*”, in contrast to brittle materials.

From a practical point of view, the part Oab in Fig. 1.2a is the most important one. Since the strain at a is about 0.1% and at b about 1-2%, the part is redrawn in Fig. 1.2b on a stretched strain scale. The upper and lower yield points are indicated by σ_u ($u = \text{upper}$) and σ_p ($p = \text{plastic}$), respectively. The slope of the elastic branch is equal to the modulus of elasticity E (Young's modulus) and the slope of the hardening branch is called E_s . For mild steel E_s is only 2-5% of E . The yielding of steel can be seen on the test piece by the

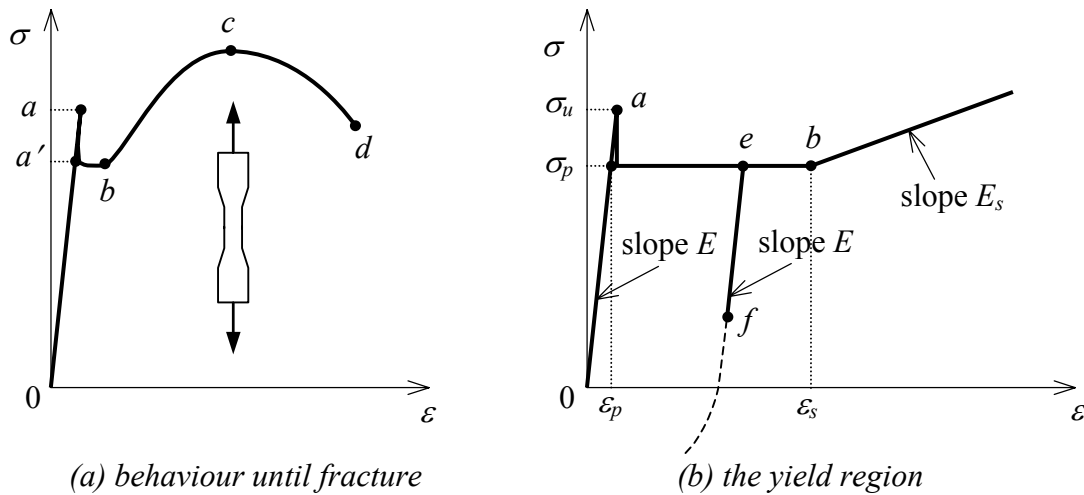


Fig. 1.2: Stress-strain diagram for mild steel under tension.

formation of so-called “Lüder's lines”, which make an angle of about 45° with the axis of the test piece showing that yielding occurs in planes with the largest shear stress (Tresca, see chapter 6).

If in Fig. 1.2b firstly the path Oae is passed into the plastic zone after which the stress is reduced, the material becomes elastic and path ef is followed the slope of which is equal to the modulus of elasticity E . In the zone of compression a deviation from the linear behaviour can be established, which is known as the *Bauschinger effect*. When the stress is increased, again the same elastic path is followed back in opposite direction until point e is reached and yielding occurs at the lower yield point σ_p after which the deformation continues on plastic branch eb . After the first cold deformation, the upper yield point disappears. For modelling of the material behaviour of steel the upper yield limit, which is strongly dependent on the load rate and the details of the test specimen, is neglected. The Bauschinger effect is generally not taken into account too. If on top of that hardening is neglected too, one speaks of an *elastic ideal-plastic* material, with identical stress-strain curves for tension and compression. The ultimate stress state corresponds to the state of yielding.

Fig. 1.3a shows the stress-strain diagram for this elastic ideal-plastic material, while in Fig. 1.3b the model is further simplified to *rigid ideal-plastic* material behaviour, where only the irreversible plastic strains occur.

- *Brittle material behaviour*

For a brittle materials like concrete the same type of modelling is possible, with the difference however that the yield strain is considerably less, namely in the order of 0.2-0.3%. Further, compared to the compressive stresses only small tensile stresses are possible. Therefore, in elementary calculations tensile stresses are neglected (Fig. 1.3c).

Section 6.4 pays more attention to material modelling, especially the more-dimensional stress states will be discussed.

The coming calculations are based on the models provided in Fig. 1.3. The influence and the importance of hardening will be covered in chapter 4.

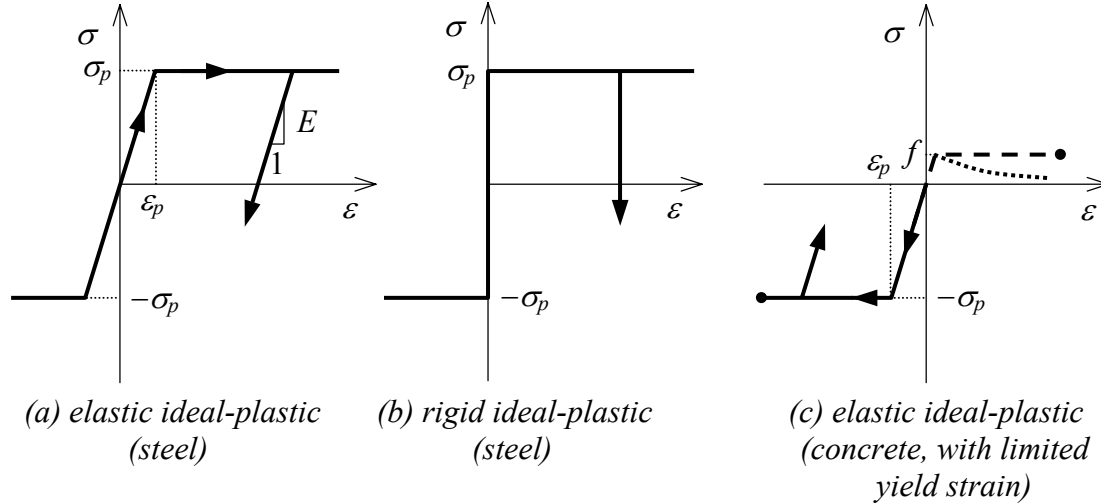


Fig. 1.3: Material modelling for one-dimensional load cases.

1.3 The elastic-plastic behaviour of simple bar structures

As an introduction, the principles of an elastic-plastic calculation with material modelling according to Fig. 1.3 will be demonstrated by a simple example. The stress free, statically indeterminate bar structure of Fig. 1.4, with bar cross-section A , passes during loading the following stages:

1) Elastic stage: $F < F_e$

The following set of equations has to be satisfied:

$$u_1 = u_2 = u \quad (\text{kinematical conditions}) \quad (1.1)$$

$$u_1 = \frac{S_1 * l}{EA} \quad ; \quad u_2 = \frac{S_2 * 2l}{EA} \quad ; \quad S_1, S_2 \leq A\sigma_p \quad (\text{constitutive conditions}) \quad (1.2)$$

$$S_1 + 2S_2 = F \quad (\text{equilibrium condition}) \quad (1.3)$$

From (1.1) and (1.2) it follows:

$$S_1 = 2S_2 \quad (1.4)$$

Substitution of (1.3) provides:

$$S_1 = \frac{1}{2}F \quad ; \quad S_2 = \frac{1}{4}F \quad (1.5)$$

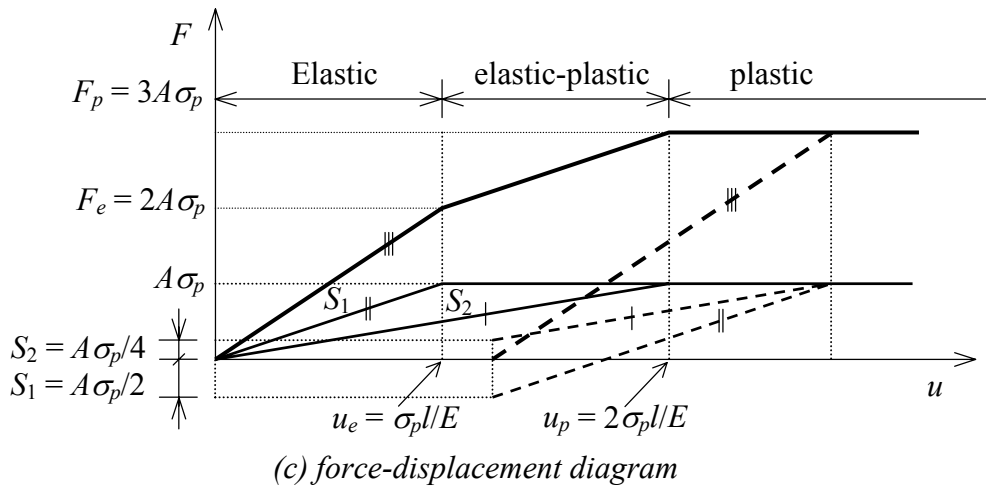
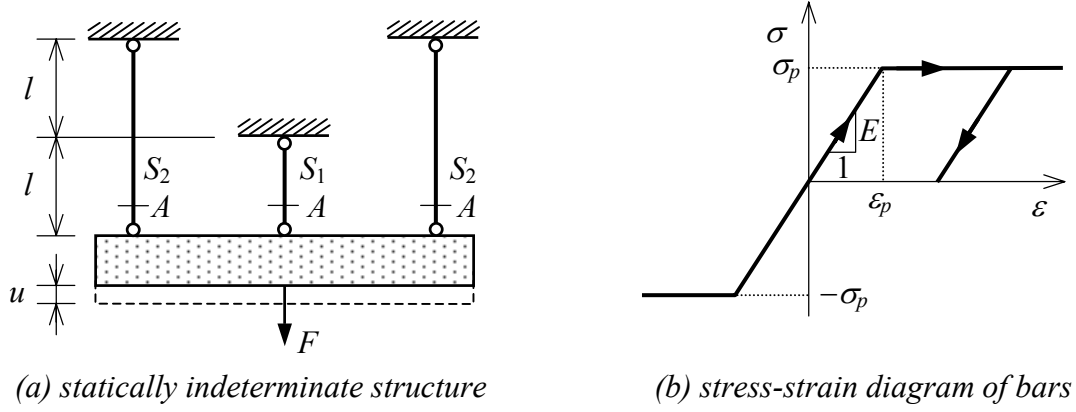


Fig. 1.4: Elastic-plastic behaviour of a simple bar structure.

Combination with (1.2) delivers:

$$u = \frac{Fl}{2EA} \quad (1.6)$$

The relations (1.5) and (1.6) are graphically displayed in Fig. 1.4c.

2) **Elastic limit state:** $F = F_e$

The elastic limit state is determined by the yielding of the middle bar, such that:

$$S_1 = A\sigma_p \quad ; \quad S_2 = \frac{1}{2}A\sigma_p \quad (1.7)$$

$$F_e = S_1 + 2S_2 = 2A\sigma_p \quad (1.8)$$

$$u_e = \frac{\sigma_p l}{E} \quad (1.9)$$

3) **Elastic-plastic stage:** $F_e < F < F_p$

The elastic-plastic stage (in the meantime the structure has become statically determinate) is determined by:

$$u_1 = u_2 = u \quad (\text{kinematical conditions}) \quad (1.1)$$

$$u_2 = \frac{S_2 * 2l}{EA} \quad ; \quad S_1 = A\sigma_p \quad ; \quad S_2 \leq A\sigma_p \quad (\text{constitutive conditions}) \quad (1.10)$$

$$F = S_1 + 2S_2 \quad (\text{equilibrium equation}) \quad (1.3)$$

Substitution of (1.10) and (1.3) in (1.1) delivers (see fig. 1.4c):

$$u = \frac{(F - A\sigma_p)l}{EA} \quad (1.11)$$

4) **Plastic limit state:** $F = F_p$

The end of the elastic-plastic stage is reached if all three bars are plastic and the system does not allow another increase of the external load. The kinematical condition in this case is that the structure has become a “collapse mechanism”. The failure load (ultimate load) immediately follows – without making use of the preceding load path – from the equilibrium equation and constitutive condition at failure:

$$S_1 = S_2 = A\sigma_p \quad (1.12)$$

$$F_p = S_1 + 2S_2 = 3A\sigma_p \quad (1.13)$$

For the displacement at failure from (1.11) it follows:

$$u_p = \frac{2\sigma_p l}{E} \quad (1.14)$$

For the calculation of this displacement information about the preceding load path is required. After reaching the elasticity limit $F_e = 2A\sigma_p$ the load can be increased by another 50% up to $F_p = 3A\sigma_p$, where the displacement doubles. Bar 1 experiences a plastic elongation of $u_{p1} = \sigma_p l / E$.

5) **Behaviour during unloading**

Now it will be investigated what will happen when the load $F = 3A\sigma_p$ is removed completely. In order to make Fig. 1.4 less confusing, unloading will take place only after a certain amount of plastic deformation of all bars, i.e. movement as a mechanism, is allowed. On basis of the adopted material model all bars will spring back elastically during unloading and therefore the whole structure will react elastically.

In Fig. 1.4, it can be seen that after complete unloading permanent deformation results.

Further, the force change in the individual bars is important. The load reduces by $3A\sigma_p$. According to (1.5) bar S_1 accounts for half of this amount and the bars S_2 for a quarter, so that $\Delta S_1 = -1.5A\sigma_p$ and $\Delta S_2 = -0.75A\sigma_p$. During failure in both bars a tensile force of $A\sigma_p$

was present. Thus the result is that after unloading residual forces remain, being $S_1 = -0.5A\sigma_p$ and $S_2 = 0.25A\sigma_p$ (see Fig. 1.4). These residual forces, the resultant of which is zero of course, see to it that during reloading the system behaves elastically until the failure load is reached. So “nature” provides an elegant way of prestressing. Anticipating on the general theory in chapter 3 it already can be seen that the failure load is insensitive to for example forces introduced into the system during assembly of the structure.

1.4 Elasticity versus plasticity approach

For a number of reasons, the theory of elasticity is applied frequently in practice. Although the target of the formal theory of elasticity is to obtain an extreme stress, this goal in most cases cannot be satisfied completely. Implicitly in such cases plastic considerations are taken into account in order to find the stresses (plastic excuse), Fig. 1.5 provides some examples.

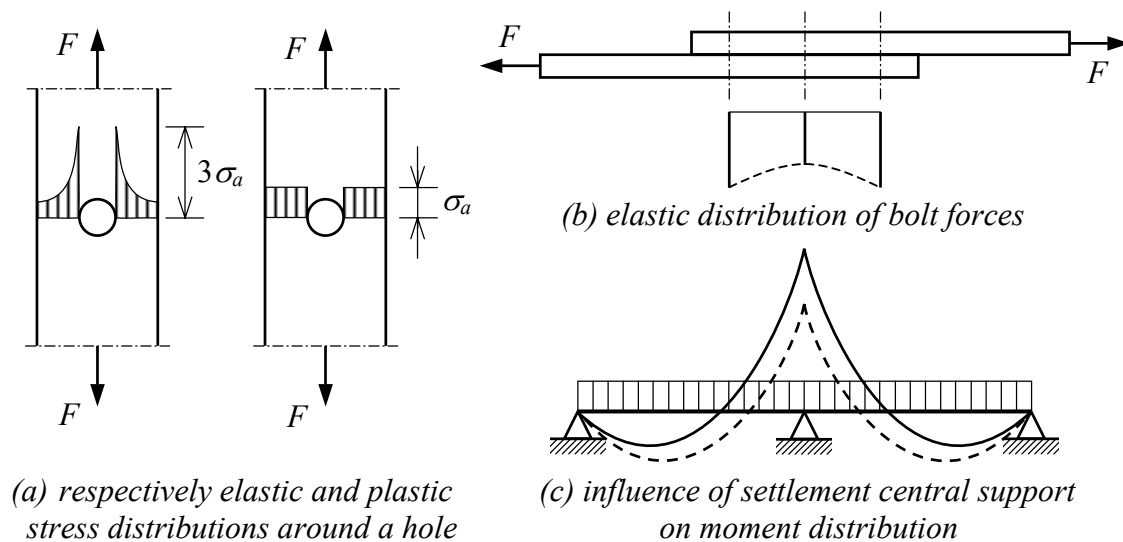


Fig. 1.5: Plastic excuse for elastic calculations.

- The stress distribution in a bar with a hole in tension is considered to be uniform in practice, while the theory of elasticity provides a stress along edge of the hole which is about three times the average value;
- For a number of bolts in series, the individual bolt force is obtained by division of the total load by the number of bolts. The elastic distribution of the bolt forces does not correspond with this assumption;
- During the calculation of beams and frames, the theory of elasticity assumes initially stress free structures and fixed supports. In reality, in statically indeterminate structures assembly stresses will be generated, which cannot be dealt with by the theory of elasticity. The real moment distribution will not coincide with the calculated one because of settlement of the supports. However, the differences are allowed as will be shown later on bases of plasticity considerations.

It may also happen that the theory of elasticity leads to paradoxical conclusions for structures made out of ductile material. For a stiffness ratio of 1.5 between the vertical columns and horizontal girder in Fig.1.6, the support moment and maximum field moment are equal. Suppose that, for whatever reason, the column is replaced by one having a

heavier cross section, bringing the stiffness ratio between the beams to 3. The result of a new elastic calculation is that the support moment increases from 6.25 kNm to 7.14 kNm. The load that can be supported by the frame in that case reduces to $(6.25/7.14) \cdot 100\% = 87.5\%$ of the original load. The fact that addition of material leads to a lower load bearing capacity is clearly in contradiction with the engineering judgement.

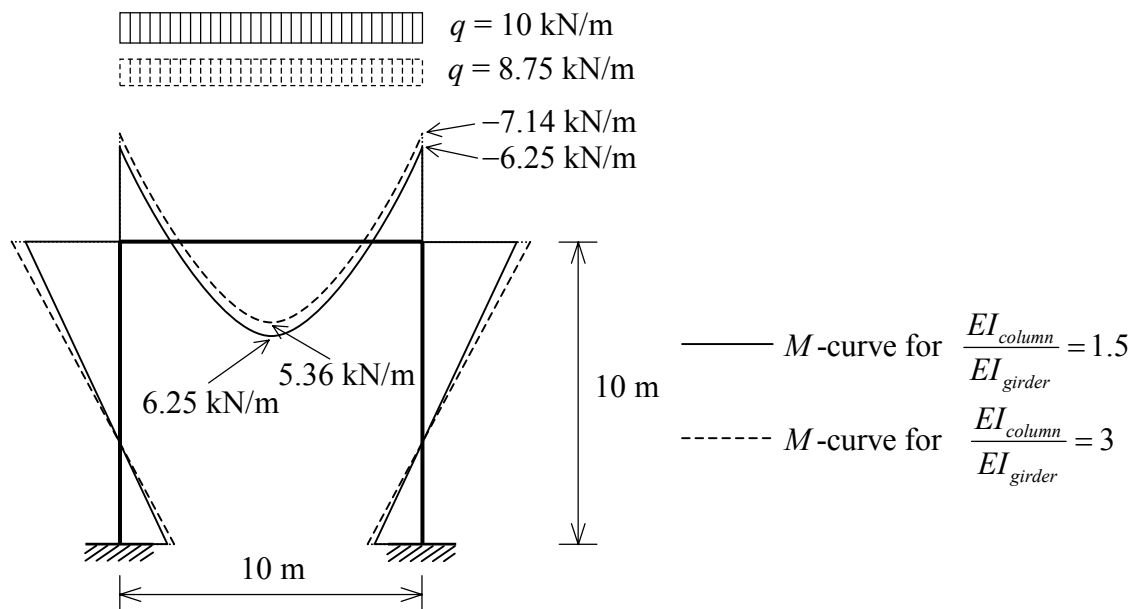


Fig. 1.6: The use of heavier columns leads according to the theory of elasticity to a lower limit load.

It may be concluded that the theory of plasticity may give valuable extra qualitative and quantitative information regarding the load carrying capacity and thus the reliability of a structure. A good engineer should consider them both.

1.5 Historical overview

From a historical point of view, the development of the computational techniques for building structures started with the determination of the ultimate load bearing capacity. Some well-known examples are the calculation of a restrained wooden beam subjected to bending by Galilei (1638), the buckling formula of Euler (1757) and the vertical excavation by Coulomb (1773). The theoretical analysis about the failure behaviour remained inadequate. The second half of the 18th century and the entire 19th century can be considered as the most prosperous time for the theory of elasticity. Modelling on basis of Hooke's law (1678) made many problems suitable for a mathematical analysis. The development of the theory of elasticity into an engineering science is especially stimulated by the construction of bridges and coverings with large spans. Since analytical solutions for complicated structures quickly leads to large sets of unmanageable equations, graphostatics* was developed around 1900 for the calculation of frameworks. With the adjustment method of Hardy Cross* (1932) it also became possible to analyse statically indeterminate frameworks. The success of the theory of elasticity pushed the influence of real material properties, which used to be the starting point, to the background. With the

exception of some solutions in soil mechanics, the calculation of the state of failure where non-linear material properties play a role fell into oblivion too.

The abandoning of Hooke's law at higher stress levels and the accounting for non-linear material properties in the plastic range introduce considerable complications. Undoubtedly this must have discouraged practitioners of mechanics in the 19th century, being well aware of the non-linear behaviour of materials. In the beginning of the 20th century this attitude changed with the recognition of the importance of the ductility on the behaviour of especially steel structures. Then it was also realised that for the calculation of the ultimate load, on basis of an elastic ideal-plastic material, it was not necessary to calculate the entire load path.

Names such as Kazinczy (1914), Kist (1917) and Maier-leibnitz (1929) are attached to the begin period of this method*, which finally became mature around 1950. Around 1940 the theory of plasticity got an important impulse by the work of Baker and his co-workers at the university of Cambridge in Great Britain and by van den Broek (a student of Kist) attached to the university of Michigan in the United States.

In the wake of the developments of the general theory of plasticity for continua by Drucker and Prager and others, around 1950 Greenberg, Prager and Home formulated the fundamental principles of the limit analysis, which was applied intuitively up to that time. In the nineteen sixties a lot of work was done on the operational applications by Beedle and co-workers of the Lehigh University in the United States, Home in great Britain, Massonet in Belgium and at TNO in the Netherlands. Recent developments are related to the research on stability, constructional details, computer applications and calculations of supporting structures at fire. Now, in almost all national regulations for steel and concrete and also in the Eurocode next to the theory of elasticity, calculations based on the limit load bearing capacity are allowed.

Following the Anglo-Saxon title "limit design" or "limit analysis" the method in the Netherlands was called "bezwijkanalyse". Now, the method is considered as a part of the general theory of plasticity.

* These methods have fallen into disuse because of introduction of the computer.

2 The elastic-plastic calculation

2.1 The moment-curvature relation for the rectangular cross-section

A beam element of elastic ideally-plastic material is loaded in pure bending (Fig. 2.1). The cross-section of the beam has a rectangular shape. The relation will be derived between the bending moment M and the resulting curvature κ .

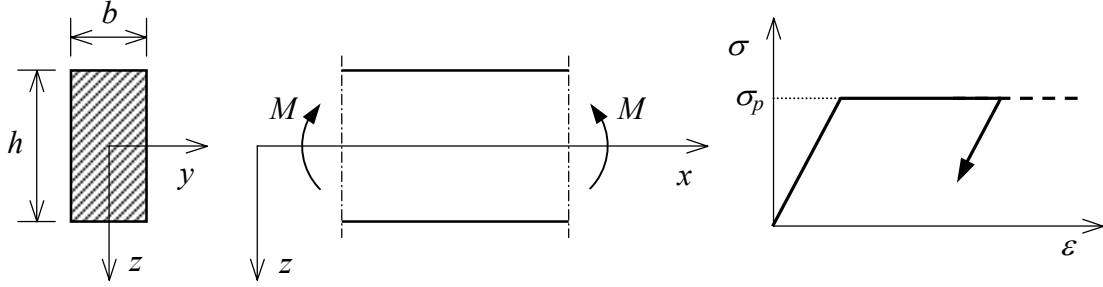


Fig. 2.1: Part of beam with rectangular cross section subjected to bending, with ideal-plastic material behaviour.

It is assumed that the beam element in unloaded state is straight and free of stress. For small curvatures the material will respond elastically and the relation between moment and curvature can be derived as follows:

$$\varepsilon_{xx} = \kappa * z \quad (\text{kinematical equation}) \quad (2.1)$$

$$\sigma_{xx} = E\varepsilon_{xx} \quad (\text{constitutive equation}) \quad (2.2)$$

$$M = \int_A z\sigma_{xx} dA \quad (\text{equilibrium equation}) \quad (2.3)$$

The kinematical equation agrees with the well-known hypothesis of Bernoulli (flat cross-sections remain flat during deformation), where the strain of the centre fibre is zero on bases of symmetry (neutral fibre). So, the strain is proportional with the distance to the neutral fibre, and the same holds for the stress because of the linear material behaviour. Combination of above three equations finally results in the required relation between M and κ :

$$M = EI\kappa \quad \text{with} \quad I = \int_A z^2 dA = \frac{1}{12}bh^3 \quad (2.4)$$

This well-known derivation according to the theory of elasticity is valid until the yield stress σ_p is reached in the extreme fibres, i.e. until:

$$M = M_e = \frac{1}{6}bh^2\sigma_p \quad (2.5)$$

and:

$$\kappa = \kappa_e = \frac{2 \sigma_p}{h E} \quad (2.6)$$

The corresponding stress-strain curve is displayed in Fig. 2.2a

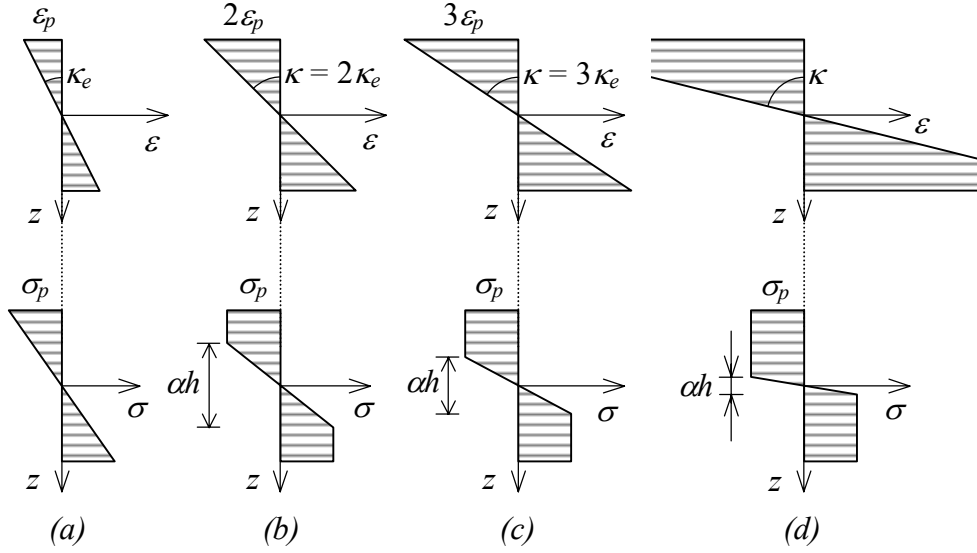


Fig. 2.2: Stresses and strains for a load above M_e .

When the moment or the curvature is further increased, it is assumed that the hypothesis of Bernoulli still holds. The strain distribution remains as given by (2.1). Naturally, during the plastic stage equilibrium is satisfied too, as given by (2.3)*. What does change, however, is the relation between stress and strain. As long as no unloading occurs, it is given by:

$$\sigma = E\varepsilon \quad \text{for } |\varepsilon| < \varepsilon_p \quad (2.7)$$

$$\sigma = \pm\sigma_p \quad \text{for } |\varepsilon| \geq \varepsilon_p \quad (2.8)$$

From this material behaviour it is possible to determine the stresses and moment for a given strain distribution. Suppose that yielding has progressed so far that the elastic inner area has been reduced to αh (see Fig. 2.2). The stress distribution is then given by:

$$\sigma = E\varepsilon \quad \text{for } |z| < \frac{1}{2}\alpha h$$

$$\sigma = \pm\sigma_p \quad \text{for } |z| \geq \frac{1}{2}\alpha h$$

* For the determination of (2.1) and (2.3) use has been made of symmetry. In this case the symmetry properties also are valid in the plastic stage. However this is not always the case, as for example for unequal yield stresses for tension and compression.

The corresponding bending moment equals:

$$M = \sigma_p \left(\frac{1}{2}bh \right) \left(\frac{1}{2}h \right) - \sigma_p \left(\frac{1}{2}b * \frac{1}{2}\alpha h \right) \left(\frac{1}{3}\alpha h \right) = \sigma_p \left(\frac{1}{4}bh^2 \right) \left(1 - \frac{1}{3}\alpha^2 \right)$$

The first term corresponds to the so-called fully plastic stress distribution. The second term is a correction for the elastic inner area (please check!). From Fig. 2.2 the following relation between α and κ can be derived: $0.5\alpha h\kappa = \varepsilon_p$, or through (2.6):

$$\alpha\kappa = \kappa_e$$

Now the relation between M and κ in the elastic-plastic phase can be written as:

$$M = M_p \left(1 - \frac{1}{3}\alpha^2 \right) = M_p \left[1 - \frac{1}{3} \left(\frac{\kappa_e}{\kappa} \right)^2 \right] \quad \text{for } \kappa \geq \kappa_e \quad (2.9)$$

$$M_p = \frac{1}{4}bh^2\sigma_p \quad (2.10)$$

As indicated, formula (2.9) is valid for $\kappa \geq \kappa_e$; if $\kappa = \kappa_e$ the moment M is equal to $2M_p/3$ or $bh^2\sigma_p/6$. The elastic and elastic-plastic branches are connected. In this case, it even can be shown that the M - κ diagram does not have a slope discontinuity, because it holds:

$$\left(\frac{\partial M}{\partial \kappa} \right)_{\kappa=\kappa_e} = \left(\frac{2}{3}M_p \frac{\kappa_e^2}{\kappa^3} \right)_{\kappa=\kappa_e} = \frac{2}{3} \frac{M_p}{\kappa_e} = \frac{M_e}{\kappa_e}$$

If κ increases further, the moment M approaches asymptotically to the value M_p (Fig. 2.3). This value is called the *fully plastic moment*, because for $\kappa = \infty$ the elastic inner area is reduced to zero and in all fibres of the cross-section the yield stress is present (Fig. 2.2d). The full-plastic moment M_p is the maximum moment that can be transmitted by a cross-section. The ratio between the maximum plastic moment and the maximum elastic moment is called the *shape factor* η . For a rectangular cross-section the shape factor equals:

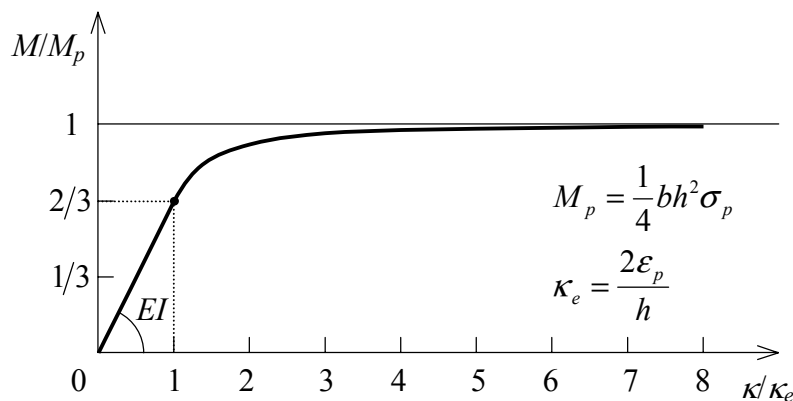


Fig. 2.3: The moment-curvature diagram.

$$\eta = \frac{M_p}{M_e} = \frac{\frac{1}{4}bh^2\sigma_p}{\frac{1}{6}bh^2\sigma_p} = 1.5$$

The shape factor indicates the plastic reserve of the cross-section with respect to the start of yielding. Naturally, the utilisation of this reserve involves extra deformations. In that case one speaks about a *plastic hinge*.

The $M-\kappa$ diagram according to Fig. 2.3 is valid only if the moment or curvature increases monotonously. When at a certain stage the moment is reduced, the cross-section will not react plastic but completely elastic. After all, all fibres yielding under compression will be elongated (unloaded) and vice versa. Suppose the cross-section was nearly loaded up to M_p and then the moment is removed completely. In Fig. 2.4 it is indicated what will happen: an elastic moment distribution with a maximum stress in the extreme fibre of $3\sigma_p/2$ is superimposed on a full-plastic stress distribution. The result is a so-called *residual-stress distribution*, the resulting moment and resulting normal force of which are equal to zero. Note that at the bottom of the beam a compressive stress remains, while the strain is still positive. Such a phenomenon often occurs during plastic deformation and one should be cautious for it; stress and strain are not uniquely related anymore, but their relation is also determined by the whole *load history*.

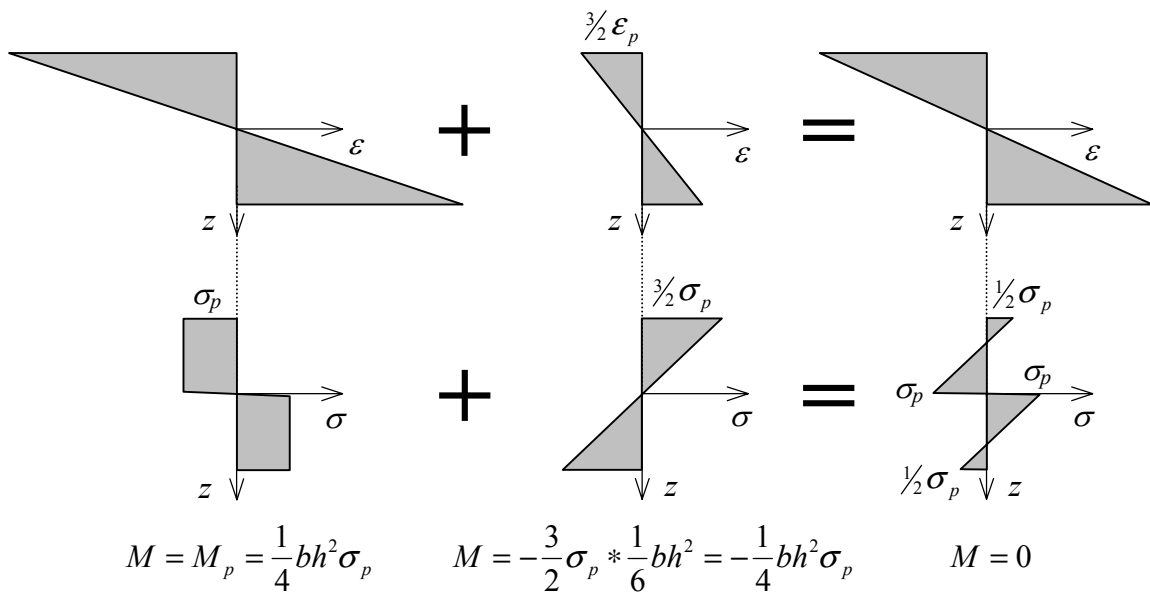


Fig. 2.4: Unloading of a beam, which was loaded up to M_p .

When the moment is further reduced to $-M_e/2$, the cross-section remains elastic, since in totally $2M_e$ can be subtracted before the extreme fibres start yielding in the opposite direction (Fig. 2.5). After that again plastic zones develop and finally an ultimate moment of $-M_p$ can be carried. *Moment variations* can be carried with a total range of $2M_p$, inducing so-called alternating yielding. The number of alternations should not become too high, as in that case a heavy form of fatigue occurs (low-cycle fatigue or plastic fatigue; important for example in earthquake calculations). Stress fluctuations within the range of

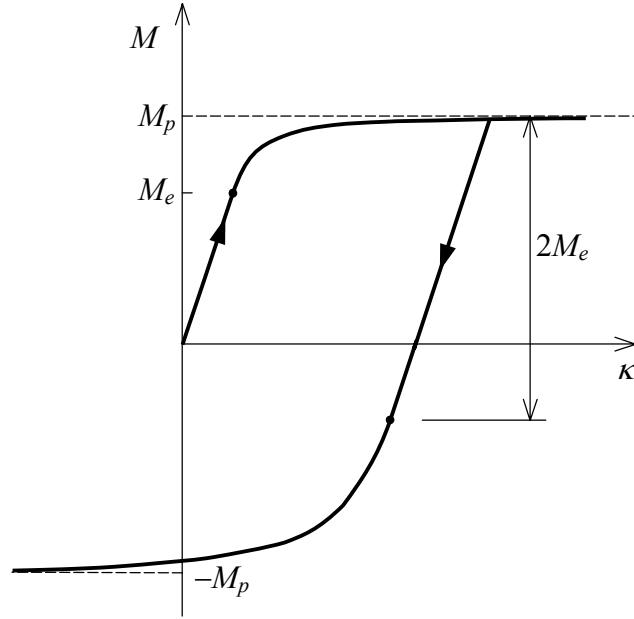


Fig. 2.5: The M - κ curve during loading, unloading and reloading up to $-M_p$.

$2M_e$ are completely elastic. In this case depending on the amplitude, only for a much larger amount of alternations fatigue fracture occurs.

2.2 Arbitrary cross-sections

The analysis carried out in section 2.1 can be applied to every arbitrary cross-section. In Fig. 2.6 the most important properties are collected, i.e. the elastic section factor, the plastic section factor and the shape factor, where the *plastic section factor* is defined by:

$$W_p = \frac{M_p}{\sigma_p} \quad (2.11)$$

The shape factor heavily depends on the choice of cross-section. A big shape factor occurs for example for circular sections ($\eta = 1.70$) and a low factor for an I section ($\eta = 1.15$).

For the determination of the plastic resistance capacity W_p , firstly double-symmetrical sections will be considered, with bending about one of the symmetry axis (Fig. 2.7). The procedure for this type of profiles is almost identical to the one for rectangular cross-sections. After an increase of the curvature to several times the elastic limit value, practically the whole area $z > 0$ yields in tension and the area $z < 0$ yields in compression. From (2.3) the full-plastic moment then can be computed as:

$$M_p = \int_A z \sigma_{xx} dA = \sigma_p \int_{z>0} z dA + (-\sigma_p) \int_{z<0} z dA$$

Since the cross-section is symmetrical, for W_p it finally follows:

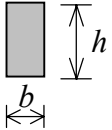
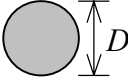
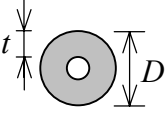
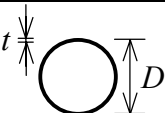
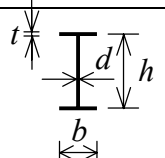
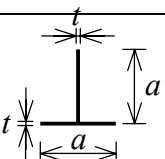
cross section	W_e	W_p	η
Rectangle 	$\frac{1}{6}bh^2$	$\frac{1}{4}bh^2$	1.50
circle 	$\frac{\pi}{32}D^3$	$\frac{1}{6}D^3$	1.70
thick-walled tube 	$\frac{\pi}{32}D^3 \left[1 - \left(1 - \frac{2t}{D} \right)^4 \right]$	$\frac{1}{6}D^3 \left[1 - \left(1 - \frac{2t}{D} \right)^3 \right]$	± 1.50
thin-walled tube 	$\frac{\pi}{4}tD^2$	tD^2	1.27
I-section 	$bht + \frac{1}{6}dh^2$	$bht + \frac{1}{4}dh^2$	± 1.15
T-section 	$\frac{5}{18}ta^2$	$\frac{1}{2}ta^2$	1.80

Fig. 2.6: Plastic section properties for various cross-sections.

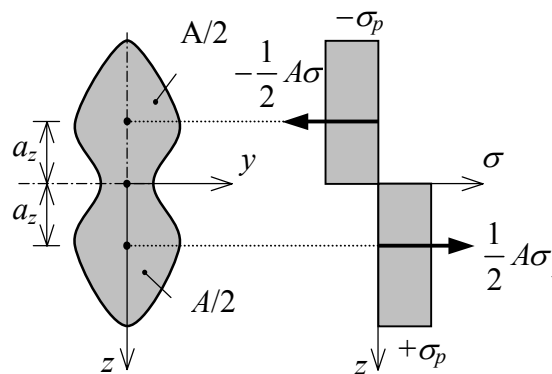


Fig. 2.7: The fully plastic moment of an arbitrary double-symmetrical cross-section equals $2S\sigma_p = a_z A \sigma_p$.

$$W_p = 2S \quad (2.12)$$

with:

$$S = \int_{z>0} z dA \quad \text{or} \quad S = a_z \left(\frac{1}{2} A \right) \quad (2.13)$$

S is the static moment of half the cross-section about the centre of gravity of the cross-section; further A is the area of the entire cross-section and a_z the distance from the centre of gravity of the upper half of the cross-section to the centre of gravity of the whole cross-section. Sometimes it is convenient (for example for an I-section) to divide the cross-section into more parts and to use:

$$W_p = \sum_{i=1}^n S_{zi} \quad \text{with} \quad S_{zi} = a_i \Delta A \quad (2.14)$$

In this relation is S_i the (absolute) static moment of part i with area ΔA_i and distance between the centres of gravity a_i . For the I-section (Fig. 2.6) in this manner it can be found:

$$W_p = \left(\frac{1}{2} h \right) (bt) + \left(\frac{1}{4} h \right) \left(\frac{1}{2} hd \right) + \left(\frac{1}{4} h \right) \left(\frac{1}{2} hd \right) + \left(\frac{1}{2} h \right) (bt) = bht + \frac{1}{4} dh^2$$

As mentioned before the I-section has a low shape factor. This is related to the effective place of the material in the elastic phase. In relation to this, the M - κ diagram has another character (Fig. 2.8). As soon as the point $M = M_e$ is passed almost immediately complete

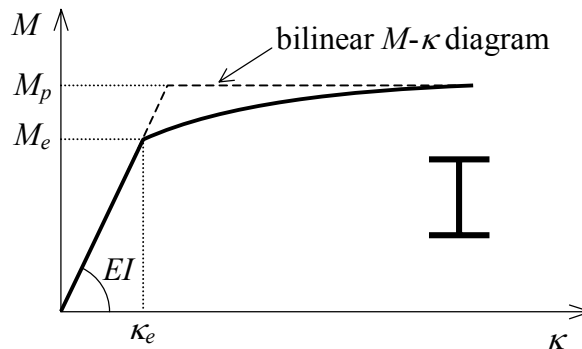
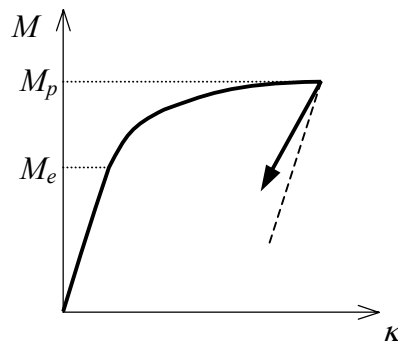
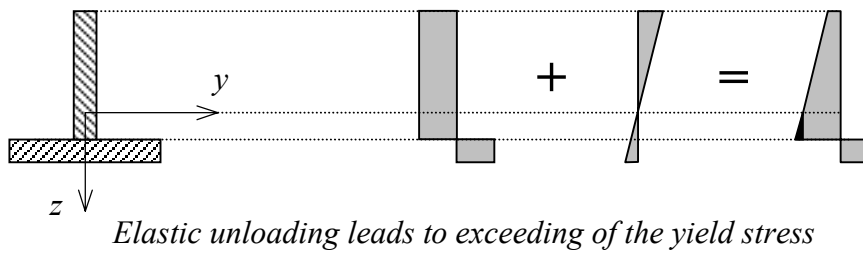
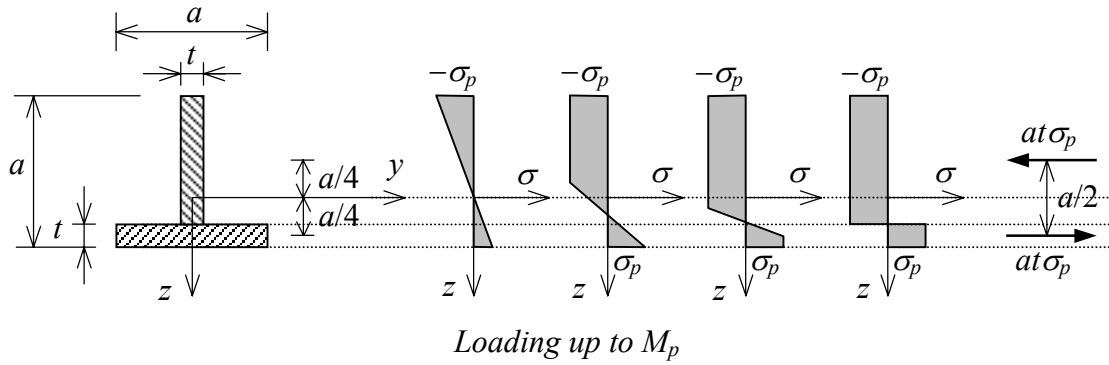


Fig. 2.8: Approximation of the M - κ curve of an I-section by a bilinear M - κ diagram.

yielding takes place in the upper and lower flanges (for $t \ll h$). The stiffness EI of the whole section reduces to the stiffness of the web and the diagram shows a slope discontinuity. During the increase of κ the value M_p is soon reached. This leads to the idea to approximate the displayed behaviour by two straight branches: the so-called bilinear M - κ diagram, where M_e is set equal to M_p . By the way, this approximation is used in calculations with other cross-sections too.

The behaviour of *asymmetrical cross-sections* is more complicated than the behaviour of symmetrical cross-sections. As an example, the T-section is chosen of Fig. 2.9, where $t \ll a$. In the elastic phase, the neutral line passes through the centre of gravity of



The M - κ diagram: the path of unloading is not parallel to the initial elastic branch

Fig. 2.9: Stress development in a T-section.

the cross-section. The stresses at the top are three times larger than at the bottom (for these specific dimensions). After loading beyond M_e only the top part yields and the lower flange remains elastic. The neutral line cannot remain fixed at its position, because else the increase in total tensile force will be larger than the increase in total compressive force, which is impossible from equilibrium point of view. So, in the plastic phase the neutral line shifts to the flange. Further increase of the moment finally causes the lowest fibre to yield too. After that, the plastic areas grow at both sides. When both plastic areas have almost approached each other, the fully plastic moment is reached.

The determination of the M - κ diagram is a very labour-intensive procedure. In most cases only the value of the fully plastic moment is important, which can be found quite easily. The key is that the place of the neutral line in the full-plastic phase is uniquely defined; this line has to divide the cross-section into two parts of equal area, in order to zero the resulting normal force. One says that the neutral line coincides with the *bisection line*. For an *arbitrary asymmetrical* cross-section the full-plastic moment then can be determined as follows (Fig. 2.10):

$$M_p = W_p \sigma_p \quad ; \quad W_p = S_1 + S_2 = \frac{1}{2} A (a_1 + a_2) \quad (2.15)$$

S_1 and S_2 are the absolute values of the static moments of the respective parts above and under the bisection line. The static moments can be determined about the centre of gravity of the cross-section as well as about the bisection line.

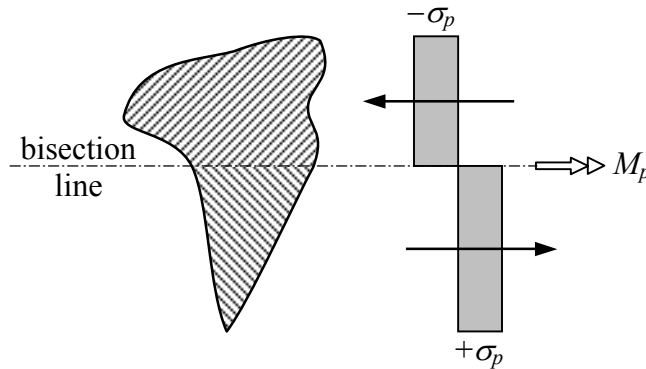


Fig. 2.10: For a non-symmetrical cross-section the full-plastic moment M_p is given by $(|S_1| + |S_2|) \sigma_p$, where S_1 and S_2 are the static moments of the parts above and below the bisection line.

For the considered T-section, it is found that the bisection line coincides with the top surface of the flange. For a positive moment the flange as a whole will yield positively and the whole body negatively. The yield force in both parts equals σ_p , the arm is $a/2$, so that a yield moment results of $(1/2)a^2t\sigma_p$. Through the formal way this result can be obtained too from (2.15). To achieve that the static moments about the centre of gravity of the section are determined:

$$W_p = \frac{1}{2} A (a_1 + a_2) = \frac{1}{2} (2at) \left(\frac{1}{4} a + \frac{1}{4} a \right) = \frac{1}{2} a^2 t \quad ; \quad M_p = \frac{1}{2} a^2 t \sigma_p$$

Finally, for the T-section it still is interesting to find out what happens if after reaching M_p the load is reduced (by a small amount). In first instance, it is assumed that the beam reacts completely elastic just as for the rectangular cross-section. However, in Fig. 2.9 it clearly can be seen (black triangle) that in the area between the centre of gravity and the bisection line the yield stress has to be exceeded, which is impossible. Therefore, it can be concluded that the section has to behave elastic-plastic during unloading. Also for the T-section completely elastic load alterations in the range of $2M_e$ are possible. This phenomenon does not occur instantly but after a number of oscillations. The analysis of this process is called *yield-stop analysis*.

2.3 The moment-curvature relation of reinforced concrete

Fig. 2.11 shows the cross-section of a concrete beam. The cross-section is rectangular with width b and height h . The reinforcement with area A_s is situated at the bottom of the beam. The ratio $A_s/(bh)$ is the geometrical reinforcement ratio indicated by ω , i.e.:

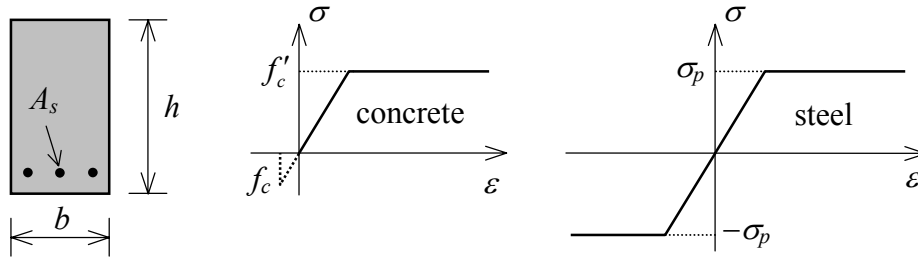


Fig. 2.11: Nomenclature of reinforced concrete.

$$\omega = \frac{A_s}{bh} \quad (2.16)$$

The material behaviour of steel and concrete are indicated in Fig. 2.11 too. The load case is considered where the beam is loaded by a pure moment. So, the normal force is equal to zero.

When the load is gradually increased from $M = 0$, initially the cross-section will behave elastically (see Fig. 2.12a). The neutral line is situated just below the centre of the beam, because steel has a higher E-modulus than concrete. In this stage, the stiffness is about the same as for an unreinforced section. At a certain moment at the bottom of the beam the tensile strength of the concrete is reached and cracking occurs.

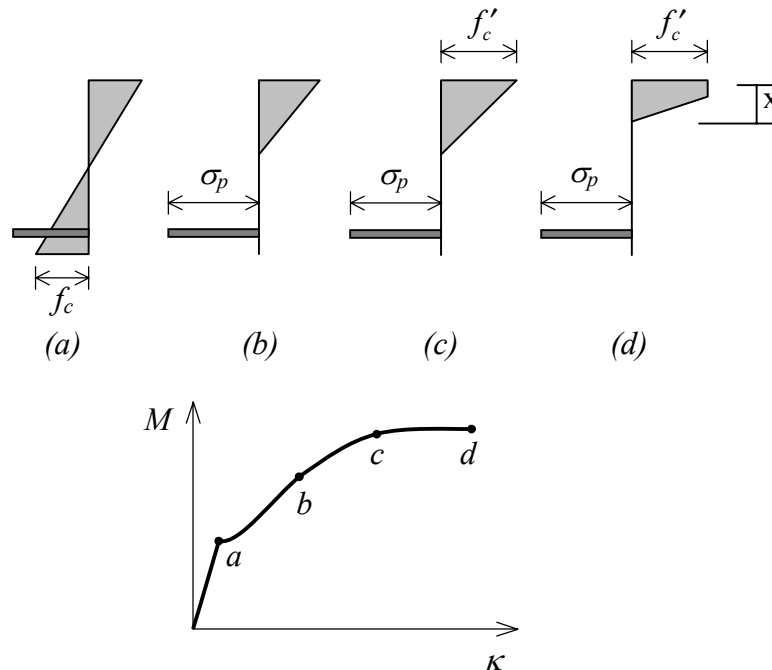


Fig. 2.12: Stress evolution in reinforced concrete.

The behaviour after the cracking-moment is reached depends on the amount of reinforcement and the softening properties of the concrete. During increasing curvature in most cases the moment initially will drop slightly, but will rise again after that. The cracked zone progresses upwards during this process. The stress distribution is given in Fig. 2.12b. Finally, the branch is reached corresponding to the “cracked” cross-section.

Then for a well-designed cross-section the point is reached where the steel will yield too. The moment still increases because the neutral line goes further upwards, increasing the internal lever arm. This situation is displayed in Fig. 2.12c. Finally, in the concrete compression zone, the maximum capacity is reached and the neutral line stops its upward movement. The limit load bearing capacity is reached with the stress distribution according to Fig. 2.12d. The entire $M-\kappa$ diagram is given in Fig. 2.12e. The ultimate moment M_u can be determined to be:

$$M_u = A_s \sigma_y (h' - \alpha x) \quad (2.17)$$

where h' is the distance from the reinforcement bars to the top surface of the beam ($= h - d - \phi/2$, with d the concrete cover and ϕ the bar diameter), σ_y is the yield stress of the steel, x is the height of the concrete compression zone and α a factor depending on the stress distribution in the concrete. If the concrete tensile stress is neglected and the concrete stress in the entire compression zone is assumed constant and equal to f'_c then the factor α equals 0.5 and x can be determined from the horizontal equilibrium of forces:

$$A_s \sigma_y = b x f'_c \quad (2.18)$$

so that:

$$M_u = \omega b h^2 \sigma_y \left(1 - \frac{1}{2} c\right) \quad (2.19)$$

or:

$$M_u = c b h^2 f'_c \left(1 - \frac{1}{2} c\right) \quad \text{with} \quad c = \frac{A_s \sigma_y}{b h f'_c} = \omega \frac{\sigma_y}{f'_c} \quad (2.20)$$

where c is called the *material reinforcement ratio*. In order to get an impression of its order of magnitude the following realistic values are chosen: $\omega = 1\%$, $\sigma_y = 240$ MPa and $f'_c = 24$ MPa. For c it then follows: $c = \omega \sigma_y / f'_c = 0.01 * 240 / 24 = 0.10$.

2.4 The elastic-plastic behaviour of a statically indeterminate beam

Fig. 2.13 shows a beam, which is restrained at both sides and loaded by a uniform surface load f . It is assumed that for $f = 0$ the beam is straight and stress free and that the $M-\kappa$ diagram can be assumed to be bilinear for each cross-section. When the load is increased in the beam the well-known elastic moment distribution develops with field moment $f l^2 / 24$ and fixed-end moment $f l^2 / 12$. The load can be increased elastically until the fixed-end moments become equal to the full-plastic moment M_p . The distributed load then is:

$$f = \frac{12 M_p}{l^2}$$

What will happen if now the load is increased further? On basis of the $M-\kappa$ diagram, it can be concluded that at the fixed ends no further increase of the moment is possible. However, the curvatures can increase. In other words, during a further load increase Δf , the fixed-

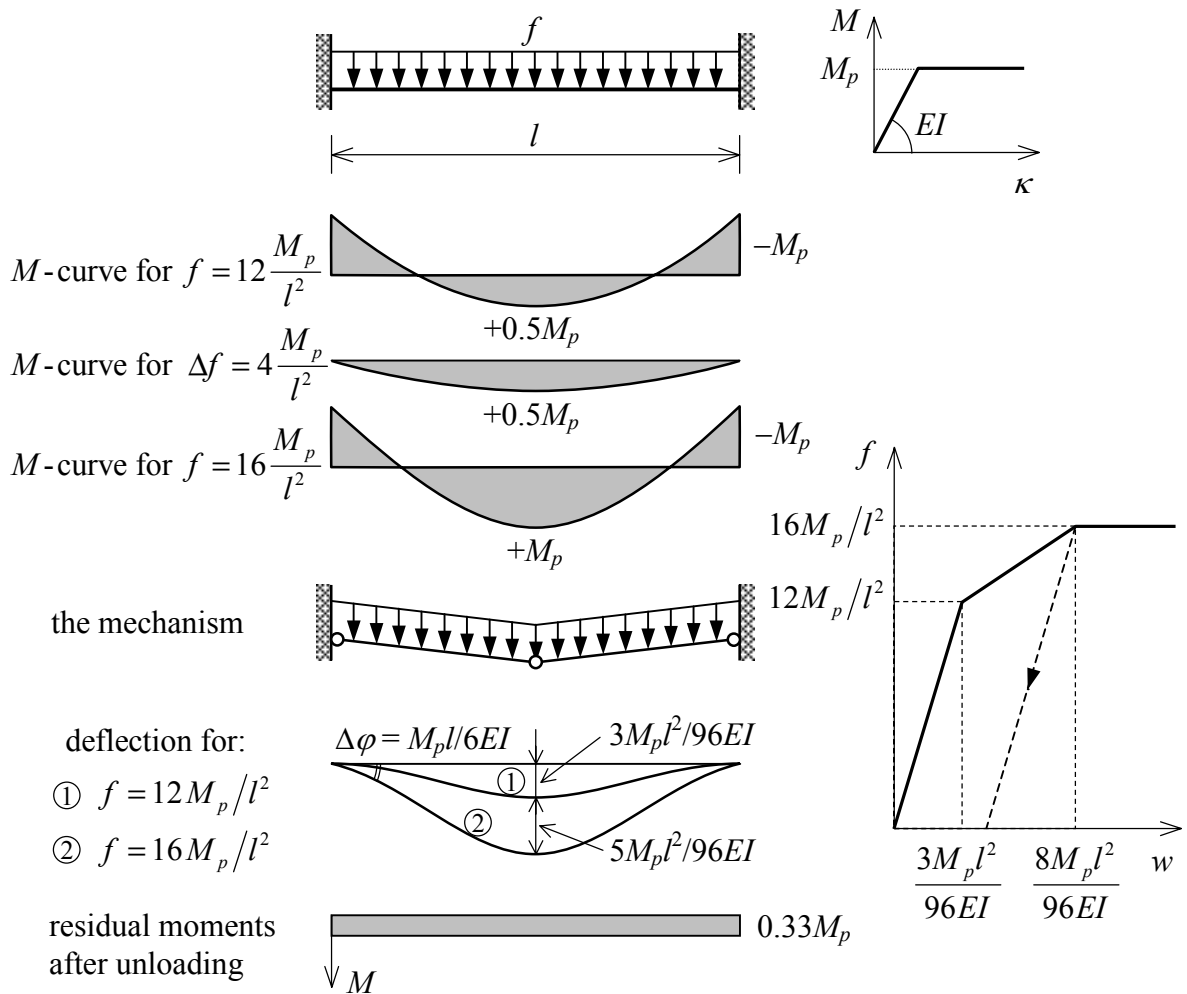


Fig. 2.13: Elastic-plastic analysis of a beam, which is restrained at both sides and is loaded by a uniformly distributed load.

ends act as simple supports with a maximum field moment of $\Delta f l^2 / 8$. Now, further increase of the load is possible until in the middle of the beam the full-plastic moment is reached too. So, the field moment increases from $f l^2 / 24 = 0.5 M_p$ at the end of the elastic phase to M_p at the end of the plastic phase. The possible increment can then be calculated to be:

$$0.5 M_p + \frac{1}{8} \Delta f l^2 = M_p \rightarrow \Delta f = \frac{4 M_p}{l^2}$$

The total load then becomes:

$$f_{tot} = \frac{12 M_p}{l^2} + \frac{4 M_p}{l^2} = \frac{16 M_p}{l^2}$$

The resulting moment distribution is given in Fig. 2.13. The field moment and both fixed-end moments are equal to M_p . A further increase of the load is not possible, because for any additional Δf at both fixed ends and at the middle of the beam, a plastic hinge will be created. Such a structure is not capable of carrying any load increment. The smallest

thinkable increment will cause infinite displacements. The structure has become a *mechanism* and the *ultimate load bearing capacity* or *limit load* is reached. The limit load can also be directly determined from the moment distribution at failure, the equilibrium equation reads:

$$2M_p = \frac{1}{8} fl^2 \quad \rightarrow \quad f = \frac{16M_p}{l^2}$$

So, the ultimate load bearing capacity obtained from the plasticity theory equals $16M_p/l^2$, which is 33% higher than the value according to the elasticity theory. It can be said that the structure has a redistribution factor of 1.33. The extra plastic load carrying capacity is originated from the indeterminate character of the structure. A statically determinate structure always has a redistribution factor of 1. In statically indeterminate structures some of the underloaded parts still can supply an extra contribution after the formation of one or more plastic hinges, which finally delivers a factor >1 . This phenomenon is called the *redistribution of stresses*. An important conclusion is that the “safety against failure” of statically indeterminate structures designed according to the elasticity theory is completely different from the one based on plastic design.

The increase of the load above the elastic limit load, however, is accompanied by larger deformations. At the end of the elastic phase the midspan deflection is given by:

$$u = \frac{1}{384} \frac{\Delta f l^4}{EI} = \frac{1}{32} \frac{M_p l^2}{EI}$$

In the elastic-plastic phase the increase of u is:

$$\Delta u = \frac{5}{384} \frac{\Delta f l^4}{EI} = \frac{5}{96} \frac{M_p l^2}{EI}$$

Although the load increment Δf is only 1/3 part of the elastic load step, the displacement is more than 1.5 times larger, as can be seen from the *load-displacement diagram* in Fig. 2.13.

The deflection curves are interesting too. In Fig. 3.13, it can be seen that the slopes of the lines at the fixed ends are unequal to zero. Because of the plastic hinge at the fixed end, the following rotation is present at the point of failure:

$$\Delta \varphi = \frac{\Delta f l^2}{24EI} = \frac{M_p l^2}{6EI}$$

Such a rotation is called a *plastic (hinge) rotation* and develops in each structure where during a certain load increase a plastic hinge is present. In the present modelling, a plastic rotation is a finite angular displacement of a single cross-section. It is called a “point hinge”. The finite angular displacement over an infinitely small distance would imply an infinitely large curvature. It is clear that this is impossible. Therefore, the reality is somewhat more complicated, in chapter 4 more attention will be paid to this phenomenon.

Finally, some attention will be paid of how the failed statically indeterminate beam responds on load removal. It is assumed that during unloading the cross-section is, and remains, completely elastic (So, the cross-section cannot be a T-section). The fixed-end moment resulting from the load reduction is equal to $fl^2/12 = 1.33M_p$ and the field moment $fl^2/24 = 0.67M_p$. The consequence is that for both the resulting fixed-end and field moments a value of $0.33M_p$ remains. Also for the intermediate points a value of $0.33M_p$ results. This easily can be seen by considering the fact that the second derivative of the moment is equal to the external load, which in this case is equal to zero, i.e.: the moment line must be linear between the calculated points. The moment distribution, which arises like this, is called a *residual moment distribution*. This residual moment distribution (the same as with residual stresses) makes it possible to take up load alterations, which are completely elastic.

It is for the reader to determine the residual stress distribution across the cross-sections in the middle and at both ends of the beam. These residual stresses then should deliver a moment of $0.33M_p$.

2.5 The elastic-plastic behaviour of a frame

The behaviour of an arbitrary frame is basically the same as that of the beam previously discussed. At low load levels the frame responds linear elastic. The elastic phase ends as soon as somewhere in the structure the bending moment becomes equal to the plastic moment M_p . At that spot a plastic hinge develops: the cross-section still transmits M_p but behaves as a hinge under a load increment. Subsequently, more plastic hinges may develop during the increase of the load. This process continues until in the structure such a configuration of plastic hinges is present that a mechanism is formed, which means that the structure can deform unlimited without any load increase.

In Fig. 2.14 this process is demonstrated for a simple portal frame. The frame has a height and width equal to l . It is horizontally loaded by the force $0.5F$ and vertically loaded by the force F . Both the columns and the cross girder have a bilinear $M-\kappa$ diagram with bending stiffness EI and full-plastic moment M_p .

In the elastic stage the largest moment occurs in cross-section (4). The moment has a value of $0.190Fl$ and therefore the first plastic hinge occurs for a value of $F = 5.25M_p/l$. During a further increase of the load, the construction responds as if in cross-section (4) a hinge is present. The corresponding moment distribution is also given in Fig. 2.14. In order to find out where the second hinge develops, for all sections the load increment ΔF has to be determined for which M_p is reached. For example for cross-section (1) the first hinge is generated for $M=0.53M_p$. So, the moment is allowed to increase by $0.47M_p$. For cross-section (1) the value of ΔF equals:

$$0.47M_p = 0.24\Delta Fl \rightarrow \Delta F = 1.96M_p/l$$

Similarly for cross-section (2) it follows $\Delta F = 14.5M_p/l$, for cross-section (3) $\Delta F = 0.35M_p/l$ and for cross-section (5) $\Delta F = 0.15M_p/l$. So, at cross-section (5) the second hinge develops because it provides the smallest force increment. The load then is increased to $F = 5.40M_p/l$. During further increase of the load, subsequently plastic hinges are formed in the cross-sections (3) and (1). By the presence of these four hinges a mechanism is formed and no further load increase is possible. The limit load equals $F_u = 6.00M_p/l$.

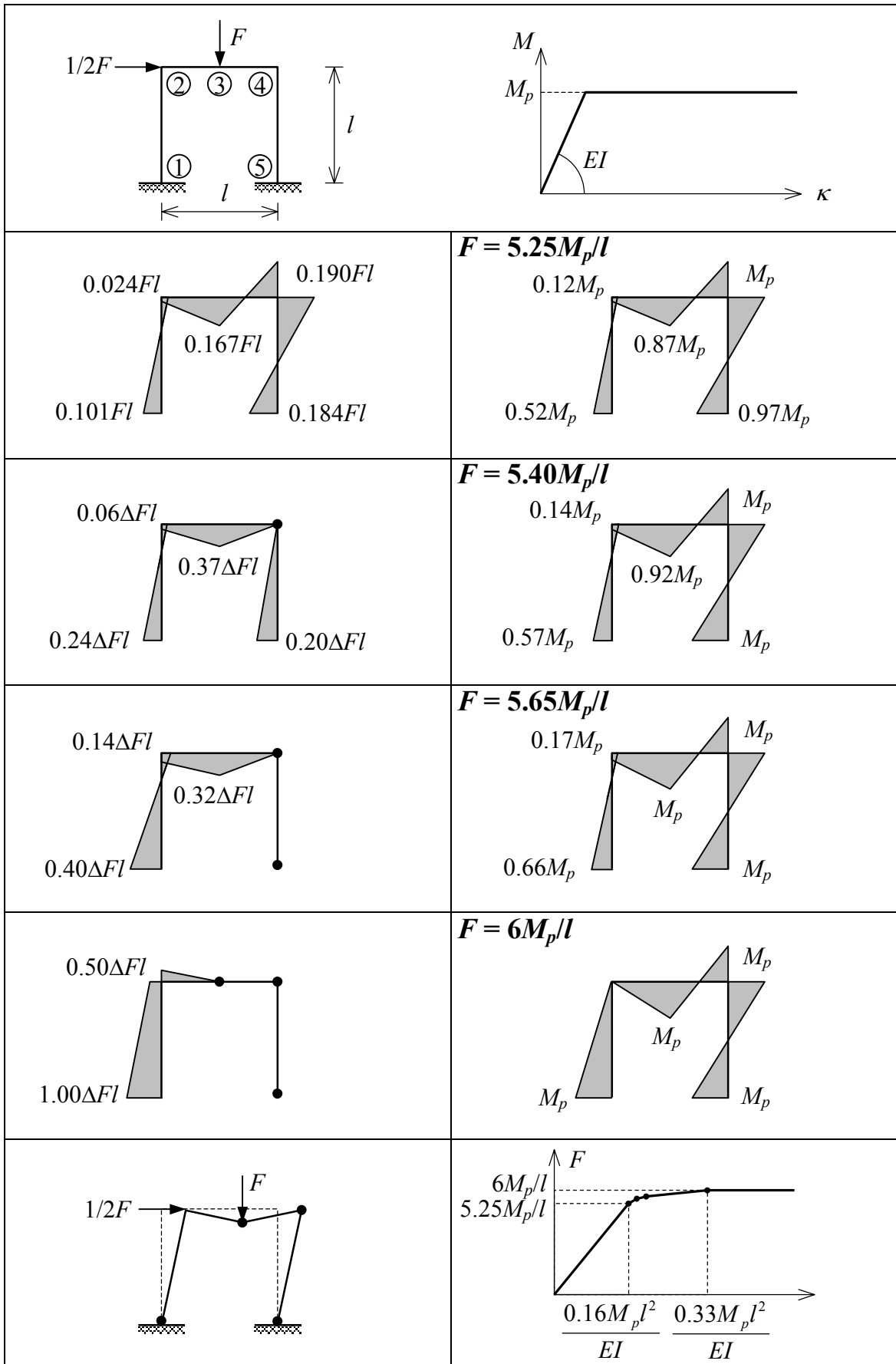


Fig. 2.14: Elastic-plastic analysis of a portal frame.

At the bottom of Fig. 2.14 the relation is displayed between the load F and the horizontal displacement u of the cross girder. The relation consists of a number straight branches. The first long branch is the elastic one, which is followed by a number of short straight branches with reducing slope generated at the formation of each plastic hinge. Finally, a horizontal branch is formed when the limit load is reached.

The difference between the ultimate elastic and ultimate plastic load bearing capacity for this portal frame is $0.75M_p/l$ or 14%. The redistribution factor of the structure is 1.14. The displacements in the plastic stage are relatively large: the 14% stress increase requires the same displacement as the entire elastic branch. By the way, in absolute sense the displacements do not need to be large at all.

An interesting aspect, in view of coming chapter, is the degree of statically indeterminacy. Initially the portal frame is 3rd-order statically indeterminate. At the formation of each hinge, the degree of statically indeterminacy reduces by one. After the formation of the 3rd hinge the structure become statically determinate and the 4th hinge changes it into a mechanism.

For the mechanism the complete moment distribution at failure can easily be determined and the ultimate load can directly be obtained independently from the load history, being the sequence of formation of the plastic hinges (check this!). The important consequence is that the incremental procedure does not have to be followed in order to obtain the ultimate load. The problem is shifted to the tracing of the proper collapse mechanism. In chapter 3, more attention will be paid to this aspect.

Summarising the following statement can be formulated: a n^{th} -order statically indeterminate structure fails after the formation of $n + 1$ plastic hinges. This is a good guideline, in spite of the fact that to both sides (more or less hinges) exceptions are possible.

3 Plastic limit state analysis

3.1 Introduction

In previous chapter, the limit load of a structure was calculated through an elastic-plastic calculation. The limit load can also be determined directly from the upper- and lower-bound theorems of the theory of plasticity. In this chapter, both theorems will be introduced, corresponding working methods discussed and demonstrated. After that it will be shown how the actual limit load can be enclosed by making a systematic use of both theorems.

In this chapter, beam structures will be considered with one-dimensional stress states, in which case the upper- and lower-bound theorems easily can be proved. For structures with two- or three-dimensional stress states (for example with normal and shear stresses), additional hypotheses are required. These will be discussed in chapter 6.

Further, it is assumed that the deformation capacity will be sufficient all the time. Attention to this aspect will be paid in chapter 4.

3.2 Upper-bound theorem

General formulation:

“Starting from an arbitrary mechanism, the corresponding equilibrium equation will provide an upper-bound solution for the limit load.”

The proof will be postponed till section 3.3. We will first clarify the theorem and show some examples.

The equilibrium equation mentioned in the theorem can best be formulated through the principle of virtual work. According to this principle for a virtual displacement field $\delta \underline{u}$ the virtual work done by the external load equals the virtual work of the internal stresses:

$$\iiint_V \underline{\sigma}^T \delta \underline{\varepsilon} dV = \lambda \underline{F}^T \delta \underline{u} \quad (3.1)$$

where δ is the general symbol for the virtual increase, \underline{F} is the external loads vector, λ is the load factor with which all external loads are multiplied, \underline{u} is the vector with the displacements, $\underline{\sigma}^T = [\sigma_{xx} \sigma_{yy} \sigma_{zz} \sigma_{xy} \sigma_{xz} \sigma_{zy}]$ is the stress vector and $\underline{\varepsilon} = [\varepsilon_{xx} \varepsilon_{yy} \varepsilon_{zz} \varepsilon_{xy} \varepsilon_{xz} \varepsilon_{zy}]^T$ is the strain vector. The superscript T stands for “transposed”.

In the case of a two-dimensional beam structure subjected to purely bending, in x -direction, which is coinciding with the beam axis, only the stresses σ_{xx} and the strains ε_{xx} are present (Fig.3.1). This reduces (3.1) to:

$$\iiint \sigma_{xx} \delta \varepsilon_{xx} dV = \lambda \underline{F}^T \delta \underline{u} \quad (3.2)$$

For pure bending, the strain is given by:

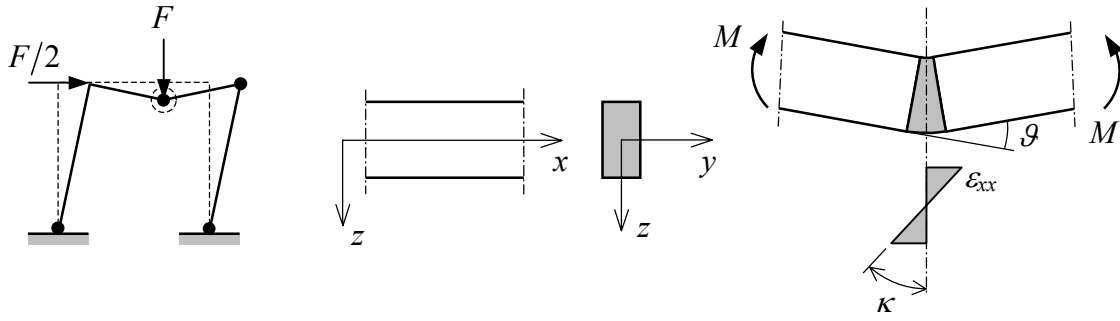


Fig. 3.1: Moment and rotation in a plastic hinge.

$$\varepsilon_{xx} = \kappa z \quad (3.3)$$

Further, the moment is given by (also see (2.3)):

$$M = \iint z \sigma_{xx} dy dz \quad (3.4)$$

Combination with (3.2) yields:

$$\sum \int M \delta \kappa dx = \lambda \underline{F}^T \delta \underline{u} \quad (3.5)$$

The sigma symbol indicates summation over all bars. The displacement field of a plastic mechanism only contains displacements that are allowed by the mechanism. So, the (concentrated) bending only occurs in the plastic hinges, as indicated in Fig. 3.1.

Therefore, in (3.5) the summation over all bars can be replaced by the summation over all plastic hinges. The integration takes place over the “length” of the hinge. However, this length is very small, theoretically it is approaching zero. In practice of course, some finite length is present. More attention to this aspect is paid in chapter 4. For the moment the length of the hinge is considered to approach zero and its curvature to approach infinity. This results into a finite angular displacement in the plastic hinge:

$$\vartheta = \int \kappa dx \quad (3.6)$$

The virtual work equation for a mechanism now becomes:

$$\sum_{k=1}^m M_{pk} \delta \vartheta_k = \lambda \underline{F}^T \delta \underline{u} \quad (3.7)$$

where m is the number of plastic hinges. From now on the variation symbol will be omitted. Further, only point loads are considered and therefore the vector notation can be replaced by the summation over the external work of all point loads. This delivers the following result:

$$\sum_{k=1}^m M_{pk} \vartheta_k = \lambda \sum_{i=1}^q F_i u_i \quad (3.8)$$

where q is the number of point loads. It is good to note that the both \mathcal{G} and M have the same sign. A positive moment goes together with a positive angular displacement and vice versa. This follows from the fact that the considered displacement field is not arbitrarily chosen but corresponds with the mechanism.

The procedure for an upper-bound calculation now is as follows:

1. Choose a mechanism;
2. Determine in each plastic hinge the plastic rotation \mathcal{G}_k ;
3. Determine in each hinge the full-plastic moment M_{pk} and its sign;
4. Determine the displacements of the point loads F_i ;
5. Determine the virtual work done in the plastic hinges;
6. Determine the virtual work done by the external loads;
7. Determine the load factor λ from (3.8).

The found value of λ is an upper bound for the load factor λ_c of the limit load.

Example 3.1

Consider the portal frame of Fig. 3.2a. From the elastic-plastic analysis in the previous chapter, the collapse mechanism is known. This mechanism including the magnitude of the

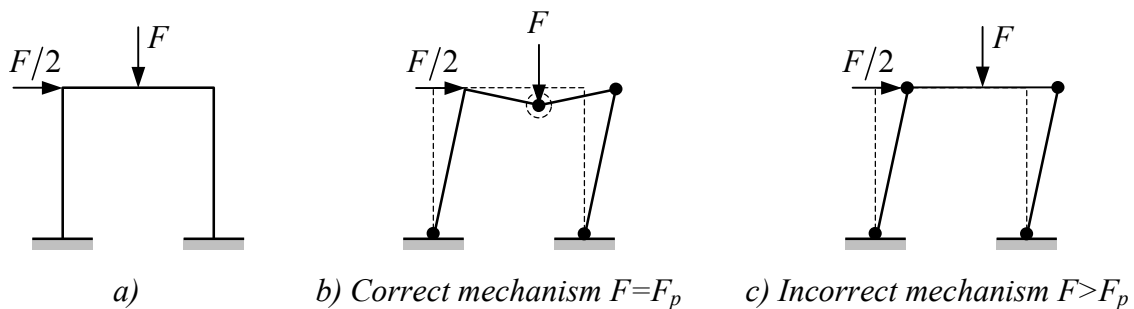


Fig. 3.2: Simple example of a mechanism.

angular displacements in the plastic hinges (bullets) and the displacements of the external point loads are indicated in Fig. 3.2b. The work equation (3.8) then becomes:

$$M_p \mathcal{G} + M_p (2\mathcal{G}) + M_p (2\mathcal{G}) + M_p \mathcal{G} = \lambda \left[(F/2)(l\mathcal{G}) + (F)(l\mathcal{G}/2) \right]$$

From this it follows $\lambda F = 6M_p/l$, which is exactly the same result as obtained in chapter 2 after the performance of a very extensive elastic-plastic calculation. The answer is the same since the proper mechanism was used. However, suppose the mechanism of Fig. 3.2c was chosen. Then the work equation becomes:

$$4M_p \mathcal{G} = \lambda (F/2)(l\mathcal{G})$$

This leads to $\lambda F = 8M_p/l$, which is an overestimation of the failure load, exactly as predicted by the upper-bound theorem. From this last example, it also can be shown that the virtual work equation agrees with the equilibrium equation corresponding to the mechanism. Both columns have a top-end moment of $+M_p$ and a bottom-end moment of

$-M_p$. The transverse force in both columns therefore is $2M_p/l + 2M_p/l$. This also provides $\lambda F = 8M_p/l$.

3.2.1 Systematic application

It is relatively simply to carry out upper-bound calculations with mechanisms. However, the solution is always higher than the limit load and principally at the unsafe side. Therefore, a sharp upper bound has to be found. An effective method is to find and check all possible mechanisms. For a frame out of straight prismatic beams having point supports and loaded with point loads this is possible in principle. Then the procedure is as follows:

1. Determine the degree of statically indeterminacy (n);
2. Determine the number of places where a hinge may develop (m);
3. Obtain a set of $e = m - n$ elementary mechanisms;
4. Determine all combination mechanisms.

The spots where a possible hinge may develop can simply be identified. All beam-ends and points of action of the external loads are possible candidates. Between these points, the moment line is linear and no maximum can occur there. Thus, in the example of Fig. 3.2 $n = 3$, $m = 5$, $e = 2$ and the number of hinges is $n + 1 = 4$.

A set of elementary mechanisms can be found by starting from an arbitrary mechanism and then subsequently replacing hinges by other ones:

Location	1	2	n	$n+1$	m
First mechanism	1	2	n	$n+1$			
Second mechanism		2	3	$n+1$	$n+2$		
Third mechanism			3	4	$n+2$	$n+3$	
Etc.									

In the first mechanism of above scheme plastic hinges are present in the first $n + 1$ of the in totally m positions. This is exactly the number required to get an ordinary mechanism for a n^{th} -order statically indeterminate structure. The second mechanism can be obtained by replacement of the first plastic hinge by the one on position $n + 2$, etc. In this manner mechanisms are created which are not a combination of the already existing set. If the highest number is equal to the number of places m , no further shifting is possible. Obviously the number of elementary mechanisms follows from the equation $n + e = m$, so that it holds $e = m - n$. Given a set of “ e ” elementary mechanisms, all mechanisms can be found by superposing two or more of the elementary mechanisms in such a ratio that the total number of appearing and disappearing hinges are the same.

In above text it is assumed that an n^{th} -order statically indeterminate structure leads to $n+1$ plastic hinges. This is not necessarily always the case. In Fig. 3.3a for example a mechanism is depicted with 3 hinges in a 3^{rd} -order statically indeterminate structure. Such a mechanism is called a *partial mechanism*. In Fig. 3.3b, its counterpart is present, the *over-complete mechanism*: there are 3 hinges in a 1^{st} -order statically indeterminate structure. Finally, Fig. 3.3c shows a mechanism that is both over-complete and partial (the structure contains one hinge more than necessary, but still is statically indeterminate). It is important to know that for all these mechanisms the upper-bound theorem holds too.

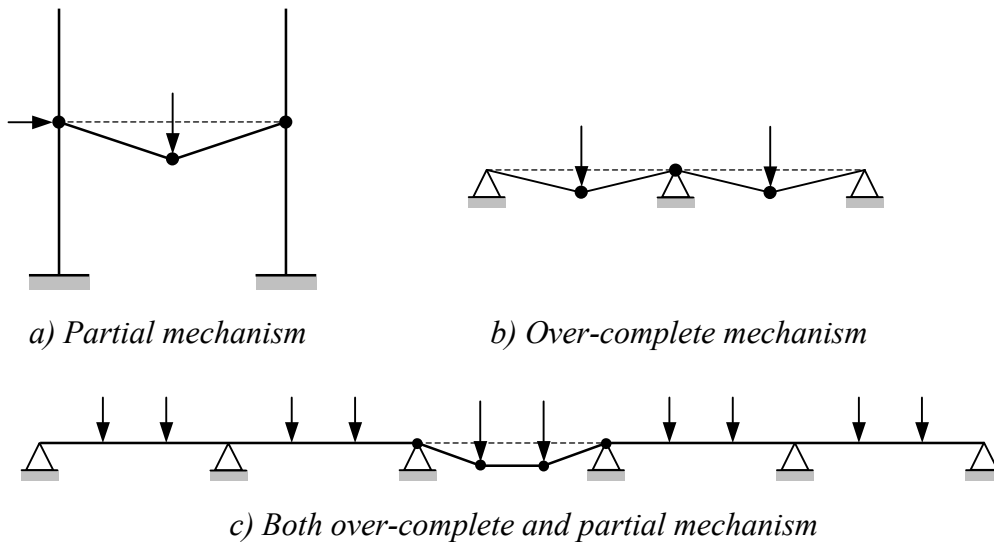


Fig. 3.3: Several types of mechanisms.

Example 3.2

Again, the portal frame of chapter 2 is considered, also see Fig. 3.4. The structure is 3rd-order statically indeterminate and there are 5 possible places for the development of plastic hinges. Therefore, $e = m - 1 = 5 - 3 = 2$ elementary mechanisms can be identified. Which ones are chosen is not that important. In this case, the following mechanisms are chosen:

- the sway mechanism
- the beam mechanism

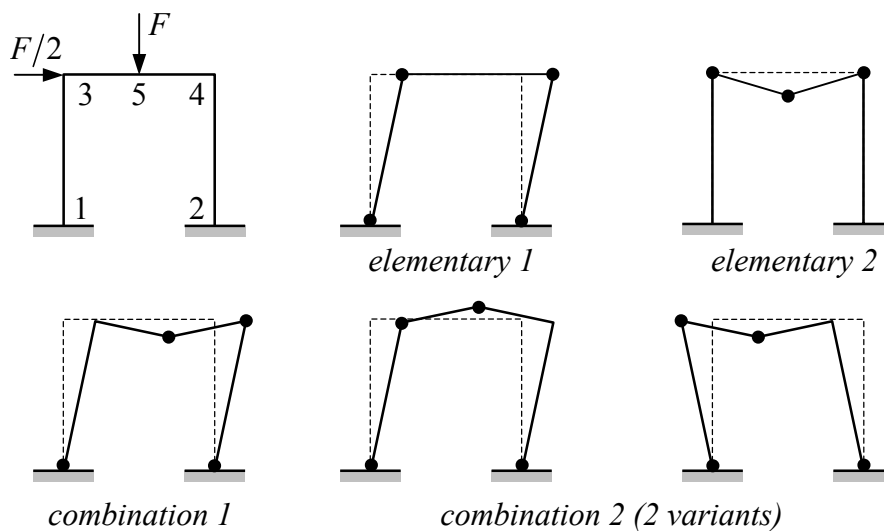


Fig. 3.4: Example of portal frame with $m = 5$, $n = 3$, $e = 2$.

Note that the second one is actually a partial mechanism: the angular rotation at location 2 is zero, so basically three hinges are present. Now combination mechanisms are investigated where the joint hinges 2, 3 and 4 will disappear one by one.

Location	1	2	3	4	5
Sway mechanism	$+\mathcal{G}$	$+\mathcal{G}$	$+\mathcal{G}$	$+\mathcal{G}$	
Beam mechanism		0	$-\mathcal{G}$	$+\mathcal{G}$	$+2\mathcal{G}$
Combination mechanism 1	$+\mathcal{G}$	$+\mathcal{G}$		$+2\mathcal{G}$	$+2\mathcal{G}$
Combination mechanism 2	$+\mathcal{G}$	$+\mathcal{G}$	$+2\mathcal{G}$		$-2\mathcal{G}$

The first combination mechanism (also indicated in Fig. 3.4) is obtained by addition of both elementary mechanisms. At position 3 (upper left corner) the plastic hinge disappears and at position 4 (upper right corner) the angular displacement doubles. In the middle of the horizontal beam (position 5) the beam mechanism still provides the hinge with rotation $+2\mathcal{G}$. The rotations \mathcal{G} at the fixed ends are maintained.

In addition, a combination can be made such that the joint hinge 4 disappears. Then a mechanism is created for which one of the two loads always performs negative work. This mechanism might still be possible, but with reduced chance to success.

The third combination has to be created by the disappearance of hinge 2. However, in this case this is not possible because the beam mechanism is a partial one.

Example 3.3

Not all examples are that simple as the previous one. For example, take the two-storey portal frame of fig. 3.5. The structure is 6th-order statically indeterminate ($n = 6$) and 16 possible places for the creation of plastic hinges are present ($m = 16$). Therefore, 10 elementary mechanisms can be identified ($e = 16 - 6 = 10$). It is not important which ones exactly, as long as they are independent. The following choice is made:

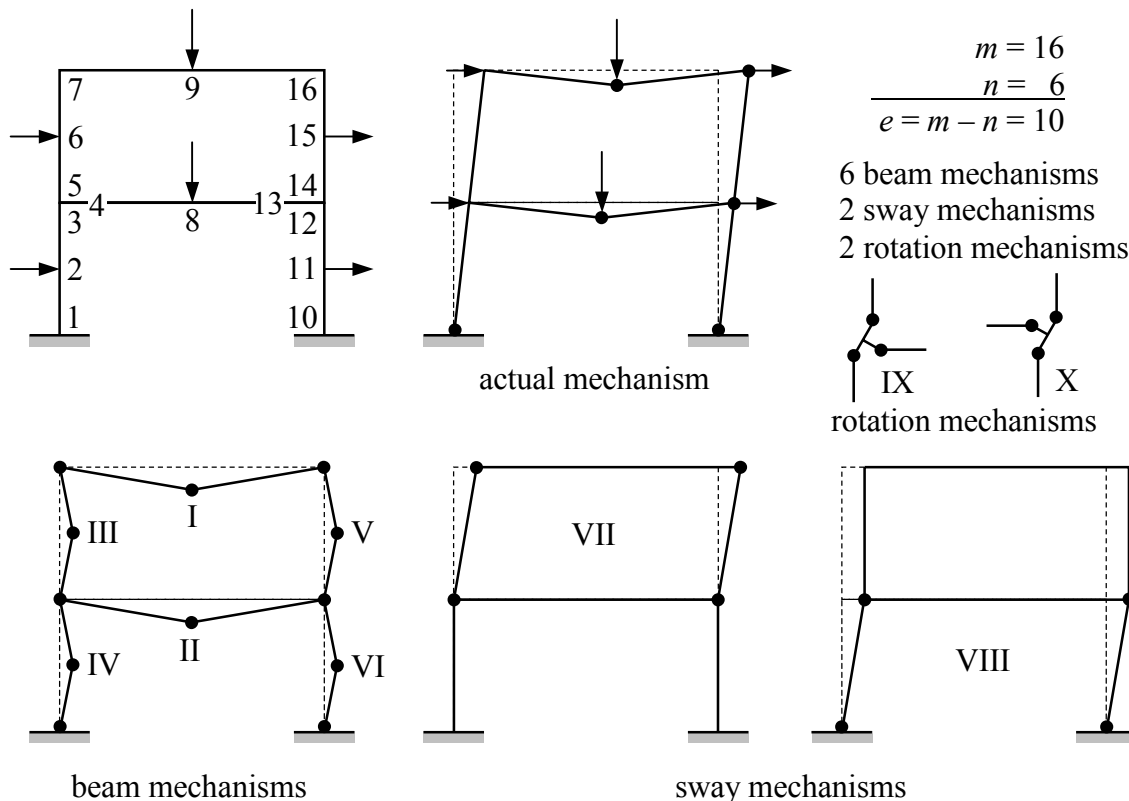


Fig. 3.5: Two-storey portal.

- 6 beam mechanisms
- 2 sway mechanisms
- 2 rotation mechanisms

In a rotation mechanism, the entire node rotates. This mechanism occurs independently only if in the node an external torsional moment is present. However, as elementary mechanism it plays an excellent role, even if the specific torsional load is not present in a certain case. Again, combinations of the elementary mechanisms can be investigated. Doing so, the actual mechanism as shown in Fig.3.5 can be found. It is a combination of the mechanisms I, II, VII and VIII and the rotation mechanisms IX and X.

3.2.2 Special cases

Although, computer programmes with automatic search procedures can carry out this type of procedures for finding the decisive mechanism, they hardly are applied. However, handy for manual calculations are the cases with very low levels or on the other hand very high levels of statically indeterminacy.

Suppose the structure is statically determinate, then just one hinge is required for the creation of a mechanism. That means that in total m mechanisms exist, which can be found easily. Is the construction 1st-order statically indeterminate two hinges are required for a mechanism. For the first hinge, m positions are possible and for the second hinge $(m-1)$ positions.

After correction for the double counting, finally $m(m-1)/2$ mechanisms are possible. Normally this amount is still manageable. For a 2nd-order statically indeterminate structure the number of mechanisms becomes $m(m-1)(m-2)/6$. For $m=10$ this comes down to 120 mechanisms, which makes the analysis complicated.

At the other side of the scale, the highly statically indeterminate structures can be found. For example, take a structure that is $(m-1)$ -order statically indeterminate. Then only $e = (m - n) = 1$ elementary mechanism can be found. Such a construction is called *kinematically determinate*.

A $(m-2)$ -order statically indeterminate structure has m elementary mechanisms. These can easily be found by assuming hinges in each possible position and then repeatedly removing one hinge in one of the positions. In a $(m-3)$ -order statically indeterminate structure combinations of 2 hinges have to be removed repeatedly.

Summarising:

n	$e = m - n$	total number	description
0	m	m	statically determinate, 1 hinge only
1	$m-1$	$1/2m(m-1)$	1 st -order stat. indet., all comb. of 2 hinges
2	$m-2$	$1/6m(m-1)(m-2)$	
$m-3$	3	$1/2m(m-1)$	2 positions without hinge
$m-2$	2	m	1 position without hinge
$m-1$	1	1	kinematically determinate, but a mechanism

Fig. 3.6 shows an overview and some examples. The already discussed portal frame is included as well, having $m = 5$ possible hinge positions and $n + 1 = 4$ required hinges. In all cases, one position does not contain a hinge. The exclusion of the restrained column ends leads to the same partial beam mechanism.

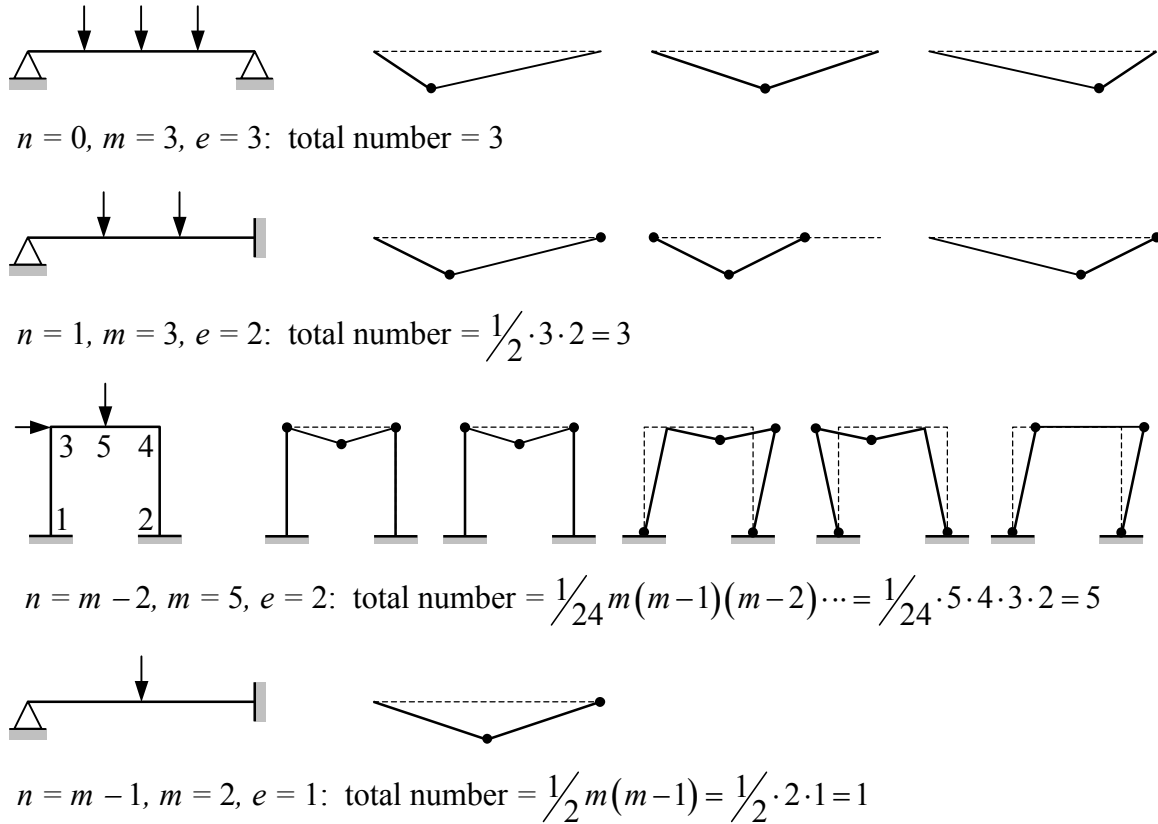


Fig. 3.6: Total number of mechanisms for different cases.

3.2.3 Uniformly distributed load

When a uniformly distributed load is present (or a continuous elastic support, or non-prismatic or curved beams) the analysis becomes more complicated. The positions of the hinges are not fixed anymore and have to be found through a process of optimisation.

Example 3.4

Consider the example of Fig. 3.7. The beam is 1st-order statically indeterminate, so 2 plastic hinges are required for failure. Firstly, the mechanism is considered with a plastic hinge in the middle of the beam and a plastic hinge at the restrained end. The virtual work equation for this mechanism reads:

$$2M_p \vartheta + M_p \vartheta = \frac{1}{2} qa \left(\frac{1}{2} a \vartheta \right)$$

The limit load then becomes:

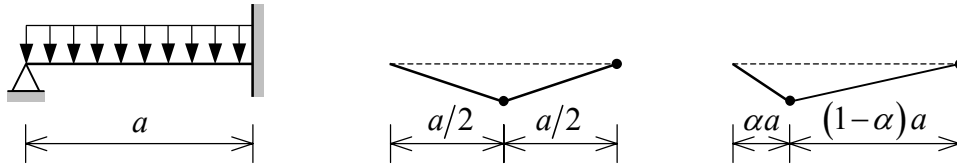


Fig. 3.7: Beam with distributed load: mechanisms for upper-bound calculation.

$$\frac{qa^2}{M_p} = 12$$

The mechanism was arbitrarily chosen, therefore this solution is an upper bound. The actual failure load can be found through an upper-bound calculation by positioning the plastic hinge at an arbitrary distance “ αa ” from the simple support (see Fig. 3.7). The virtual work equation for this case becomes:

$$M_p \vartheta + M_p \vartheta + M_p \vartheta \left(\frac{1-\alpha}{\alpha} \right) = qa \frac{1}{2} (1-\alpha) a \vartheta \rightarrow M_p \left(2 + \frac{1-\alpha}{\alpha} \right) = qa^2 \frac{1-\alpha}{2}$$

This can be worked out to:

$$\frac{qa^2}{M_p} = \frac{2(1+\alpha)}{\alpha(1-\alpha)}$$

For each value of α an upper-bound solution can be found. The lowest upper bound, and thus the correct value of α , can be found by minimisation of this function. Differentiation and equating the numerator to zero provides:

$$\frac{2\alpha(1-\alpha) - 2(1+\alpha)(1-2\alpha)}{\alpha^2(1-\alpha)^2} \rightarrow \alpha^2 + 2\alpha - 1 = 0 \rightarrow \alpha = -1 + \sqrt{2}$$

Substitution in the expression for qa^2/M_p gives:

$$\frac{qa^2}{M_p} = \frac{2\sqrt{2}}{(-1+\sqrt{2})(2-\sqrt{2})} = 11.66$$

Indeed this value is smaller than the previously found one, however the difference is small.

3.2.4 Proof of the upper-bound theorem

As a conclusion of this section, proof of the upper-bound theorem will be given for the case of prismatic straight beams, loaded by point loads only.

Suppose the real collapse mechanism is given by a displacement field u and rotations ϑ in the plastic hinges. Thus, the load factor λ_c corresponding to the ultimate load can be determined through:

$$\lambda_c \sum F_i u_i = \sum M_k \vartheta_k \quad (3.9)$$

The values of M_k are the full-plastic moments M_{pk} where the sign follows from the sign of the rotations ϑ_k .

Now consider an arbitrary mechanism with displacement field u'_i and plastic rotations ϑ'_k . This displacement field leads to a limit load with level λ given by:

$$\lambda \sum F_i u'_i = \sum M'_k \vartheta'_k \quad (3.10)$$

The values of M'_k are the full-plastic moments M_{pk} at hinge k where the sign follows from the sign of the rotations ϑ'_k .

Since the real solution (λ_c, M_k) satisfies the equilibrium equation, the real solution also has to satisfy the virtual work equation corresponding with the arbitrary mechanism given by (u'_i, ϑ'_k) . Therefore, it holds:

$$\lambda_c \sum F_i u'_i = \sum M_k \vartheta'_k \quad (3.11)$$

Because the work $\sum F_i u'_i$ in both equations (3.10) and (3.11) is the same it follows:

$$\frac{\sum M_k \vartheta'_k}{\lambda_c} = \frac{\sum M'_k \vartheta'_k}{\lambda} \quad (3.12)$$

As $\sum M'_k \vartheta'_k \geq \sum M_k \vartheta'_k$ (see below) it follows that $\lambda \geq \lambda_c$, which had to be proved.

That $\sum M'_k \vartheta'_k \geq \sum M_k \vartheta'_k$ can be seen quite easily. Suppose that in hinge k of the arbitrary mechanism $\vartheta'_k > 0$, then $M'_k = M_{pk} \geq M_k$ and the inequality is valid. On the other hand if $\vartheta'_k < 0$, then $M'_k = -M_{pk} \leq M_k$ and the inequality is valid too. Moreover, if the inequality holds for one hinge, it holds for the sum over the hinges too.

3.3 Lower-bound theorem

General formulation:

“Each arbitrary moment distribution, that is in equilibrium with the external load and for which nowhere the yield condition is violated, delivers a lower bound for the limit load.”

3.3.1 Application

Lower-bound solutions for simple structures normally can be found quite easily. Note that the ordinary elastic solution provides a lower-bound solution too. The advantage of a lower-bound solution is that it is always at the safe side. However, the derivation of such a solution can be very uneconomical. Sometimes, the search for the best lower-bound solution can be done analytically or numerically, but in most cases, a trial and error method is applied.

Example 3.5

Given is the portal frame according to Fig. 3.8. The structure is 1st-order statically indeterminate. If the reaction force H in point B is introduced as the redundant, the

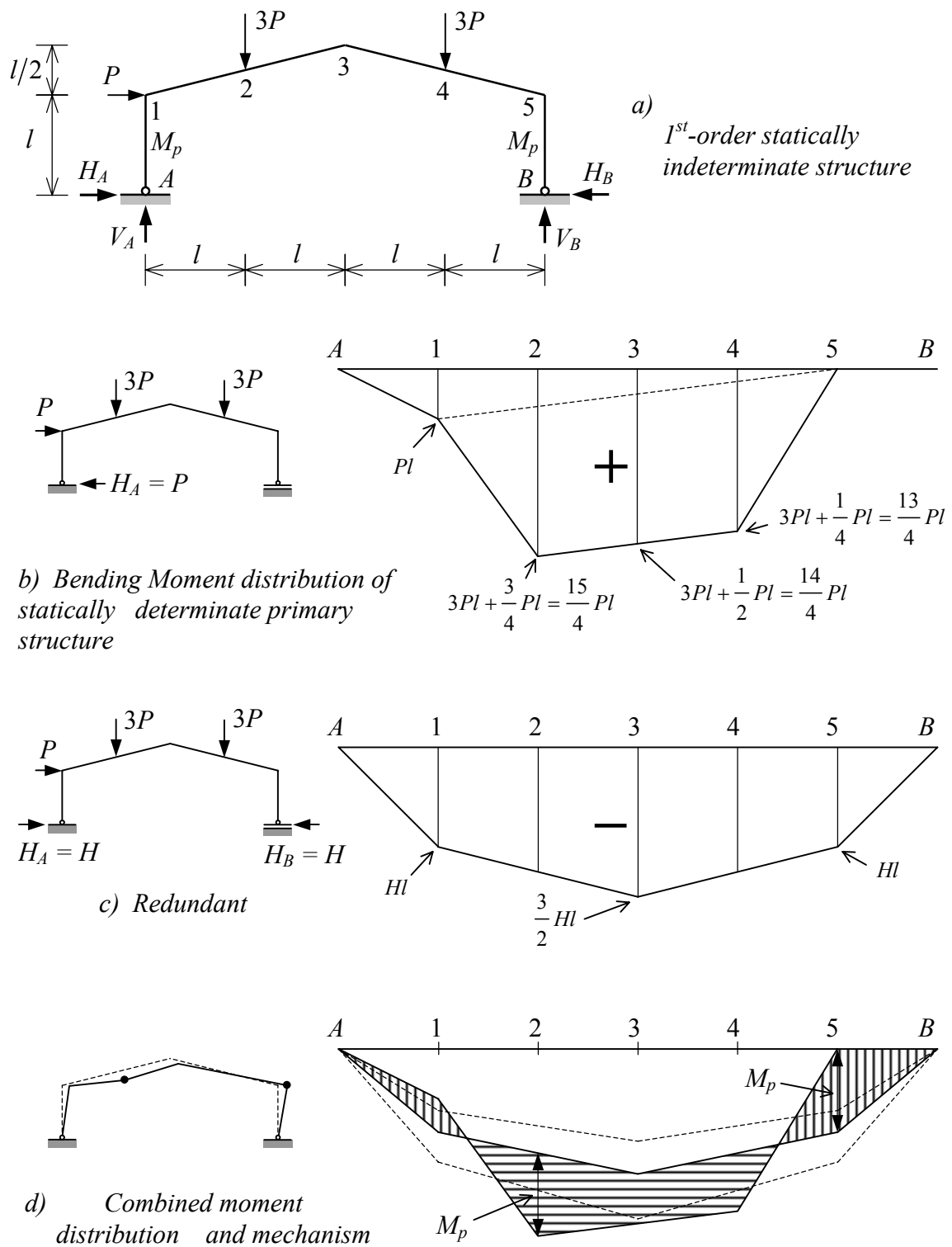


Fig. 3.8: Failure mechanism of a 1^{st} -order statically indeterminate portal frame.

structure becomes statically determinate. The moment line is calculated for the statically determinate primary structure together with the moment line caused by the redundant. Then both lines are combined. For a handy chosen value of H the moment line of Fig. 3.8d can be obtained, of which in the points 2 and 5 the moment is equal to the full-plastic

moment M_p . In the other points, the moment is lower. The limit load P_p and H can be determined from:

$$\left. \begin{aligned} M_2 &= \frac{15}{4} * P_p * l - \frac{5}{4} * H * l = M_p \\ M_2 &= 0 * P_p * l - 1 * H * l = M_p \end{aligned} \right\} \rightarrow \begin{cases} H = \frac{M_p}{l} \\ P_p = \frac{3}{5} \frac{M_p}{l} \end{cases}$$

3.3.2 Uniformly distributed load

Again, consider the problem of Fig. 3.7. For the lower-bound calculation the moment distribution is used as drawn in Fig. 3.9. Suppose the reaction at the simple support is equal to Q , then $M(x)$ is given by:

$$M(x) = Qx - \frac{1}{2}qx^2$$

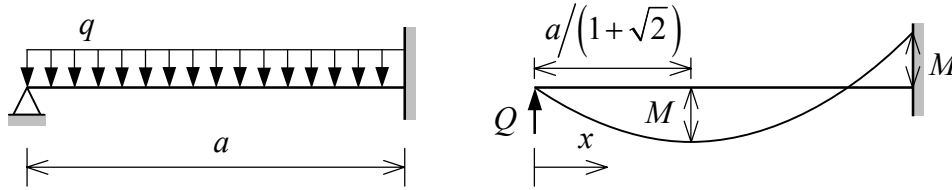


Fig. 3.9: Beam with distributed load and moment curve for lower-bound calculation.

At the fixed end ($x = a$) a moment can be supported equal to $M = -M_p$ and the value of Q follows then from:

$$-M_p = Qa - \frac{1}{2}qa^2 \rightarrow Q = -\frac{M_p}{a} + \frac{1}{2}qa \quad (a)$$

The field moment is maximal for:

$$Q = qx$$

The value of this maximum is set equal to $+M_p$. Combination with the first relation yields:

$$M_p = \frac{Q^2}{q} - \frac{1}{2} \frac{Q^2}{q} = \frac{1}{2} \frac{Q^2}{q} \quad (b)$$

The results (a) and (b) together provide:

$$Q^2 = 2qM_p = \left(-\frac{M_p}{a} + \frac{1}{2}qa \right)^2 \rightarrow M_p^2 - 3M_pqa^2 + \frac{1}{4}(qa^2)^2 = 0$$

The lower-bound solution finally becomes:

$$\frac{qa^2}{M_p} = 11.66$$

So, the best lower-bound solution coincides exactly with the best upper-bound solution, which was previously found.

3.3.3 Proof of the lower-bound theorem

Provided is a structure of prismatic straight members, having full-plastic moments M_{pk} and loaded by point loads F_i .

Suppose that the real collapse mechanism is given by a displacement field u_i and rotations \mathcal{G}_k in the plastic hinges. Then the load factor λ_c corresponding with the failure load can be determined through:

$$\lambda_c \sum F_i u_i = \sum M_k \mathcal{G}_k \quad (3.13)$$

The M_k 's are equal to the full-plastic moments M_{pk} where the sign follows from the sign of the rotations \mathcal{G}_k .

Now, consider an arbitrary moment field M' , which is in equilibrium with a load λF and satisfies the yield conditions. Since all equilibrium equations are satisfied, the virtual work equation corresponding with the real collapse mechanism is satisfied too. So, it follows:

$$\lambda \sum F_i u_i = \sum M'_k \mathcal{G}_k \quad (3.14)$$

Since the work $\sum F_i u_i$ in both (3.13) and (3.14) is the same, it follows that:

$$\frac{\sum M_k \mathcal{G}_k}{\lambda_c} = \frac{\sum M'_k \mathcal{G}_k}{\lambda} \quad (3.15)$$

Because $\sum M_k \mathcal{G}_k \geq \sum M'_k \mathcal{G}_k$ (see below) it follows that $\lambda_c \geq \lambda$, which had to be proved.

That $\sum M_k \mathcal{G}_k \geq \sum M'_k \mathcal{G}_k$ can be shown quite easily. Firstly, assume that in hinge k of the real collapse mechanism $\mathcal{G}_k > 0$. In that case is $M_k = M_{pk} \geq M'_k$ and the inequality is valid. Conversely, if it is assumed that $\mathcal{G}_k < 0$ then $M_k = -M_{pk} \leq M'_k$ and the inequality holds again. And when it holds for one hinge it also holds for the sum over the hinges.

3.4 Combination of upper- and lower-bound theorems

The handiest way (for a manual calculation) to determine the limit load is obtained through a combination of the upper- and lower-bound theorems. The procedure then is as follows:

1. Choose a mechanism with a large chance to success;
2. Draw the corresponding moment line that satisfies equilibrium;
3. If nowhere the full-plastic moment is exceeded, the collapse mechanism is found;
4. Determine a valid lower-bound solution;

5. Determine a new mechanism with plastic hinges at the positions with the largest moments.

Example 3.6

The method is demonstrated by the problem of Fig. 3.10. It is assumed that the sway mechanism is the most likely one. This provides an ultimate load of:

$$F_u = \frac{6M_p}{a}$$

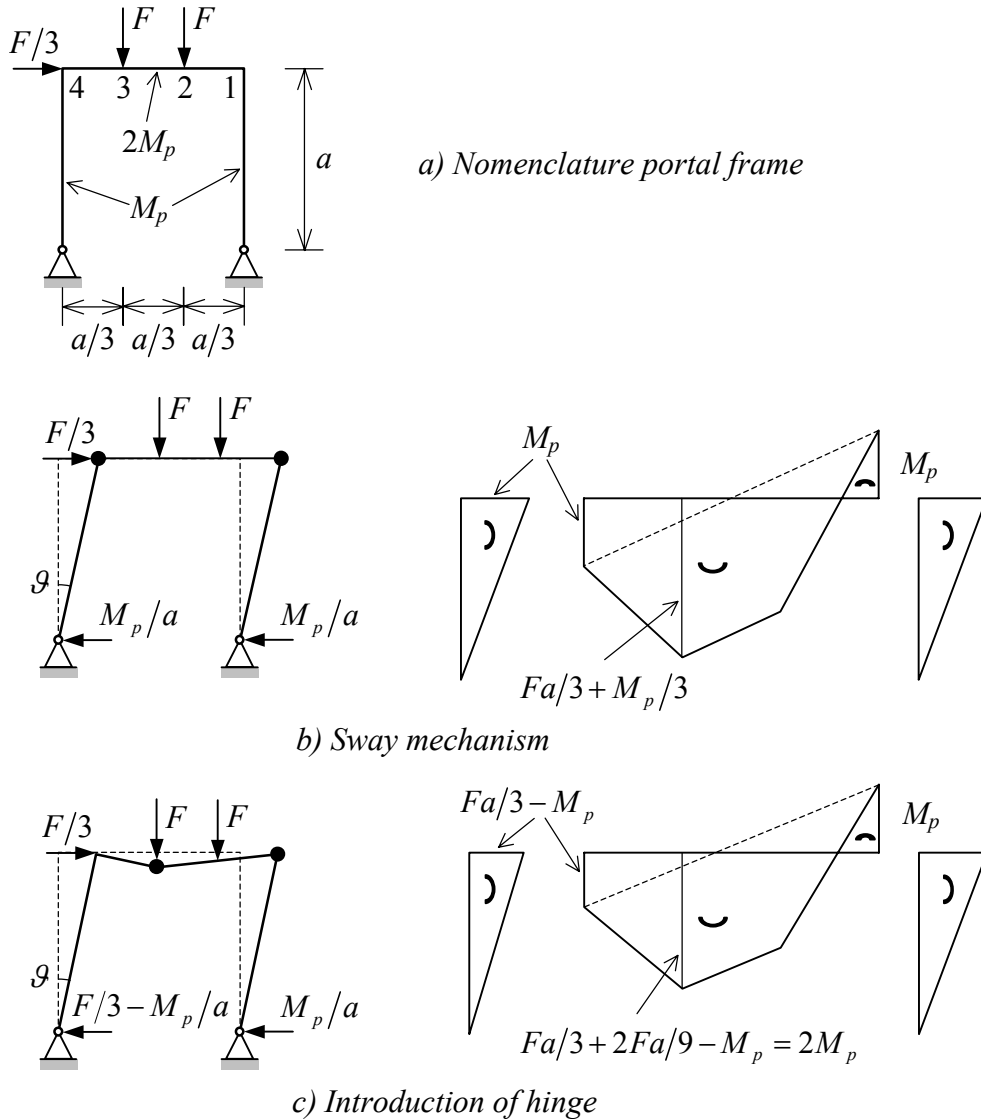


Fig. 3.10: Alternating use of upper- and lower-bound solutions.

Fig. 3.10b provides a sketch of the corresponding moment distribution. It appears that the moment in the middle of the beam becomes equal to: $2.33M_p$. So, a lower-bound estimation for the ultimate load is found equal to:

$$F_u = \frac{2}{2.33} \frac{6M_p}{a} = 5.14 \frac{M_p}{a}$$

It is clear that in the next attempt at position 3 a hinge has to be introduced in the mechanism. The problem now is to find out, which of the old hinges has to disappear. In this case the hinge at position 4 is the most obvious one (see Fig. 3.10c). This delivers a failure load of:

$$F_u = 5.4 \frac{M_p}{a}$$

The corresponding moment line can now easily be drawn. The full-plastic moment is not exceeded and the failure load has been found.

3.5 Some consequences of the lower- and upper-bound theorems

One of the outcomes of the lower- and upper-bound theorems is that a unique limit load will be found. One knows that the load factor determined through an elastic-plastic analysis is unique and does not depend on the way of how the analysis is carried out. After all, if a solution is found that satisfies equilibrium and at the same time causes a mechanism, then the hypothesis that still a higher limit load can be found contradicts the lower-bound theorem and vice versa. In next chapter more attention will be paid to this subject.

Another important observation is that the ultimate load does not appear to depend on the elastic material properties. If the mutual flexural stiffnesses are changed but the full-plastic moments are kept the same, the same value for the load factor at collapse will be found. But note that then sometimes another mechanism is found, or another moment distribution at failure.

Finally, there is the aspect of additional external loads, such as temperature, settlement, erection stresses, etc.. In elastic models they can cause large stresses in statically indeterminate structures. However, for the ultimate load they are not important: they simply are not capable of performing work during failure. The key is that these loads do not cause stresses in statically determinate structures or in a statically determinate parts of structures. And just before a mechanism is formed the structure (or for a partial mechanism a part of the structure) becomes statically determinate.

4 Rotation capacity

4.1 Introduction

For the analysis of the elastic-plastic behaviour of a structure in the previous chapters it was assumed that an unlimited redistribution of moments could take place. It even appeared that for the determination of the elementary ultimate load, no relations for the description of the deformation were necessary. The ultimate load just followed from the equilibrium of the statically determined system during collapse.

For this really to happen, the full-plastic moment M_p should be preserved during the rotations, which are necessary to create the rest of the plastic hinges. This property is called “rotation capacity”. For a more detailed discussion, it is referred back to the example of the uniformly loaded beam that is restrained at both ends of Fig. 2.13. Starting from a stress-free undeformed structure, firstly at the ends the full-plastic moments are reached during loading. In order to make the creation of a plastic hinge in the middle of the beam possible, the hinges at the ends are subjected to a certain amount of rotation. In chapter 2 it already was mentioned that this rotation cannot take place in a single cross-section. This would require infinite strains and no material can provide these. Each material has a finite breaking strain, therefore a finite length is required for the plastic deformation to take place.

4.2 Restrained steel beams

For the case of the restrained beam, the situation is further detailed in Fig. 4.1. For the provision of the required rotation, in the first place it is important that the M - κ diagram is not purely bilinear, but already starts curving as soon as the moment surpasses M_e . Further, it is important that the real material is not ideal-plastic, but demonstrates strain hardening (see Fig. 4.2). Then a situation develops as indicated in Fig. 4.1: in one part of the beam the moment is a bit higher than M_p . In Fig. 4.1 the curvature distribution is sketched too. Indeed, the required rotation $\Delta\vartheta$ can be considered to be built up out of finite curvatures over a finite but small length. Fracture occurs if the fixed-end moment exceeds the ultimate moment M_u . This information is used as a criterion for the deformation capacity of the material. This will be worked out below.

The moment at the restrained end can be written as:

$$M_{\text{fixed end}} = M_p + Qa \quad (4.1)$$

where Q is the transverse force and a the distance from the fixed end to the cross-section with $M = M_p$. The distance “ a ” can be considered as the “length” of the plastic hinge. The influence of the path between M_e and M_p is neglected. Supposing the rupture moment is equal to 1.15 times the full-plastic moment then:

$$M_u = 1.15M_p \quad (4.2)$$

In the plastic failure phase, the transverse force Q equals $Q = 8M_p/l$. Therefore, the rotation capacity is reached if:

$$0.15M_p = Qa = 8 \frac{M_p a}{l} \quad (4.3)$$

The distance a then follows as:

$$a = 0.02l \quad (4.4)$$

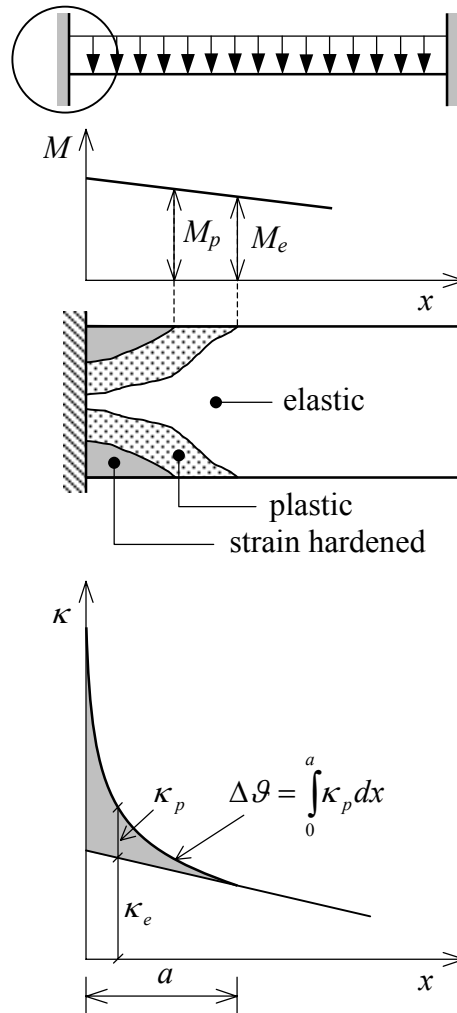


Fig. 4.1: Stresses and deformations in a plastic hinge.

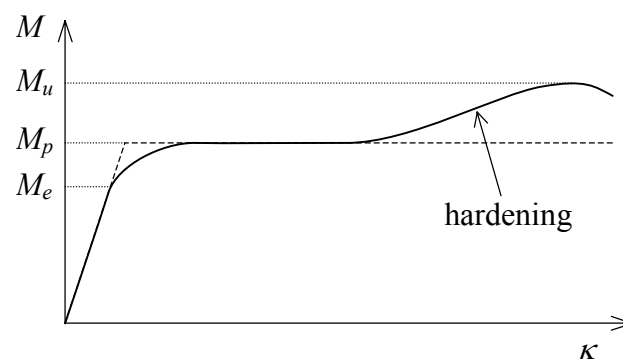


Fig. 4.2: Moment-curvature diagram.

The rotation that can occur over this distance is estimated to be (see Fig. 4.1):

$$\Delta \vartheta = \frac{1}{3} a \kappa_u = \frac{\kappa_u l}{150} \quad (4.5)$$

In chapter 2 for the restrained beam a required rotation capacity was found to be:

$$\Delta \vartheta = M_p l / 6EI = \kappa_e l / 6 \quad (4.6)$$

The requirement for sufficient rotation capacity can now be written as:

$$\frac{\kappa_u l}{150} > \frac{\kappa_e l}{6} \rightarrow \frac{\kappa_u}{\kappa_e} > 25 \quad (4.7)$$

This condition then also holds for the strains:

$$\frac{\varepsilon_u}{\varepsilon_e} > 25 \quad (4.8)$$

So, for $\varepsilon_e = 0.001$ the required deformation capacity is found to be $\varepsilon_u > 0.025$. For most types of steel this condition is satisfied. However, for some high-strength steels or at very low temperatures this condition might be a problem.

As demonstrated by above derivation, it appears that the length a of the plastic hinge is small compared to the span of the beam. On a macro scale, the assumption of a pin hinge conveniently can be made.

In the above analysis, the required rotation capacity was determined by application of the external load on the undeformed stress-free structure. In reality numerous other factors can exist, which may influence the rotation capacity. In chapter 3 it was already mentioned that factors like temperature, pre-stressing, assembly faults, settlements and the like do not affect the failure load. Also, the flexural stiffness ratios in the structure and the sequence in the application of the loads have no influence within certain limits. However, these phenomena do have an impact on the magnitude of the deformations in the failure phase. This effect can be both positive and negative. In most cases, it must be assumed that all these factors put extra requirements on the rotation capacity.

Above calculation of the rotation capacity was based on a geometrically linear consideration. Non-linear phenomena such as buckling, wrinkling, and twisting can have a negative impact on the rotation capacity of a member or a joint. In order to deliver sufficient rotation capacity, for steel structures conditions are given on the thickness-width

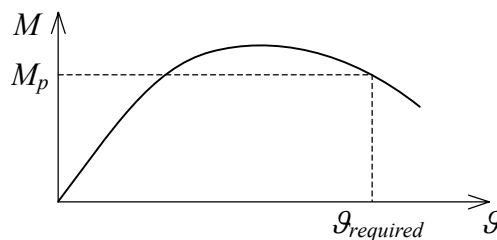


Fig. 4.3: Reduced full plastic moment.

ratio of flanges. Introduction of reduced full-plastic moments is also one of the remedies (see Fig. 4.3).

Finally, it can be remarked that a plastic hinge in the middle of a member can develop a longer length. Therefore, the problem of insufficient rotation capacity, because of reaching the breaking point of the material, is less pronounced.

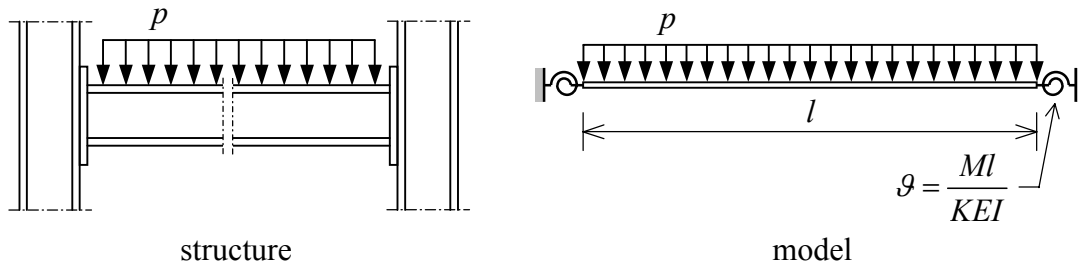


Fig. 4.4: Beam with end-plate connection.

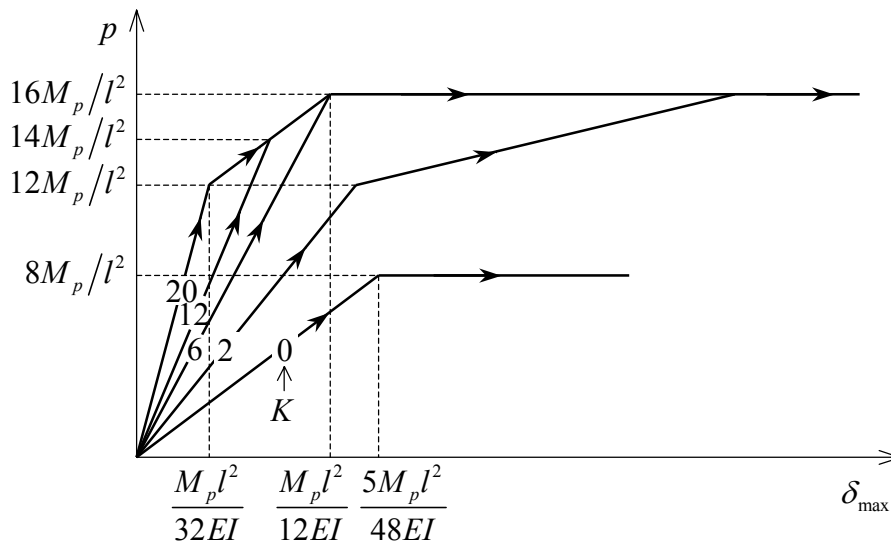


Fig. 4.5: Load-deflection diagrams.

The rotation capacity is also important for the assessment of joints. Therefore, the same restrained beam is considered, however with elastic restraints (see Fig. 4.4), the spring constant of which equals KEI/l . In Fig. 4.5, the load-deformation diagram of this structure is given for different values of the spring constant. From the figure it can be concluded that:

- For $K > 6$ the first plastic hinges appear at the restrained ends. The required rotations for the formation of a plastic hinge in the middle are partly delivered by the elastic rotation in the joints and partly by the plastic rotation in the plastic hinges at the restrained ends. Depending on the magnitude of the plastic moment, the plastic rotation is delivered by the joint itself or by the member next to the joint.
- For $K = 6$ the plastic hinges at the restrained ends and in the middle of the member appear simultaneously. So, no redistribution of moments has to take place and actually no conditions for the rotation capacity are present.

- For $K < 6$ the first plastic hinge appears in the middle of the beam. Now, conditions are imposed on the rotation capacity of the beam itself. If the spring is very weak this situation may lead to unrealistic large deformations (see section 4.4).

4.3 Experiments by Stüssi and Kollbrunner

Stüssi and Kollbrunner performed in 1935 a number of tests on beams, which have become classical. The beams were simply supported at four positions and were loaded by a point load in the middle of the centre field (see Fig. 4.6). The degree of restraint of the centre field is determined by the factor k , which is the ratio of the lengths of the end fields and the centre field.

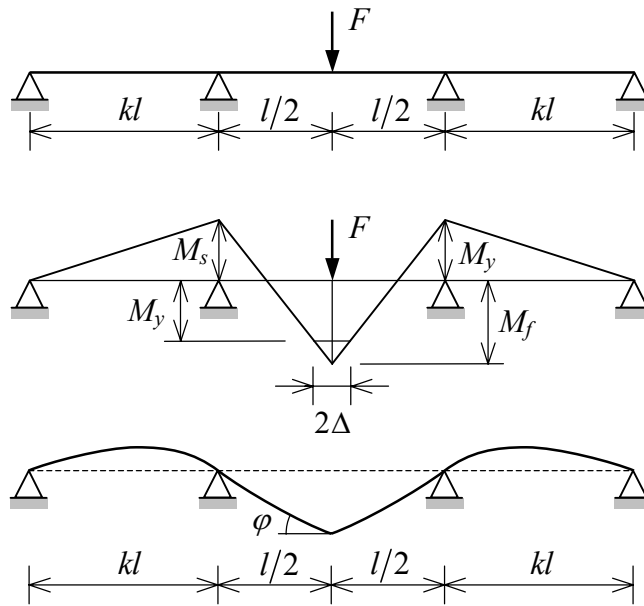


Fig. 4.6: Stüssi-Kollbrunner beam.

In Fig. 4.7 the computational results for different values of k are displayed. The result is comparable with that of Fig. 4.5. The deflection at the moment of collapse u_p increases with increasing length of the end field. For values of k larger than 3 the slope of the diagram $P > P_e$ becomes so small, that only for very large deflection the ultimate load is reached. For $k = \infty$ the ultimate load actually cannot be reached. In that case the theoretical

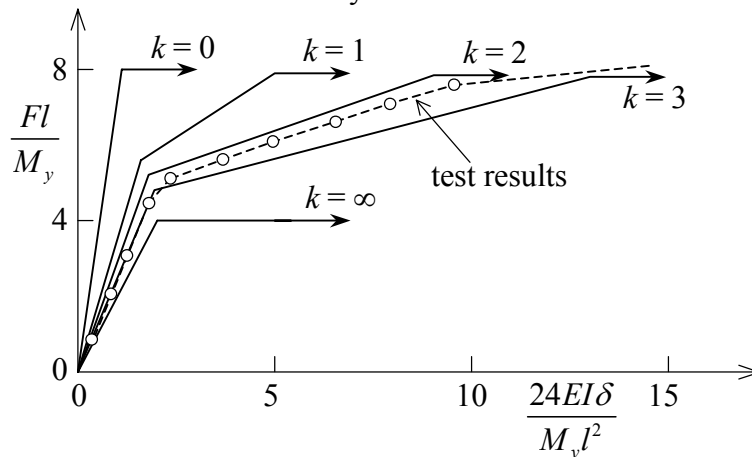


Fig. 4.7: Load-deflection relations for beam of Fig. 4.6 (from [Nea 77]).

collapse load has no practical meaning anymore. In addition, in the firstly created plastic hinge a very high rotation takes place, which may lead to premature failure by wrinkling, twisting or brittle fracture.

The experimental result for $k = 2$ is indicated by a dashed line in the figure too. It can be concluded that the theory is confirmed by the tests and that the theoretical elementary ultimate load is reached.

4.4 Reinforced concrete

For reinforced concrete, the assessment of the available plastic rotation capacity is even more complex than for steel. To start with, the more irregular moment curvature relation applies as indicated in Fig. 2.12. The redistribution of internal forces starts already after the formation of the first small cracks. Then there is a second stage of redistribution after yielding of the reinforcement due to the change in position of the neutral line and due to slip of the reinforcement. This indicates that many geometrical and mechanical parameters are involved. In the Thesis by A. Bigaj “Structural dependence of rotation capacity of plastic hinges in reinforced beams and slabs, Delft 1999” detailed information can be found. The remaining part in this chapter has also been retrieved from that thesis.

Fig. 4.8 gives a simplified estimate by showing the available rotation capacity for a simply supported beam with slenderness $a/h = 12$ as a function of the material reinforcement ratio $c = \omega \sigma_y / f'_c$ (see chapter 2). For values of c greater than 0.15 the figure gives a general linear representation as most other factors are of limited importance. For lower values, however, many other influences play a role. The top value (usually reached for $c = 0.05$) may vary from $\Delta\vartheta = 0.01$ to $\Delta\vartheta = 0.06$. The most important parameter in this region is the reinforcement parameter p given by:

$$p = (\varepsilon_u + 2\varepsilon_{sh})^{0.75} (f_t/f_y - 1)^{0.8} \quad (4.9)$$

where:

- ε_u = rupture strain of the steel
- ε_{sh} = strain at the onset of hardening
- f_t = rupture strength of the steel
- f_y = yield strength of the steel

In the case of cold worked steel the term ε_{sh} is not present. For low reinforcement ratios, the following relation holds:

$$\Delta\vartheta_{12} = 0.7p \quad (4.10)$$

where the subscript 12 indicates the beam slenderness a/h . For slenderness values of a/h different from 12 the following correction needs to be applied:

$$\Delta\vartheta_{a/h} = [(a/h)/12]^{0.85} \Delta\vartheta_{12} \quad (4.11)$$

As an example, a two sided clamped beam with uniformly distributed load is considered (see Fig. 4.9), having a span $L = 6000$ mm, cross sectional dimensions $h = 300$ mm and $b =$

150 mm, a geometrical reinforcement ratio of $\omega = 0.8\%$, and material properties $E_b = 30,000 \text{ N/mm}^2$ and $f_y = 300 \text{ N/mm}^2$. In that case it approximately holds:

$$M_p = 0.9\omega b h^2 f_y = 33 \text{ kNm}$$

$$EI = \frac{1}{12} E b h^3 = 10,000 \text{ kNm}^2$$

This means that the required rotation capacity at the clamped cross-sections can be found as (see chapters 2 and 4.1):

$$\Delta\vartheta = \frac{M_p L}{6EI} = 0.0032 \text{ rad}$$

The value of the material reinforcement ratio c in this case is about 0.1 (assuming $f'_c = 30 \text{ MPa}$). Fig. 4.8 indicates an available rotational capacity of about 0.013. This value,

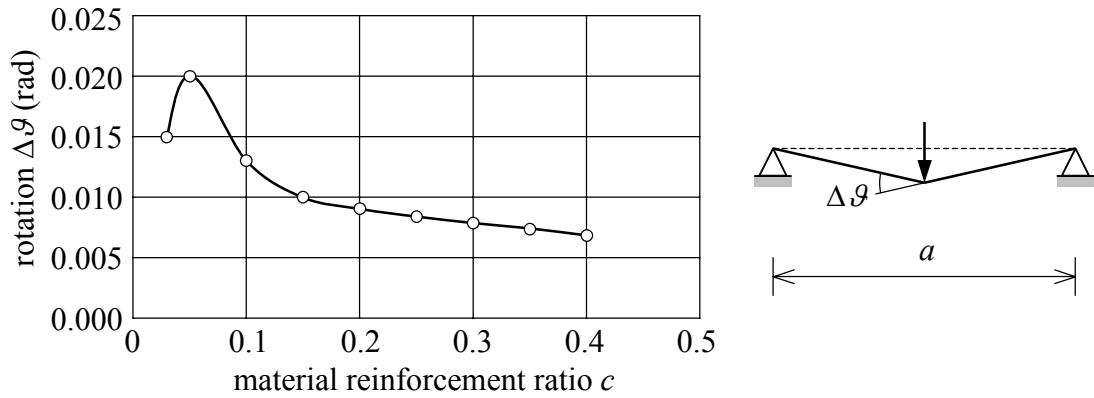


Fig. 4.8: Rotation capacity as a function of the material reinforcement ratio (for ductile steel and $a/h = 12$).

however, should be corrected for the slenderness and divided by 2 as we have only one side now (clamped in situation). The value of a in this case equals two times the distance from the clamped in section to the point of zero bending moment (see figure 4.9):

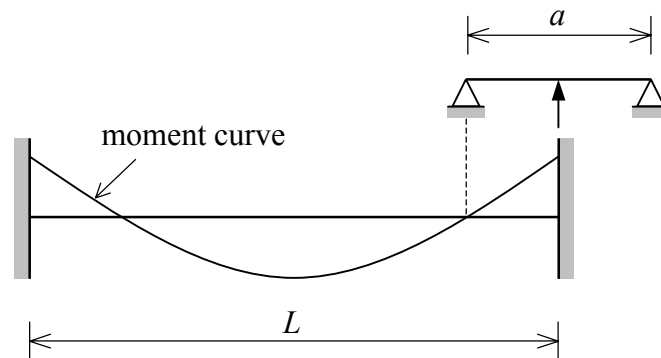


Fig. 4.9: Determination of "a" for the example of a two-sided clamped in beam.

$$a = 2 \frac{L}{8} = \frac{L}{4} = 1500 \text{ mm}$$

This leads to $a/h = 1500/300 = 5$ and so:

$$\Delta \vartheta = (5/12)^{0.85} * 0.013/2 = 0.0031 \text{ rad}$$

This is practically sufficient to deal with the condition.

5 The yield contour

5.1 Plane truss

Fig. 5.1 shows a pin-jointed plane truss, consisting out of two bars. It is loaded by a horizontal force F_x and a vertical force F_y . Both bars can sustain a yield force N_p in

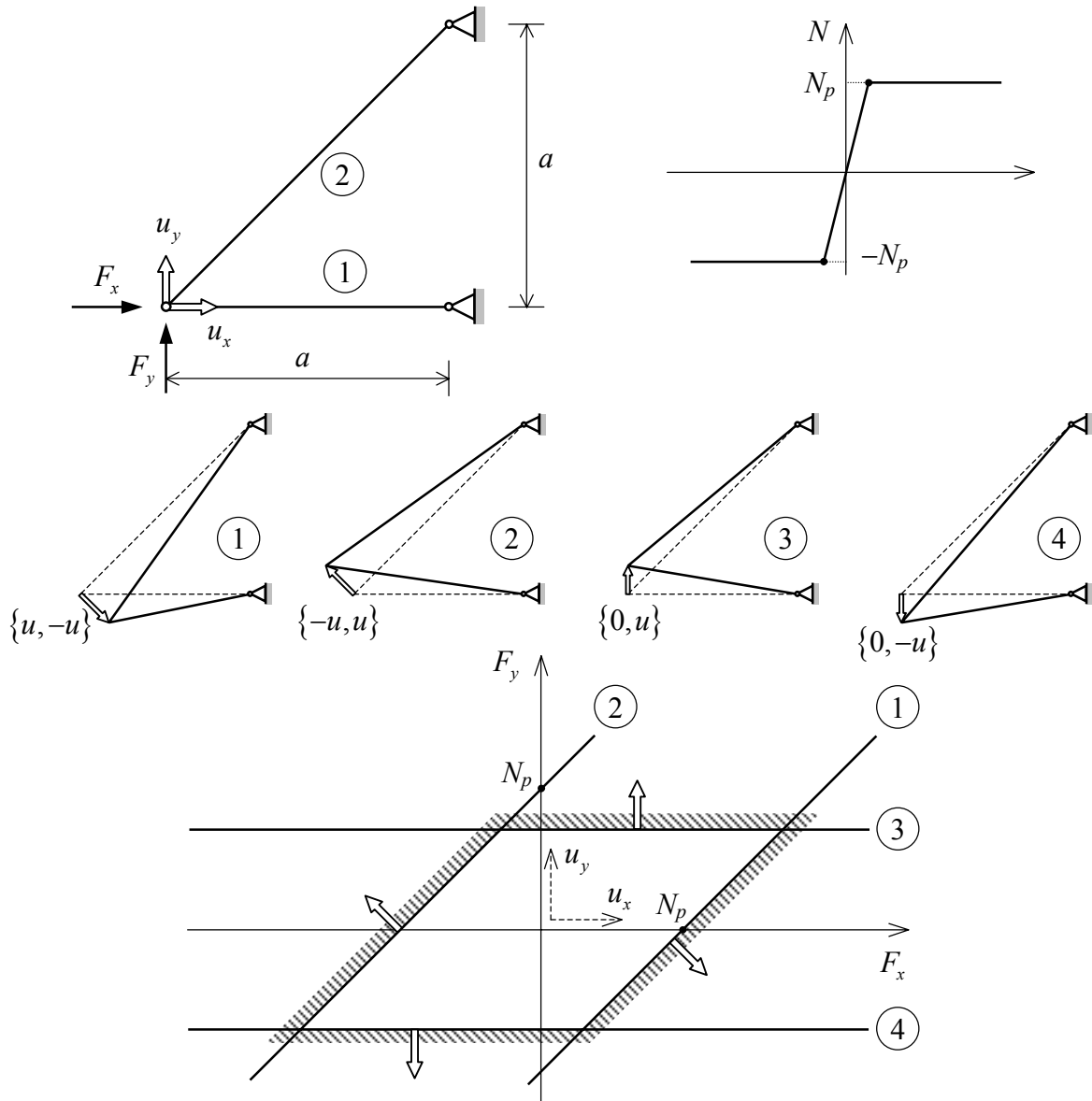


Fig. 5.1: Mechanism and yield contour for a truss with two bars.

compression as well as in extension. The structure is statically determined, which means that a mechanism is created as soon as one of the bars starts yielding. Four mechanisms can be distinguished:

- Mechanism 1: bar 1 yields in compression
- Mechanism 2: bar 1 yields in extension
- Mechanism 3: bar 2 yields in compression
- Mechanism 4: bar 2 yields in extension

The work equation for these mechanisms reads:

$$F_x u_x + F_y u_y = N_p |\Delta l_i| \quad ; \quad i = 1, 2 \quad (5.1)$$

In the table below, the relations are given between u_x , u_y , Δl with respect to a reference displacement u .

	u_x	u_y	$ \Delta l_1 $	$ \Delta l_2 $
Mechanism 1	u	$-u$	u	$-$
Mechanism 2	$-u$	u	u	$-$
Mechanism 3	0	u	$-$	$u/\sqrt{2}$
Mechanism 4	0	$-u$	$-$	$u/\sqrt{2}$

Substitution into (5.1) leads successively to the following equations:

$$\begin{aligned}
 \text{Mechanism 1: } & F_x - F_y = N_p \\
 \text{Mechanism 2: } & -F_x + F_y = N_p \\
 \text{Mechanism 3: } & F_y = N_p / \sqrt{2} \\
 \text{Mechanism 4: } & -F_y = N_p / \sqrt{2}
 \end{aligned} \quad (5.2)$$

If F_x can be written as a function of F_y or vice versa, then from (5.2) the decisive collapse mechanism can be found, including the corresponding failure load. On the other hand, if the ratio between F_x and F_y is kept free, it is possible to find out which combinations of F_x and F_y can be carried and which combinations lead to overstepping of the load carrying capacity. The best way to execute such an analysis is by setting up a F_x - F_y diagram, as indicated in Fig. 5.1c. Each of the four mechanisms is represented by a straight line. These four lines enclose an area given by:

$$\begin{aligned}
 F_x - F_y &\leq N_p \\
 -F_x + F_y &\leq N_p \\
 F_y &\leq N_p / \sqrt{2} \\
 -F_y &\leq N_p / \sqrt{2}
 \end{aligned} \quad (5.3)$$

Combinations of F_x and F_y that satisfy these inequalities are called safe or permissible combinations. Load combinations situated outside the indicated area cannot be carried by the structure. This is the unsafe area.

The line enclosing the safe area is called the *yield contour*. The yield contour is an important concept in the theory of plasticity, which is not only applied to frames and trusses, but also to cross-sections loaded by moments and normal forces, and also to two- and three-dimensional stress states in general. In all cases, the yield contour turns out to have a number of interesting properties. The first property is that a yield contour always encloses a *convex* area. This is not very surprising because the safe area can be described by a number of linear inequalities.

The second property concerns the (plastic) displacements. On the yield contour of fig. 5.1c for each mechanism, the displacement vector u is drawn of the loaded node. It can be established that for each mechanism this displacement vector is perpendicular to the yield contour. This phenomenon is called *normality* and is connected to the growth of the plastic deformations. Later in this chapter, more attention will be paid to this topic.

5.2 Yield contour of a portal frame

The portal frame of Fig. 5.2a is considered. The ratio between the forces F_1 and F_2 is left free, just as in the framework in section 5.1.

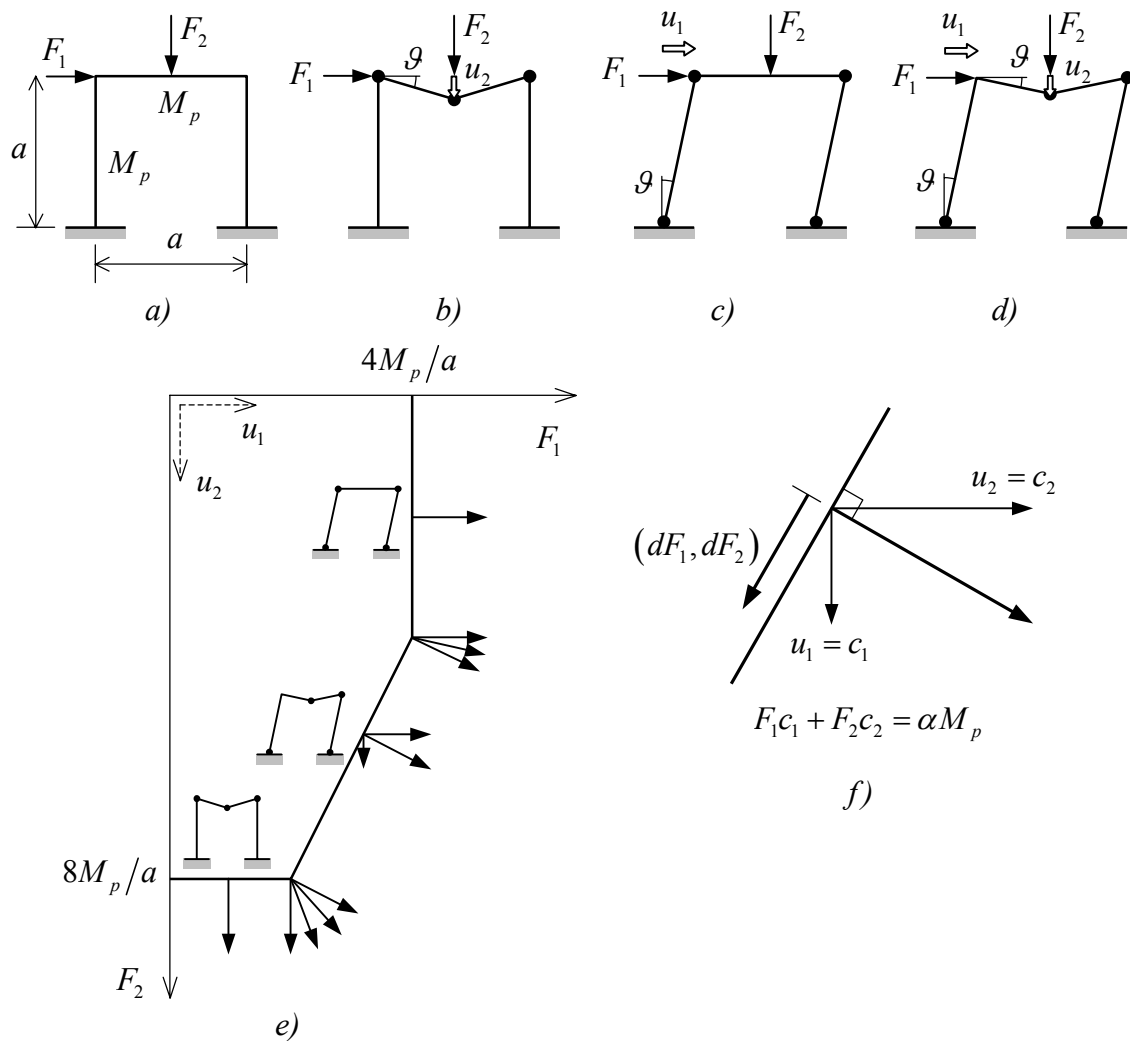


Fig. 5.2: Yield contour for a simple portal frame..

The equations for the three mechanisms are:

- a) Beam mechanism (Fig. 5.2b) : $F_2 u_2 = 4M_p \vartheta$ with $u_2 = a\vartheta/2$
 b) Sway mechanism (Fig. 5.2c) : $F_1 u_1 = 4M_p \vartheta$ with $u_1 = a\vartheta$
 c) Combined mechanism (Fig. 5.2d): $F_1 u_1 + F_2 u_2 = 6M_p \vartheta$ with $u_1 = a\vartheta$; $u_2 = a\vartheta/2$

Note that only positive values of F_1 and F_2 are considered.

The three found mechanisms can be depicted in a F_1 - F_2 diagram (Fig. 5.2e). A contour is created inside which the permissible combinations of F_1 and F_2 are situated. Load combinations lying outside the contour cannot be carried.

The total contour is built up out of three branches: the horizontal one generated by the beam mechanism, the vertical one of the sway mechanism and the slanting one of the combined mechanism. So, ratios between F_1 and F_2 can be identified for which one of the mechanisms is decisive. However, other ratios can be chosen, which make other mechanisms decisive. It is also possible that a mechanism lies completely outside the yield contour and never is decisive.

Again it can be observed that the yield contour is convex and that the normality condition is satisfied:

- For the beam mechanism the displacement $(u_1, u_2) = (0, a\vartheta/2)$ is perpendicular to the horizontal axis.
- For the sway mechanism the displacement $(u_1, u_2) = (a\vartheta, 0)$ is perpendicular to the vertical axis.
- For the combined mechanism the displacement $(u_1, u_2) = (a\vartheta, a\vartheta/2)$ is perpendicular to $F_1a + F_2a/2 = 6M_p$.

Interesting points of the yield contour are the corner points, where two mechanism lines intersect. In such an intersection point the mechanism is over-complete. Movements are possible according to the one or the other mechanism, and also for an arbitrary combination of both mechanisms with positive coefficients. That is why a whole fan of displacements is drawn in the corner points of Fig. 5.2e.

The proof for this normality condition can be delivered rather easy. The energy dissipation equation for a structural mechanism reads:

$$F_1u_1 + F_2u_2 = \alpha M_p \vartheta$$

where α is a factor depending on the mechanism. Further, for each specific mechanism the relations $u_1 = c_1\vartheta$ and $u_2 = c_2\vartheta$ can be given, which leads to:

$$F_1c_1 + F_2c_2 = \alpha M_p \quad (5.4)$$

The directional vector of this line is $\{dF_1, dF_2\}$, for which it holds:

$$dF_1c_1 + dF_2c_2 = 0 \quad (5.5)$$

It can be concluded that the dot product of the vectors $\{dF_1, dF_2\}$ and $\{c_1, c_2\}$ is equal to zero, from which it follows that these vectors are perpendicular. Therefore, also the vector $\{u_1, u_2\} = \vartheta\{c_1, c_2\}$ is perpendicular to the failure line, which completes the proof.

Another way of looking at the problem is as follows. Relation (5.4) can be rewritten as:

$$\psi = F_1u_1 + F_2u_2 - \alpha M_p \vartheta = 0 \quad (5.6)$$

The quantity ψ is called the *plastic potential*. The gradient vector $\nabla\psi$ is given by:

$$\nabla \psi = \begin{Bmatrix} \partial \psi / \partial F_1 \\ \partial \psi / \partial F_2 \end{Bmatrix} = \begin{Bmatrix} u_1 \\ u_2 \end{Bmatrix} \quad (5.7)$$

Since the yield figure $\psi = 0$ is a contour line and because the gradient is perpendicular to contour lines, the normality condition is conveniently proved.

Relation (5.7) is often used in the reversed way, where starting from the plastic potential the displacements are determined.

The plastic potential is not uniquely defined, since all terms can be multiplied with a certain factor. This means that only the direction of the displacement vector can be obtained. In order to find the magnitude of the displacements an undetermined (or through other circumstances a determined) positive scale factor λ is introduced, i.e.:

$$\begin{Bmatrix} u_1 \\ u_2 \end{Bmatrix} = \lambda \begin{Bmatrix} \partial \psi / \partial F_1 \\ \partial \psi / \partial F_2 \end{Bmatrix} \quad (5.8)$$

Above relation (5.8) is the usual formulation of the normality principle.

Finally the following: suppose the structure is loaded by $F_1 = F_2 = F = 4M_p/a$. Normally, it is assumed that this situation is reached by a slowly and proportional increase of F_1 and F_2 until failure occurs. Proportional in this case means that $\Delta F_1 = \Delta F_2$. However, it is also possible to follow another load path and firstly apply $F_1 = 4M_p/a$ followed by $F_2 = 4M_p/a$. The yield contour in Fig. 5.3 shows that this is possible, since all combinations of F_1 and F_2 are situated inside the yield contour. Therefore, failure occurs at the same load as for the

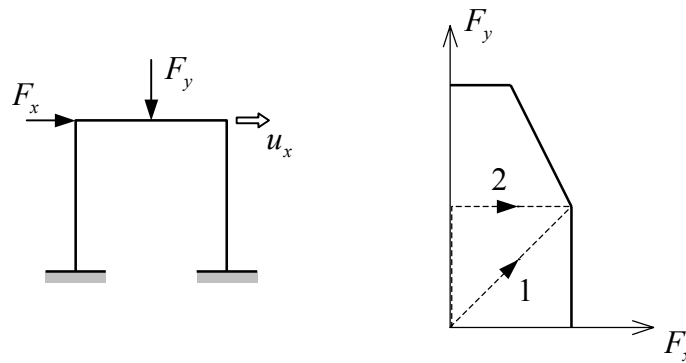


Fig. 5.3: Load path has no influence on failure load and type of mechanism.

proportional load case. The failure load appears to be independent from the followed load path, which is known as the proposition of the *invariant failure load*. Important of course is that the whole path is inside the yield contour, if not so, premature failure will occur (see Fig. 5.4).

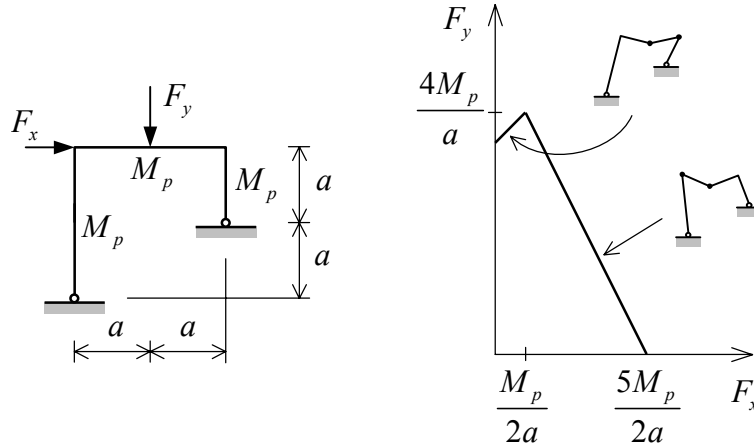


Fig. 5.4: The point $(F_x, F_y) = (0.5M_p/a, 4M_p/a)$ cannot be reached by application of firstly a vertical load and secondly a horizontal load.

5.3 Normality

In the previous text it is established twice that the yield contour is convex and that the plastic displacement increments have directions, which are coinciding with the outward-pointing normal on the yield surface. These two properties will be investigated in this and next sections. Consider an arbitrary framework or truss including point loads F_j . In a number of cross-sections i plastic hinges may develop, the full-plastic moments of which are M_{pi} . For an arbitrary mechanism it then can be written:

$$\sum F_j u_j = \sum M_{pi} |\mathcal{G}_i| \quad (5.9)$$

where u_j are the displacements of the points of action of F_j in the direction of the forces and \mathcal{G}_i are the rotations corresponding with M_{pi} . For convenience's sake, it is assumed that the full-plastic moments are the same for both positive and negative curvature. The computation for asymmetrical sections is not essentially different, but requires more paper work. The summations in (5.9) have to be done over all loads and all (potential) plastic cross-sections. For a fixed mechanism, the right-hand side is completely determined except for the factor \mathcal{G} , which is a proportionality factor for the displacements.

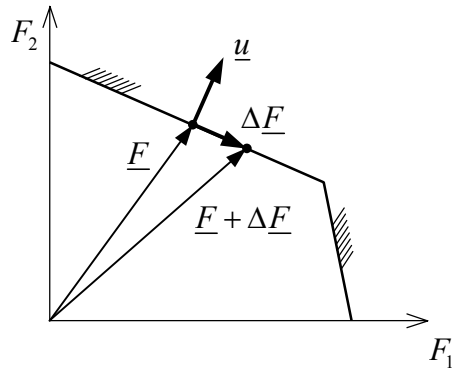
Now, consider a neighbouring load case $F_j + \Delta F_j$. It is assumed that the mechanism remains the same one and that this load case causes failure too (Fig. 5.5a). It then holds:

$$\sum (F_j + \Delta F_j) u_j = \sum M_{pi} |\mathcal{G}_i| \quad (5.10)$$

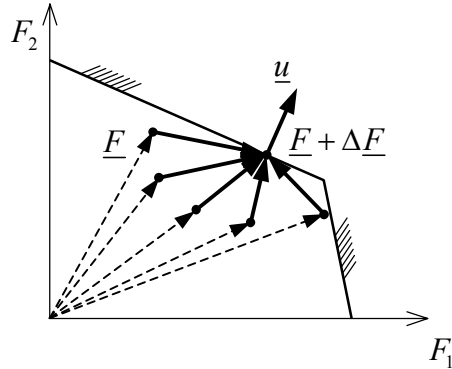
From (5.9) and (5.10) it then follows:

$$\sum \Delta F_j u_j = 0 \quad (5.11)$$

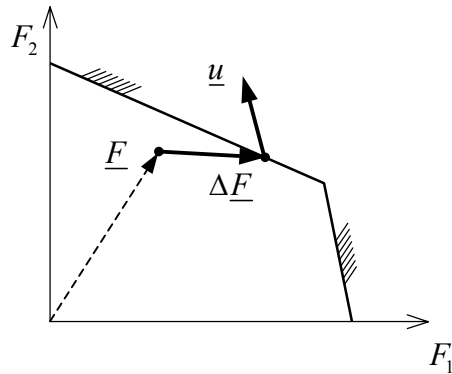
The geometric interpretation of this is that $\Delta \underline{F}$ and \underline{u} , both considered and plotted out as vectors, are perpendicular to each other (normality)(see Fig. 5.5a). For the physical interpretation, the idea is abandoned that F_j represents a failure state with respect to the



a) State of failure \underline{F} and neighbouring state of failure $\underline{F} + \underline{\Delta F}$, belonging to the same mechanism



b) The state of failure $\underline{F} + \underline{\Delta F}$ is reached by several load paths; \underline{F} is an arbitrary safe load and $\underline{\Delta F}$ is the last load increment leading to failure



c) If the plastic displacement vector is not perpendicular to the yield contour, it is always possible to choose \underline{F} and $\underline{\Delta F}$ in such a manner that negative work is done

Fig. 5.5: State of failure and normality.

considered mechanism. If it is assumed that F_j represents an arbitrary safe load combination (Fig. 5.5b), relation (5.9) is changed to:

$$\sum F_j u_j \leq \sum M_{pi} |\mathcal{Q}_i| \quad (5.12)$$

Combination with (5.10) in this case leads to:

$$\sum \Delta F_j u_j \geq 0 \quad (5.13)$$

The load increment ΔF_j can be considered as the last load step until failure occurs. Firstly, the safe state F_j is reached and then the last increment is imposed until failure occurs. Inequality (5.13) displays that irrespective from which side ΔF_j approaches the state of failure, it always will perform positive work. In other words, to bring a structure into a state of failure always costs energy and no energy is generated. For this to happen it is required, that u_j is perpendicular to the yield surface (apart from the corner points of the surface).

If the outcome should have been different, very strange things would happen. Suppose that the portal frame of Fig. 5.2 is almost collapsing. For complete collapse, only a small increment ΔF_1 to the right is required. It would be very strange if, after the application of the increment, the frame would move to the left instead of to the right. This is exactly the logic, which is brought to expression by the normality principle.

At first sight, normality seems to be a property that generally can be found in structures and materials. Indeed, normality can be confirmed for frames as discussed above. The key issue in this is that all considered situations can be reduced to 1-dimensional stress states. As soon as 2- or 3-dimensional stress states are involved, normality cannot be derived any more, but has to be introduced as an assumption (Postulate of Drucker). Given the above outcome this seems very plausible, which however is not the case. Normality turns out to be a material property and one just has to wait and see if the condition is satisfied. Steel does satisfy the normality condition very well, but sand for example not at all. This is because the plastic behaviour of sand is based on a frictional mechanism.

5.4 Plastic potential, convexity

According to (5.9) the mechanism equation for an arbitrary mechanism can be written as:

$$\sum F_j u_j = \sum M_{pi} |\mathcal{G}_i| \quad (5.9)$$

It is assumed that all displacements depend on one single scale parameter \mathcal{G} , because $u_j = c_j \mathcal{G}$ and $|\mathcal{G}_i| = a_i \mathcal{G}$. If further all moments M_{pi} are equal to $b_i M_p$ the mechanism equation can be rewritten as:

$$\sum \alpha_j F_j = M_p \quad (5.14)$$

Analogously to (5.6) a plastic potential is defined:

$$\psi = \sum \alpha_j F_j - M_p \quad (5.15)$$

If the loads F_j are such that $\psi < 0$, then no failure occurs for this mechanism; for $\psi \geq 0$ it does. The outward-pointing normal on the yield contour is given by $(\partial \psi / \partial F_j)$. The normality condition is then given by (also see (5.8)):

$$u_j = \lambda \left(\frac{\partial \psi}{\partial F_j} \right) = \lambda \alpha_j \quad (5.16)$$

where λ is a positive scale factor.

Generally, the yield contour is built up out of different yield functions ψ_k (Fig. 5.6). If the load on the structure is only composed out of point forces, all functions ψ_k are linear. If one part of the load is uniformly distributed, the yield line can be curved too. In fact, the curve can be assumed to be a polygon built up out of infinitesimal-small straight-line pieces (Fig. 5.7). The total yield contour, which is built up out of curved and straight-line pieces, is always convex. On the one hand, this directly follows from the definition of the yield contour, but on the other hand, this can be shown more explicitly. Therefore, two arbitrary

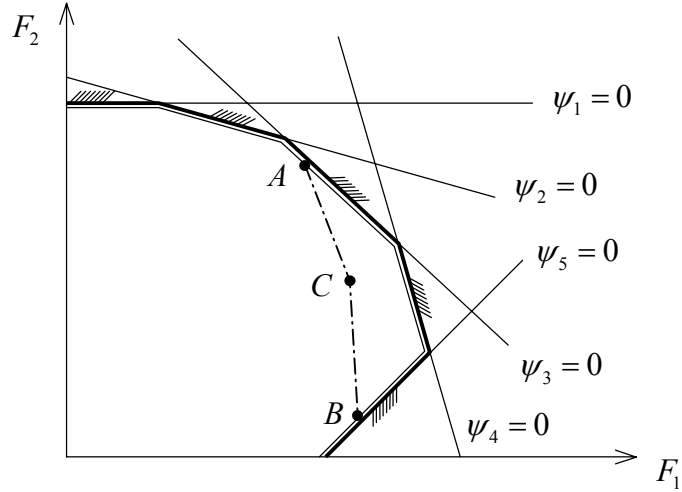


Fig. 5.6: In the case of loading by point forces, the yield contour is composed out of linear line pieces.

points A and B are considered situated on the yield contour (Fig. 5.6). It is assumed that all possible mechanisms are incorporated, so that in the points A and B moment distributions can be applied, which satisfy equilibrium and the yield condition. Now, an arbitrary load combination C is considered, situated on a straight line passing A and B . The load in C can be considered as the sum of certain proportions of the loads in A and B . These proportions are called α and $(1 - \alpha)$:

$$\underline{F}_C = \alpha \underline{F}_A + (1 - \alpha) \underline{F}_B \quad (5.17)$$

The fact that the sum of the proportions is equal to unity reflects that C is situated on a straight line through A and B . In each arbitrary point of the structure a bending moment can be defined of $M_C = \alpha M_A + (1 - \alpha) M_B$. If this is done for each point, the moment distribution for point C has been found, which satisfies equilibrium. Since further $-M_p \leq M_A \leq +M_p$ and $-M_p \leq M_B \leq +M_p$ it also holds that $-M_p \leq \alpha M_A + (1 - \alpha) M_B \leq +M_p$, which can be proved easily. So for M_c it holds $-M_p \leq M_C \leq +M_p$. So, a moment distribution in point C is found, which satisfies equilibrium and the yield conditions. Therefore, Point C is situated inside or on the yield contour, which means that the yield contour is convex.

To conclude this chapter another example with a uniformly distributed load f will be discussed. As mentioned above a curved yield contour will appear. The frame and yield contour are drawn in Fig. 5.7. Again, three mechanisms can be distinguished: a beam mechanism, a sway mechanism and a combined mechanism. The beam and sway mechanisms are self-evident and will not be discussed. For the combination mechanism the work equation reads:

$$F_x a \vartheta + (2fa) \left(\frac{1}{2} \alpha a \vartheta \right) = M_p \left(4\theta + \frac{2\alpha \vartheta}{2 - \alpha} \right) \quad (5.18)$$

where α is the position parameter of the plastic hinge in the beam. With $F_y = 2fa$ the mechanism equation is given by:

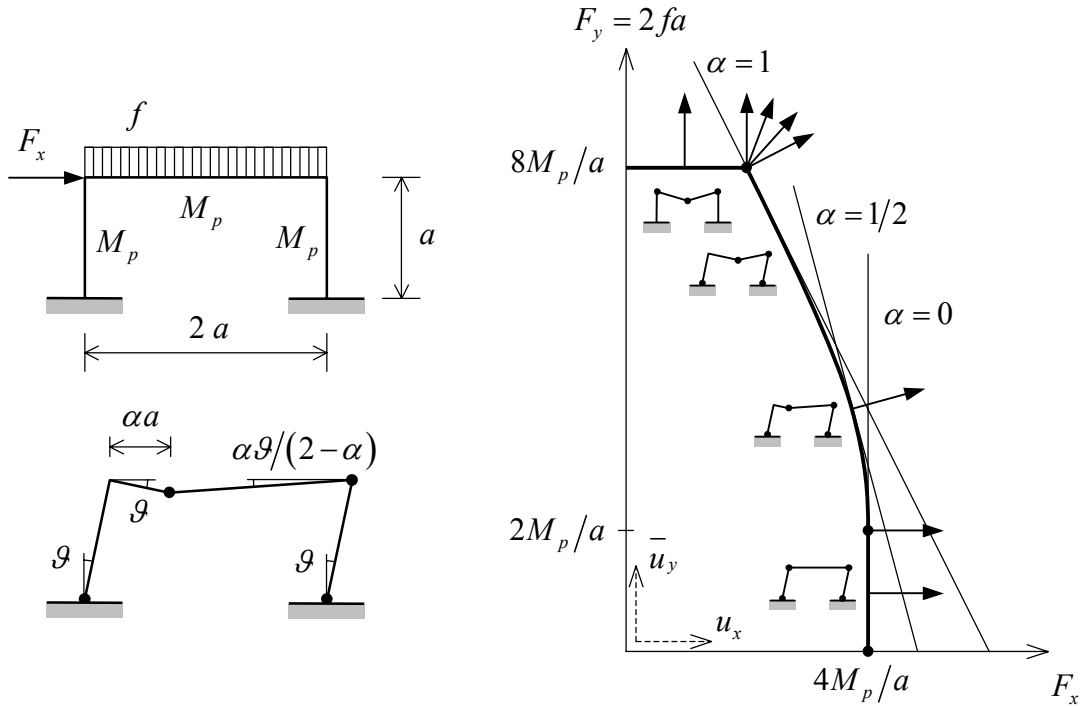


Fig. 5.7: Due to the distributed load the position of the hinge is not fixed and the yield contour is curved; the displacement component \bar{u}_y , which is important for normality, is the average displacement of all points of the upper beam.

$$F_x + \frac{\alpha}{2} F_y = \frac{M_p}{a} \left(\frac{8-2\alpha}{2-\alpha} \right) \quad (5.19)$$

In Fig. 5.7 the lines are drawn for $\alpha=0$, $\alpha=1/2$, $\alpha=1$. For $\alpha=0$ the mechanism is exactly the sway mechanism, for $\alpha=1$ the hinge is positioned exactly in the middle of the beam. For each value of α a mechanism line can be drawn with another slope in the F_x - F_y diagram. The more lines for different values of α are drawn, the more the inscribed polygon approaches the flowing curve. In order to find this curve for fixed F_y the value of F_x is determined through minimisation with respect to α :

$$F_x = \frac{M_p}{a} \left(\frac{8-2\alpha}{2-\alpha} \right) - \frac{\alpha}{2} F_y \rightarrow \frac{\partial F_x}{\partial \alpha} = \frac{M_p}{a} \frac{4}{(2-\alpha)^2} - \frac{1}{2} F_y = 0 \quad (5.20)$$

$$\alpha = 2 - \sqrt{\frac{8M_p}{F_y a}} \quad (0 \leq a \leq 2) \quad (5.21)$$

Substitution of α in (5.20) provides:

$$F_x = \frac{2M_p}{a} - F_y + \sqrt{\frac{8M_p F_y}{a}} \quad (5.22)$$

Since (5.21) is valid only for $\alpha \geq 0$, relation (5.22) is valid only for $F_y \geq 2M_p/a$. For lower values of F_y the sway mechanism holds. The transition from sway mechanism to combination mechanism is gradually, and the deformation vector $\{u_x, \bar{u}_y\}$ is unique. The transition from the combination mechanism to the beam mechanism is an abrupt one and more deformation vectors are possible (over-complete mechanism). Note that the displacement \bar{u}_y , for which in this example the normality condition holds, is not the displacement of the plastic hinge, but the “average displacement of the beam”, which is half of the hinge displacement. Namely, it is essential that the displacement related to normality, belongs to the corresponding force, in such a sense that their product represents a work. The choice of one of the two quantities is basically free. In this example the displacement of the hinge could have been chosen too, but than F_y should have been defined by $F_y = fa$.

6 Yield criteria

6.1 Introduction

In chapter 1 the yield behaviour of a 1-dimensional stress state was discussed. For more-dimensional stress states so-called *yield criteria* are required, indicating which combination of stresses will lead to limit stress states. In structural mechanics, frequently two-dimensional stress states are encountered and therefore, most attention will be paid to this in this chapter.

In chapter 1 it was discussed, that for a 1-dimensional stress state, the limit state is determined by yielding, for which:

$$\sigma = \pm \sigma_p \quad (6.1)$$

For more-dimensional stress states several yield criteria have been developed, the most important ones of which will be discussed.

6.2 The yield criterion of Tresca (steel)

Since it was observed that for tensile tests carried out on mild steel, the plastic deformations occur along planes making an angle of about 45° with the axis of the test

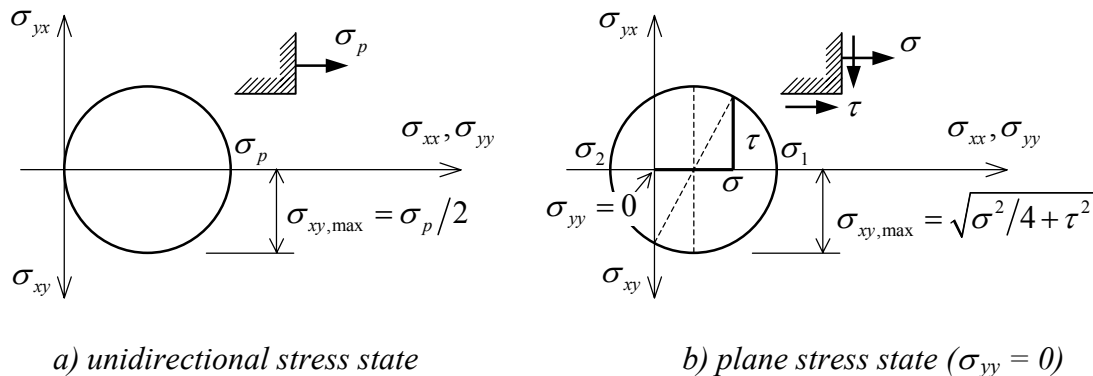


Fig. 6.1: Maximum shear stress.

specimen, it was quite logical to assume that the *maximum shear stress* was the decisive factor for yielding. The magnitude of the maximum shear stress can easily be obtained from a tensile test (Fig. 6.1a):

$$\sigma_{xy, \max} = \frac{\sigma_{xx}}{2} \quad (6.2)$$

and therefore the yield stress equals:

$$\tau_p = \pm \frac{\sigma_p}{2} \quad (6.3)$$

In the case of a special plane stress state, for example the stress state of a beam subjected to bending by a transverse force as shown in Fig. 6.1b, the maximum shear stress becomes:

$$\sigma_{xy, \max} = \frac{1}{2} \sqrt{\sigma^2 + 4\tau^2} \quad (6.4)$$

With Tresca's yield criterion according to (6.3) the yield condition for this stress state becomes:

$$\sigma^2 + 4\tau^2 = \sigma_p^2 \quad (6.5)$$

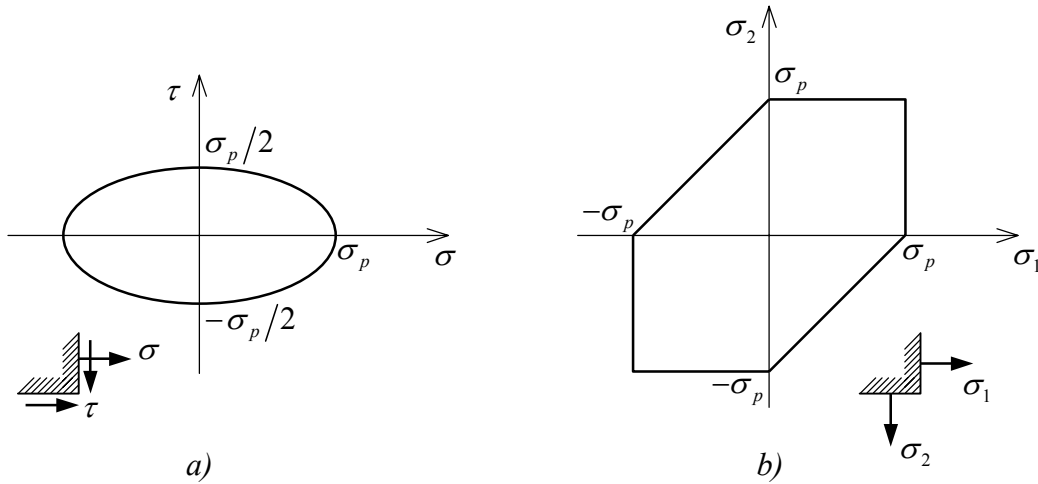


Fig. 6.2: Yield criterion of Tresca for plane stress
a) for the components σ , τ ($\sigma_{yy} = 0$);
b) in the principal stresses σ_1 , σ_2 ($\sigma_3 = 0$).

This relation is displayed in Fig. 6.2a. In the 3-dimensional stress space having principal stresses ($\sigma_1, \sigma_2, \sigma_3$) the largest shear stress is given by the largest of the absolute values of the differences given below:

$$\frac{\sigma_1 - \sigma_2}{2} ; \frac{\sigma_2 - \sigma_3}{2} ; \frac{\sigma_3 - \sigma_1}{2}$$

This changes the yield condition into:

$$\max[|\sigma_1 - \sigma_2|, |\sigma_2 - \sigma_3|, |\sigma_1 - \sigma_3|] < \sigma_p \quad (6.6)$$

In the 3-dimensional principal stress space this is a regular hexagonal prism, which is symmetrical with respect to the space diagonal $\sigma_1 = \sigma_2 = \sigma_3$. For the plane stress state with $\sigma_3 = 0$ the yield condition can be written as (Fig. 6.3b):

$$\max[|\sigma_1|, |\sigma_2|, |\sigma_1 - \sigma_2|] < \sigma_p \quad (6.7)$$

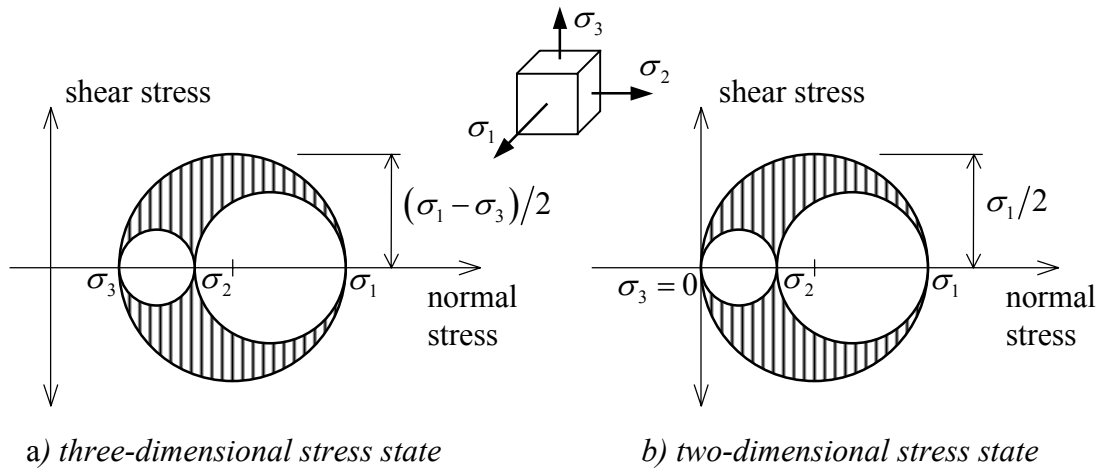


Fig. 6.3: Maximum shear stress.

This condition is sketched in Fig. 6.2b. For stress combinations inside the hexagon the material reacts elastically. Stress combinations on the hexagon cause the material to yield. Unloading takes place elastically. Outside the hexagon, no stress combinations are possible.

6.3 The yield criterion of von Mises (steel)

From experiments, it is known that the yield criterion of Tresca underestimates the yield shear stress. In this respect the yield criterion of von Mises provides a better approximation. For the 3-dimensional stress state having principal stresses $(\sigma_1, \sigma_2, \sigma_3)$ the criterion reads:

$$(\sigma_1 - \sigma_2)^2 + (\sigma_2 - \sigma_3)^2 + (\sigma_3 - \sigma_1)^2 = 2\sigma_p^2 \quad (6.8)$$

or:

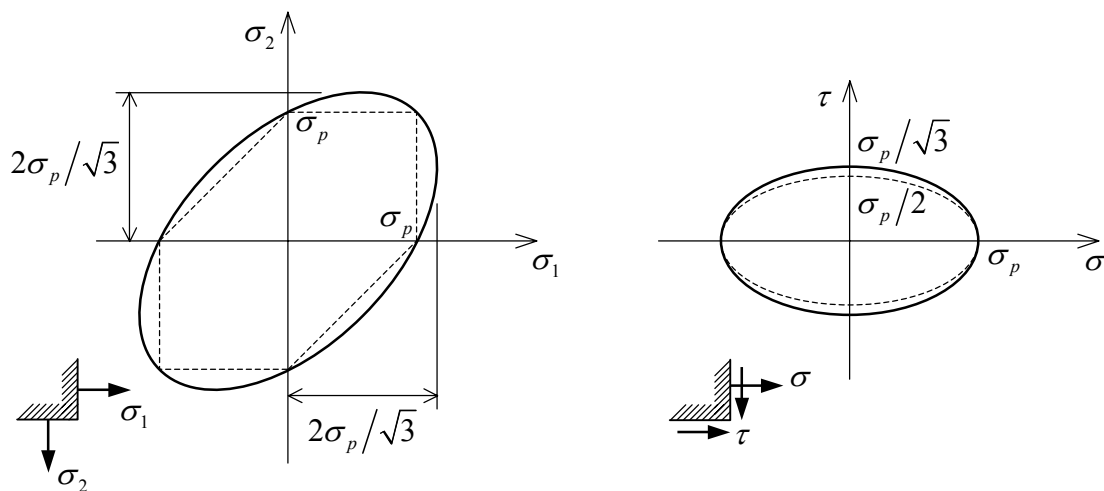


Fig. 6.4: Yield criterion of von Mises for plane stress
 a) in the principal stresses σ_1, σ_2 ($\sigma_3 = 0$);
 b) for the components σ, τ ($\sigma_{yy} = 0$);
 the dashed line shows Tresca's yield criterion.

$$\sigma_1^2 + \sigma_2^2 + \sigma_3^2 - \sigma_1\sigma_2 - \sigma_2\sigma_3 - \sigma_3\sigma_1 = \sigma_p^2 \quad (6.9)$$

In principal stress space, this is a cylinder that is symmetrical with respect to the space diagonal. For the plane stress state $\sigma_3 = 0$ the yield condition (6.9) changes into:

$$\sigma_1^2 + \sigma_2^2 - \sigma_1\sigma_2 = \sigma_p^2 \quad (6.10)$$

This is graphically represented in Fig. 6.4a. The dashed line indicates the criterion of Tresca.

For a plane stress state, defined by $\sigma_{xx} = \sigma$, $\sigma_{yy} = 0$, $\sigma_{xy} = \tau$ (bending by a transverse force), the principal stresses are (see Fig. 6.1b):

$$\sigma_{1,2} = \frac{1}{2}\sigma \pm \sqrt{\left(\frac{1}{2}\sigma\right)^2 + \tau^2}$$

Combination with (6.10) yields:

$$\sigma^2 + 3\tau^2 = \sigma_p^2 \quad (6.11)$$

This yield condition is displayed in Fig. 6.4b. The dashed line represents Tresca's criterion. From (6.11) immediately the shear stress according to von Mises follows:

$$\tau_p = \pm \frac{\sigma_p}{\sqrt{3}} \quad (6.12)$$

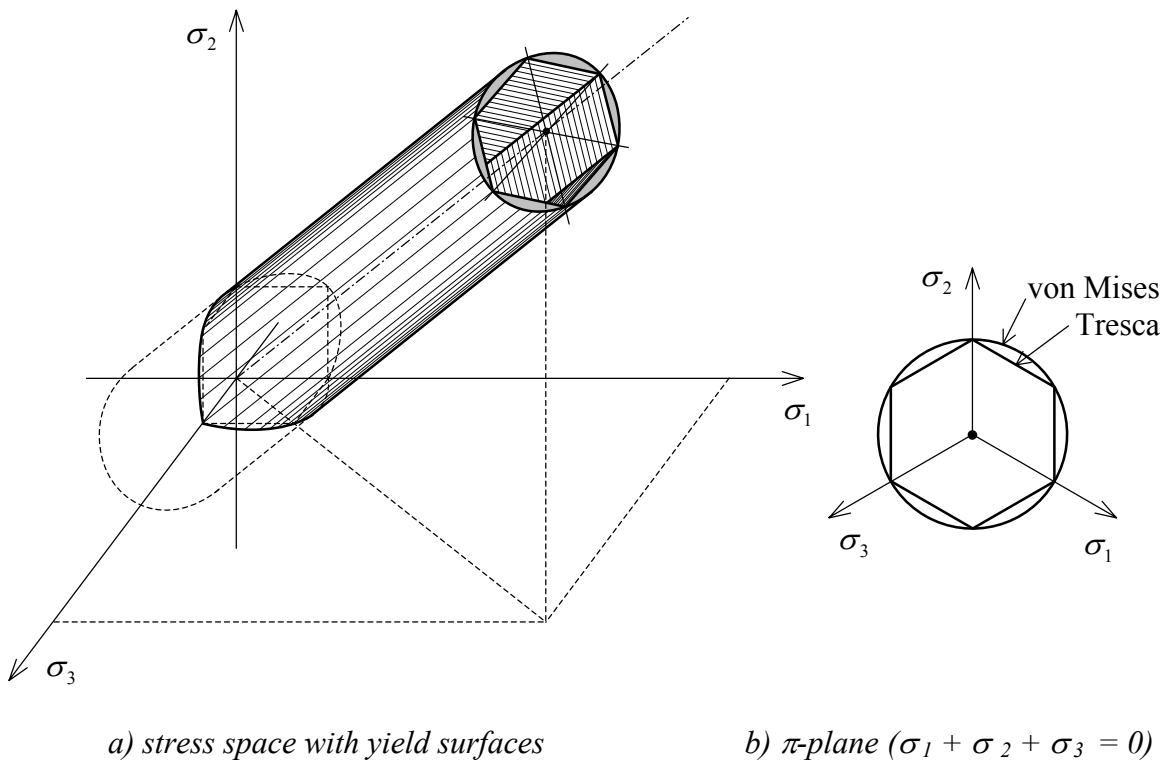


Fig. 6.5: The yield criteria of von Mises and Tresca in three-dimensional stress space.

Since the criterion of von Mises provides better results for steel and aluminium than the criterion of Tresca, it is normally applied for the calculation of steel and aluminium structures.

Finally, Fig. 6.5 shows the 3-dimensional stress space $(\sigma_1, \sigma_2, \sigma_3)$, with both Tresca's and von Mises yield criterion. The intersection of the cylinder and prism with the $\sigma_1 - \sigma_2$ plane provides an ellipse and a hexagon, respectively (Fig. 6.4a). As can be seen from the figure as well as from the structure of the criteria (6.6) and (6.8) addition of a hydrostatic stress $\sigma_1 = \sigma_2 = \sigma_3$ does not affect a critical stress state. This property is characteristic for the behaviour of isotropic materials. The structure of the yield criterion for brittle materials such as concrete and friction materials such as soil is for that reason very different.

6.4 The yield criterion of Mohr-Coulomb (concrete, rock / soil)

The yield criterion of Mohr-Coulomb is not only a good approximation for loose granular materials such as sand, but also a good first approximation for rock-like materials such as unreinforced concrete. First of all, these materials are characterised by enormous different properties for compression and tension. In the Mohr-Coulomb criterion, it is assumed that failure occurs, if in an arbitrary plane the shear stress becomes equal to the maximum allowable shear stress. This allowable shear stress depends linearly on the normal stress on the same plane. In formula form:

$$\tau_{\max} = c - \sigma \tan \varphi \quad (6.13)$$

where c is the cohesion and φ the angle of internal friction. Opposite to the normal sign convention, in soil mechanics compressive stresses are assumed positive.

The yield criterion can be displayed graphically by two straight lines in Mohr's diagram (Fig. 6.6). Immediately it can be seen that for $\varphi = 0$ the Mohr-Coulomb criterion transforms into Tresca's criterion with $c = \sigma_p / 2$. In the figure an arbitrary stress state is indicated, the shear stress of which is critical. Shear takes place along two planes, making an angle of $(\pi/4 + \varphi/2)$ with respect to the largest principal stress σ_1 , the deformation for which is unlimited.

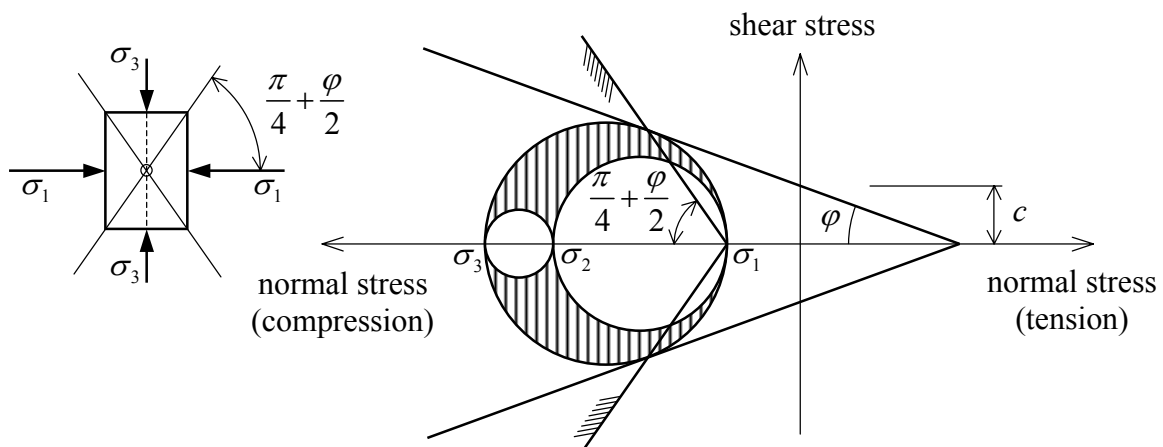


Fig. 6.6: The yield criterion of Mohr-Coulomb, tensile stresses are positive and $(\sigma_1 > \sigma_2 > \sigma_3)$.

For stress circles situated completely inside the envelope, no failure will occur and the deformations are limited. Generally, for concrete and soil, as a first approximation these deformations can be described with an isotropic linear-elastic material model.

From Fig. 6.6 it also becomes clear that contrary to the criteria of von Mises or Tresca, the addition of a hydrostatic stress $\sigma'_1 = \sigma'_2 = \sigma'_3$ to a critical stress state has a significant impact. As can be expected the influence of hydrostatic compression is positive, however the resistance against hydrostatic tensile stresses is very limited. By means of a geometrical

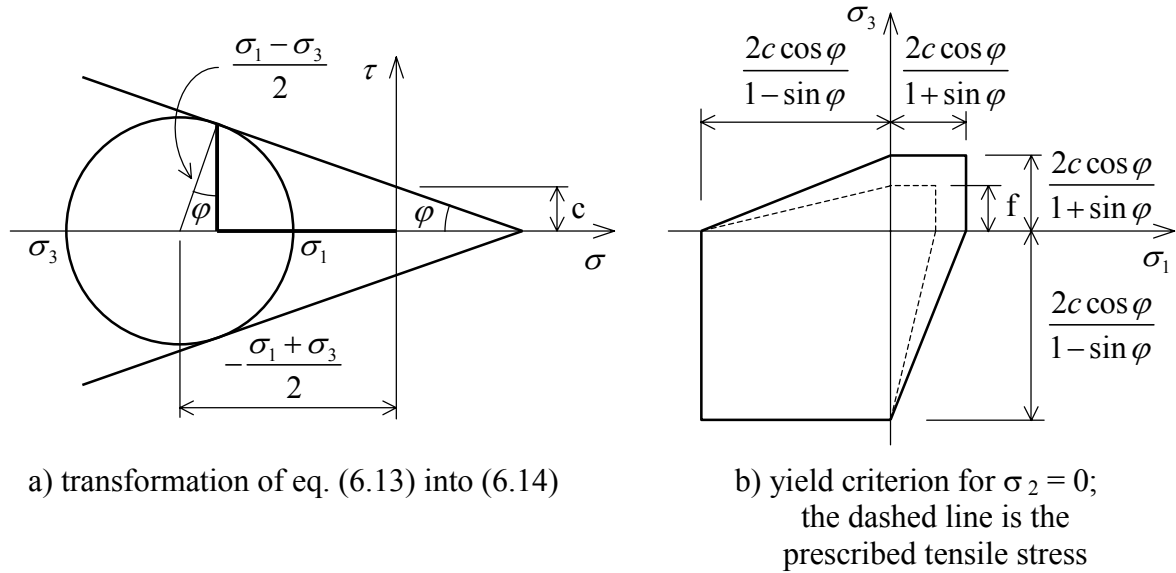


Fig. 6.7: Transformation of the Mohr-Coulomb yield criterion to principal stresses ($\sigma_1 > \sigma_2 > \sigma_3$).

transformation, the yield criterion can be displayed in principal stresses. In Fig. 6.7a this transformation is carried out for $\sigma_1 > \sigma_2 > \sigma_3$. This changes (6.13) into:

$$\sigma_1(1 + \sin \varphi) - \sigma_3(1 - \sin \varphi) = 2c \cos \varphi \quad (6.14)$$

For the 3-dimensional stress state the yield condition becomes:

$$\max \left[\begin{aligned} &\sigma_1(1 + \sin \varphi) - \sigma_3(1 - \sin \varphi), \sigma_3(1 + \sin \varphi) - \sigma_1(1 - \sin \varphi), \\ &\sigma_2(1 + \sin \varphi) - \sigma_1(1 - \sin \varphi), \sigma_1(1 + \sin \varphi) - \sigma_2(1 - \sin \varphi), \\ &\sigma_3(1 + \sin \varphi) - \sigma_2(1 - \sin \varphi), \sigma_2(1 + \sin \varphi) - \sigma_3(1 - \sin \varphi), \end{aligned} \right] = 2c \cos \varphi \quad (6.15)$$

In space this is a irregular hexagonal pyramid with apex $\sigma_1 = \sigma_2 = \sigma_3 = c \cos \varphi$.

For the plane stress state with $\sigma_2 = 0$ criterion (6.15) changes into:

$$\max \left[\begin{aligned} &\sigma_1(1 + \sin \varphi) - \sigma_3(1 - \sin \varphi), \sigma_3(1 + \sin \varphi) - \sigma_1(1 - \sin \varphi), \\ &-\sigma_1(1 - \sin \varphi), \sigma_1(1 + \sin \varphi), \sigma_3(1 + \sin \varphi), -\sigma_3(1 - \sin \varphi), \end{aligned} \right] = 2c \cos \varphi \quad (6.16)$$

which is graphically displayed in Fig. 6.7b. For $\varphi = 0$ the figure is identical to Fig. 6.2b, which is based on Tresca's criterion. During the last few decades, several modifications on the Mohr-Coulomb criterion are proposed, for both concrete and soil. In concrete mechanics, frequently use is made of the Mohr-Coulomb criterion with a prescribed maximum tensile stress. So, except for the material parameters c and φ also a maximum tensile strength f has to be introduced (see Fig. 6.7b). For principal stresses smaller than zero failure takes place through shear deformation (see Fig. 6.6), for principal stresses larger than zero failure takes place through crack formation perpendicular to the principal stress direction σ_1 .

7 Effects of normal forces on plastic frame behaviour

7.1 The influence of the normal force on the fully plastic moment

7.1.1 Introduction

In chapter 2 the calculation of the plastic moment for pure bending was discussed. In this chapter it will be discussed, to what degree the magnitude of the moment M_p is changed, under influence of a normal force N acting on the same cross-section. Just as in chapter 2, the first focus will be on the rectangular cross-section. After that, other shapes of cross-sections will be discussed. The assumptions made in chapter 2 are valid here as well.

7.1.2 Rectangular cross-section

Let us first reformulate the limit for the elastic stage (see Fig. 7.1):

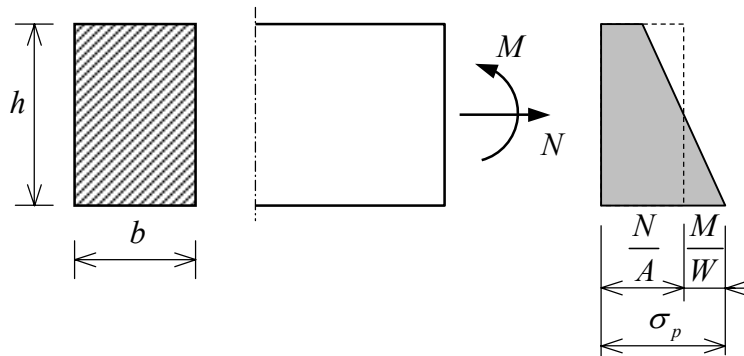


Fig. 7.1: Normal force and bending moment on rectangular cross section.

$$\frac{N}{A} + \frac{M}{W} = \sigma_p$$

This relation can also be written as:

$$\frac{N}{N_p} + \frac{M}{M_e} = 1 \quad \text{where} \quad N_p = A\sigma_p \quad \text{and} \quad M_e = W\sigma_p \quad (7.1)$$

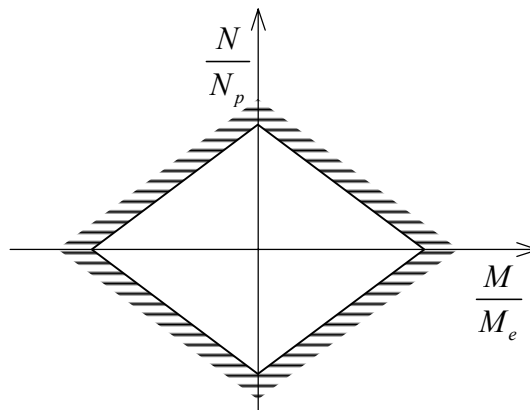


Fig. 7.2: Yield contour for elastic limit state.

Relation (7.1) can be represented graphically by a yield contour as drawn in Fig. 7.2. After reaching the yield stress in the extreme fibre, the stress distribution across the cross-section becomes elastic plastic (see Fig. 7.3). At the side where $\sigma = \sigma_p$ the yielded area is

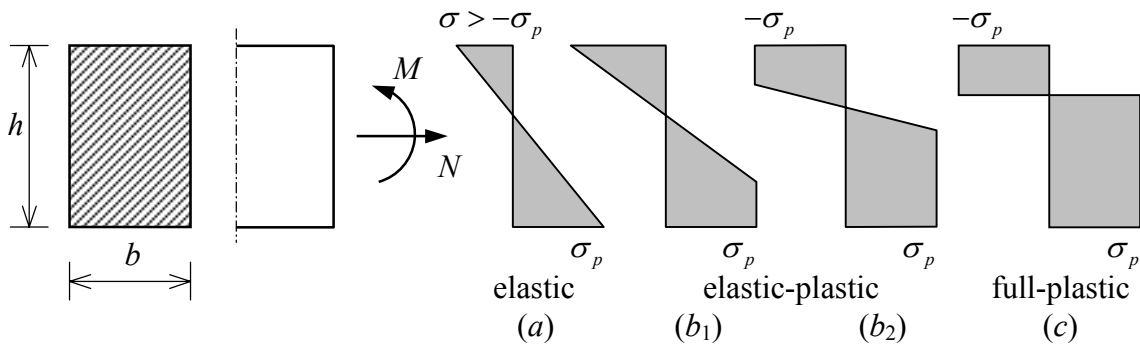


Fig. 7.3: Elastic, elastic-plastic and full-plastic state.

expanding. When at the upper side the yield stress is reached too, also here the yielded area starts growing. The state of failure is reached, when all fibres are yielding.

For the calculation of the moment and the normal force in the state of failure, it is handy to split the stress diagram of Fig. 7.3c into two parts, as indicated in Fig. 7.4. The stresses in the central part of the cross-section (with height d) are caused by the normal force only.

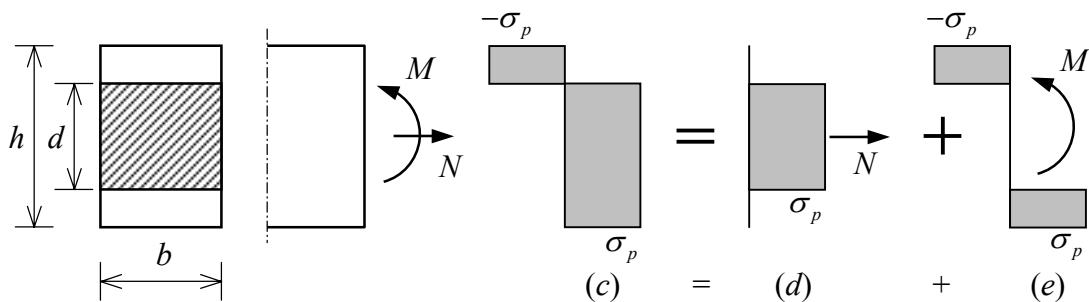


Fig. 7.4: Model for separation of the force and moment contributions.

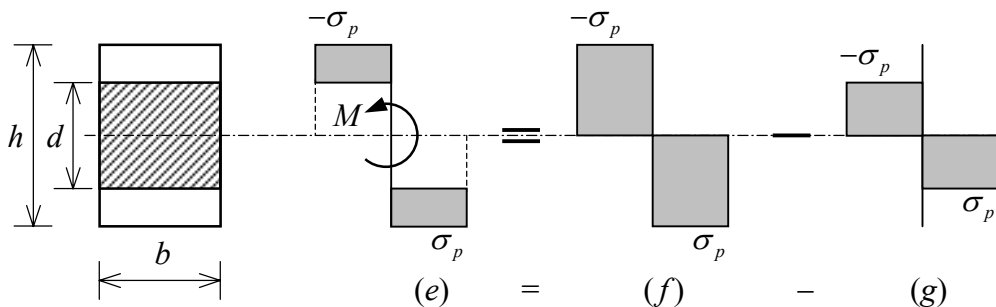


Fig. 7.5: Model for the treatment of the moment.

The remaining stresses in the rest of the cross-section deliver a pure bending moment. The stresses are distributed in such a manner that the normal force is transmitted through fibres, which are situated around the neutral line, while the moment is provided by the most effective extreme fibres. For the calculation of M (Fig. 7.4e) the fictive model of Fig. 7.5 is

used. The limits of the plastic (N, M) -combinations can be calculated through $N = bd\sigma_p$ and $N_p = bh\sigma_p$. It then follows:

$$\frac{N}{N_p} = \frac{bd\sigma_p}{bh\sigma_p} = \frac{d}{h} \quad (7.2)$$

As $M = bh^2\sigma_p/4 - bd^2\sigma_p/4$ and $M_p = bh^2\sigma_p/4$, it is found that:

$$\frac{M}{M_p} = \frac{\frac{1}{4}bh^2\sigma_p - \frac{1}{4}bd^2\sigma_p}{\frac{1}{4}bh^2\sigma_p} = 1 - \frac{d^2}{h^2} \quad (7.3)$$

Combination of (7.2) and (7.3) then leads to:

$$\left(\frac{N}{N_p}\right)^2 + \left(\frac{M}{M_p}\right) = 1 \quad (7.4)$$

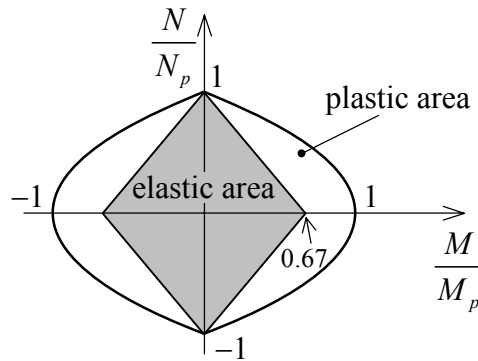


Fig. 7.6: Yield contours of elastic and plastic areas.

This relation forms the plastic yield contour, as displayed in Fig. 7.6. For comparison, the elastic contour according (7.1) is drawn inside. Because of the quadratic term $(N/N_p)^2$, small normal forces have only little impact on the fully plastic moment.

7.1.3 Arbitrary double-symmetric cross-section

Relation (7.1) derived in the previous section, being valid for the elastic area, is valid too for double symmetrical cross-sections (see Fig. 7.7). Similarly as for the rectangular cross-section, the maximum combination of M and N in the state of failure can be derived from the full-plastic stress distribution (see Fig 7.8). It is assumed that all fibres are yielding either in tension or in compression. The central part with height d , which is assumed to carry the normal force N , has a cross-sectional area A_N and a plastic section factor W_{pN} . For a certain value of the height d of the hatched central part in Fig. 7.8, the values of N and M follow from the following relations:

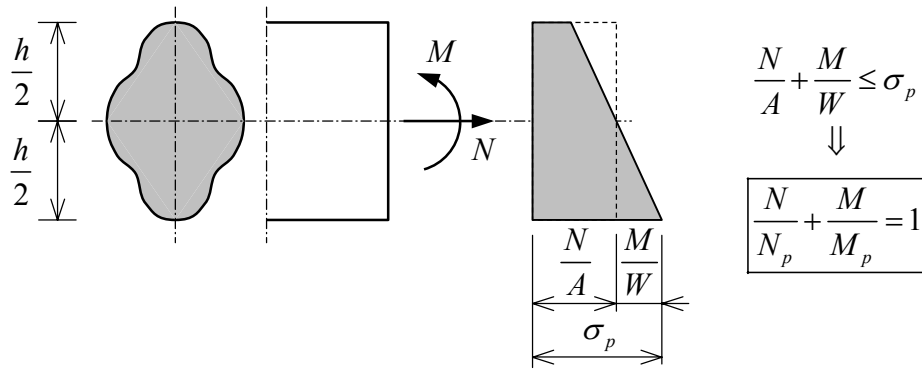


Fig. 7.7: Normal force and bending moment on double-symmetric cross section.

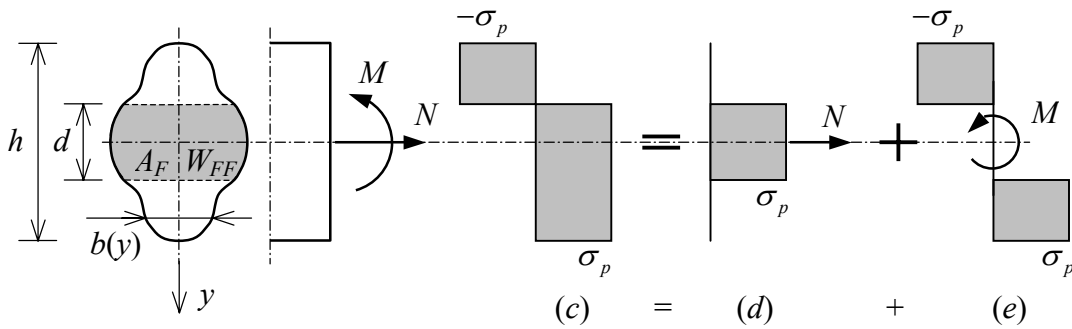


Fig. 7.8: Model for separation of the force and moment contribution.

$$N = 2\sigma_p \int_0^{d/2} b(y)dy = \sigma_p A_N \tag{7.5}$$

$$M = 2\sigma_p \int_{d/2}^{h/2} yb(y)dy = \sigma_p (W_p - W_{pN})$$

These two equations determine the plastic contour of the plastic area and obviously are independent from the geometry of the cross-section. The equations (7.5) can be rewritten as:

$$\frac{N}{N_p} = \frac{A_N}{A} \tag{7.6}$$

$$\frac{M}{M_p} = 1 - \frac{W_{pN}}{W_p}$$

Consider as an example an I-section, subjected to bending about the strong axis ($x-x$ axis). The influence of the rounding between flanges and body is neglected. So, the section is schematised as if it is composed out of rectangular bars. Two different cases may arise:

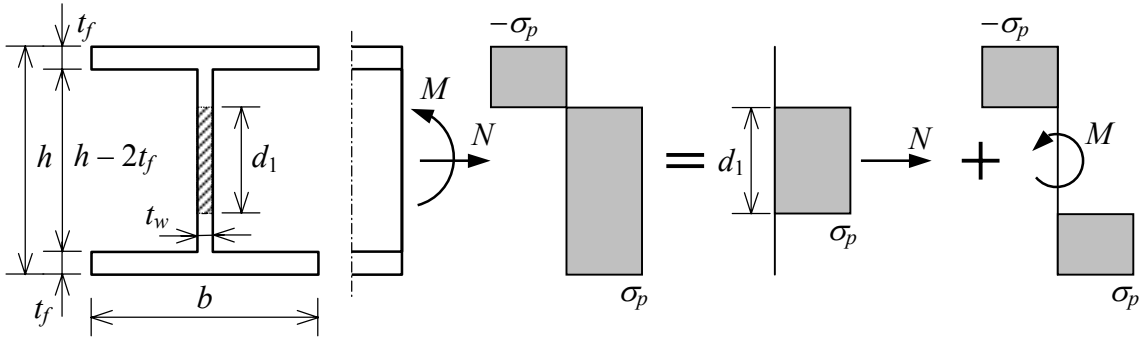


Fig. 7.9: I-section with normal force smaller than yield force of web.

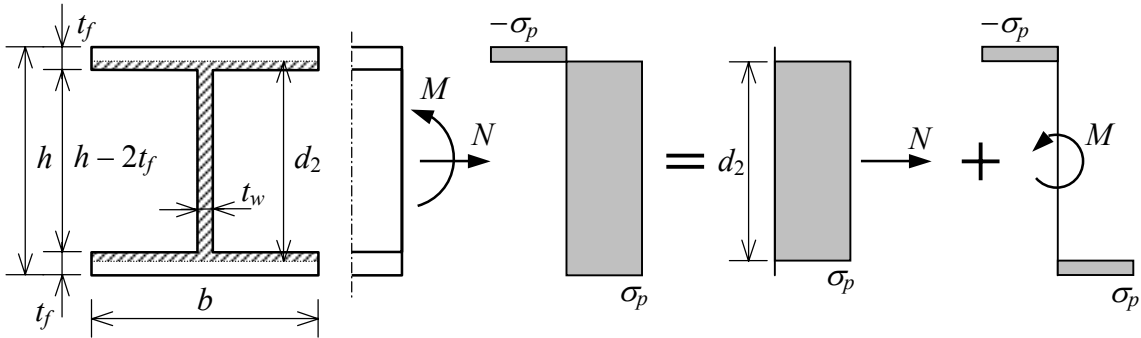


Fig. 7.10: I-section with normal force larger than yield force of web.

1. The normal force is smaller than the yield force of the web, so: $N < \sigma_p t_w (h - 2t_f)$. In the state of collapse (full-plastic) the neutral line is situated in the body (Fig. 7.9). Through $N = \sigma_p t_w d_1$ and $N = \sigma_p A$ it then can be found:

$$\frac{N}{N_p} = \frac{t_w d_1}{A} \quad (7.7)$$

2. The normal force is larger than the yield force of the web, so $\sigma_p t_w (h - 2t_f) < N < \sigma_p A$. In the state of collapse, the neutral line is situated in the flange (Fig. 7.10). Then it holds (see Figs. 7.11 and 7.12):

$$N = \sigma_p b d_2 - \sigma_p (b - t_w)(h - 2t_f)$$

$$N_p = \sigma_p A$$

and

$$M = \sigma_p \frac{1}{4} b h^2 - \sigma_p \frac{1}{4} b d_2^2$$

$$M_p = \sigma_p W_p$$

So:

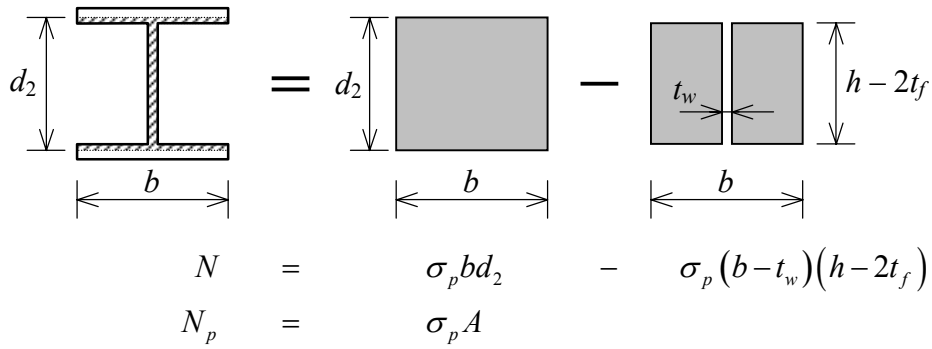


Fig. 7.11: Calculation of the plastic normal force.

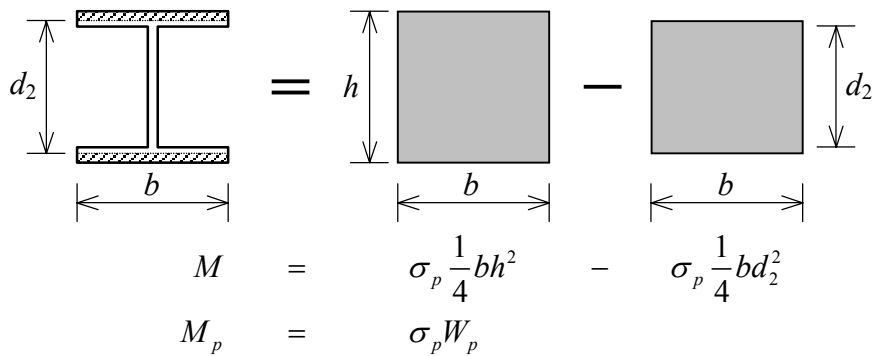


Fig. 7.12: Calculation of the plastic moment.

$$\frac{N}{N_p} = \frac{b d_2 - (b - t_w)(h - 2t_f)}{A}$$

$$\frac{M}{M_p} = \frac{b h^2 - b d_2^2}{4 W_p}$$
(7.8)

For practical applications the above curves normally are approximated by a simple contour, composed out of two straight lines per quadrant (Fig. 7.13). The slanting line in the first quadrant is given by the relation:

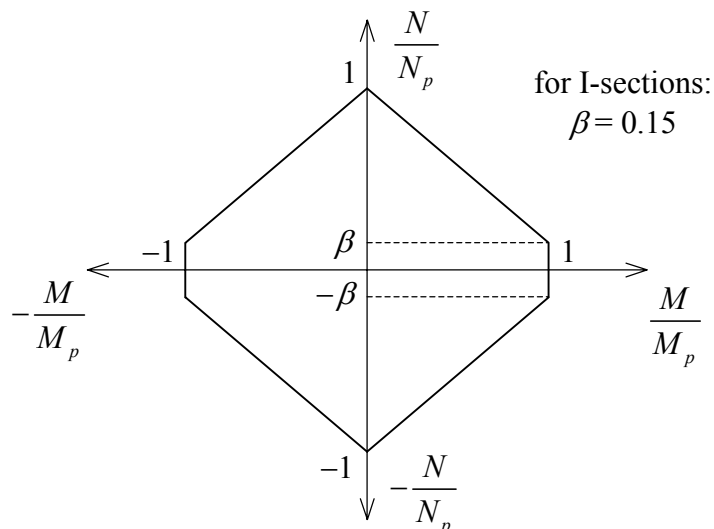


Fig. 7.13: Approximated yield contour.

$$\frac{M}{M_p} = 1.18 \left(1 - \frac{N}{N_p} \right) \leq 1$$

The approximation is quite acceptable within the framework of structural design.

7.2 The moment-curvature diagram in the presence of a normal force

In this section it is discussed how the moment-curvature diagram is affected by a normal force N . The obtained diagrams often are indicated as M - N - κ diagrams. These diagrams are used for example for the evaluation of the strength and deformation properties of columns subjected to bending and compression.

7.2.1 Rectangular cross-sections

As discussed in section 7.1.1, for increasing curvature the stress distribution passes the stages as indicated in Fig. 7.14 (compare with Fig. 7.3).

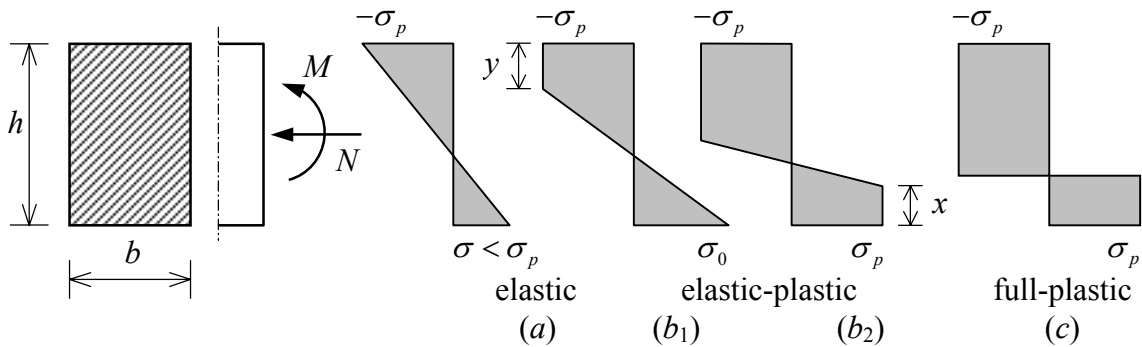


Fig. 7.14: Normal compressive force and bending moment on rectangular cross section.

For the elastic stage we have:

$$\kappa = \frac{M}{EI} \quad \text{or} \quad \frac{\kappa}{\kappa_e} = \frac{M}{M_e}$$

The end of the elastic range is reached if:

$$\frac{N}{N_p} + \frac{M}{M_e} = 1$$

For the elastic-plastic stage two steps should be considered:

1. Only the zone of compression is yielding (see Fig. 7.14):

$$N = \sigma_p b h - \frac{(\sigma_p + \sigma_0)}{2} b (h - y)$$

$$M = \frac{1}{12} (\sigma_p + \sigma_0) b (h - y)^2 + \frac{1}{4} (\sigma_p + \sigma_0) b y (h - y)$$

$$\kappa = \frac{(\sigma_p + \sigma_0)}{E(h-y)}$$

or:

$$\frac{N}{N_p} = \frac{1}{2}[(1+y') - \sigma'(1-y')] \quad (7.9)$$

$$\frac{M}{M_e} = \frac{1}{2}(1+\sigma')(1-y')(1+2y') \quad (7.10)$$

$$\frac{\kappa}{\kappa_e} = \frac{1+\sigma'}{2(1-y')} \quad (7.11)$$

where $y' = y/h$, $\sigma' = \sigma_0/\sigma_p$, $N_p = bh\sigma_p$, $M_e = \frac{1}{6}bh^2\sigma_p$ and $\kappa_e = 2\sigma_p/Eh$.
From these equations the variables σ' and y' can be eliminated, leading to:

$$\frac{\kappa}{\kappa_e} = \frac{4(1-N/N_p)^3}{[3(1-N/N_p) - M/M_e]^2} \quad (7.12)$$

Equation (7.12) is valid as long as only one side of the section yields (case b₁ in Fig. 7.14).
At the moment the bottom side starts yielding then $\sigma_0 = \sigma_p \rightarrow \sigma' = 1$. Substitution of this value in (7.9) and (7.11) provides the following condition:

$$\left. \begin{array}{l} \frac{N}{N_p} = y' \\ \frac{\kappa}{\kappa_e} = \frac{1}{1-y'} \end{array} \right\} \rightarrow \frac{\kappa}{\kappa_e} = \frac{1}{1-N/N_p} \quad (7.13)$$

2. *The zones of compression and tension are yielding (see Fig. 7.14):*

$$N = \sigma_p b(y-x)$$

$$M = \frac{1}{6}\sigma_p b(h-x-y)^2 + \sigma_p by\left(\frac{h}{2} - \frac{y}{2}\right) + \sigma_p bx\left(\frac{h}{2} - \frac{x}{2}\right)$$

$$\kappa = \frac{2\sigma_p}{E(h-x-y)}$$

or:

$$\frac{N}{N_p} = y' - x' \quad (7.14)$$

$$\frac{M}{M_e} = 1 + x' + y' + 2x'y' - 2x'^2 - 2y'^2 \quad (7.15)$$

$$\frac{\kappa}{\kappa_e} = \frac{1}{1 - x' - y'} \quad (7.16)$$

where $x' = x/h$ and $y' = y/h$.

From (7.14), (7.15) and (7.16) the variables x' and y' can be eliminated, leading to:

$$\frac{M}{M_e} = \frac{3}{2} \left[1 - \left(\frac{N}{N_p} \right)^2 \right] - \frac{1}{2 \left(\frac{\kappa}{\kappa_e} \right)^2} \quad (7.17)$$

As an illustration, the full M - N - κ curves are presented in Fig. 7.15. The maximum value of M/M_p is obtained for infinitely large curvature. So, for $\kappa/\kappa_e \rightarrow \infty$ from (7.17) it follows:

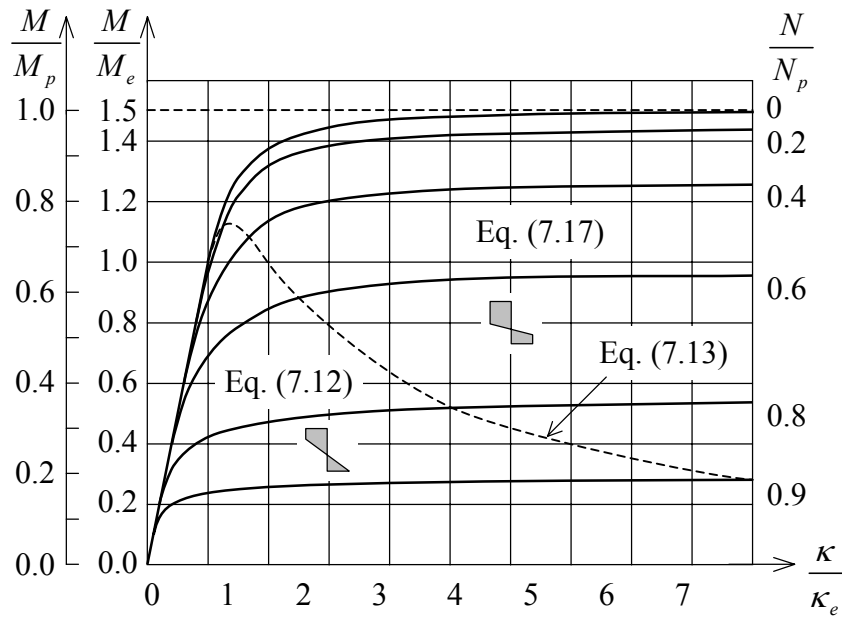


Fig. 7.15: Rectangular cross section.

$$\frac{M}{M_e} = \frac{3}{2} \left[1 - \left(\frac{N}{N_p} \right)^2 \right] \rightarrow \frac{2}{3} \frac{M}{M_e} + \left(\frac{N}{N_p} \right)^2 = 1 \quad \text{or} \quad \frac{M}{M_p} + \left(\frac{N}{N_p} \right)^2 = 1$$

Compare this result with (7.4).

7.2.2 I-shaped cross-sections

Completely analogously as for the previously described rectangular cross-section, for I-sections similar relations can be derived between the moment and curvature in the presence of a normal force of magnitude N/N_p . In Fig. 7.16 an example is given. The point of contact of the elastic-plastic part of the curve and the elastic branch is determined by (7.1): $N/N_p + M/M_e = 1$. For $\kappa/\kappa_e \rightarrow \infty$, the curves approach the limit values for M/M_p , which follow from the interaction formulae (7.7) and (7.8) as derived in section 7.1.2. Rolling stresses σ_r affect the curves of the M - N - κ diagrams. Naturally, the maximum value of M/M_p is not influenced by the rolling stresses.

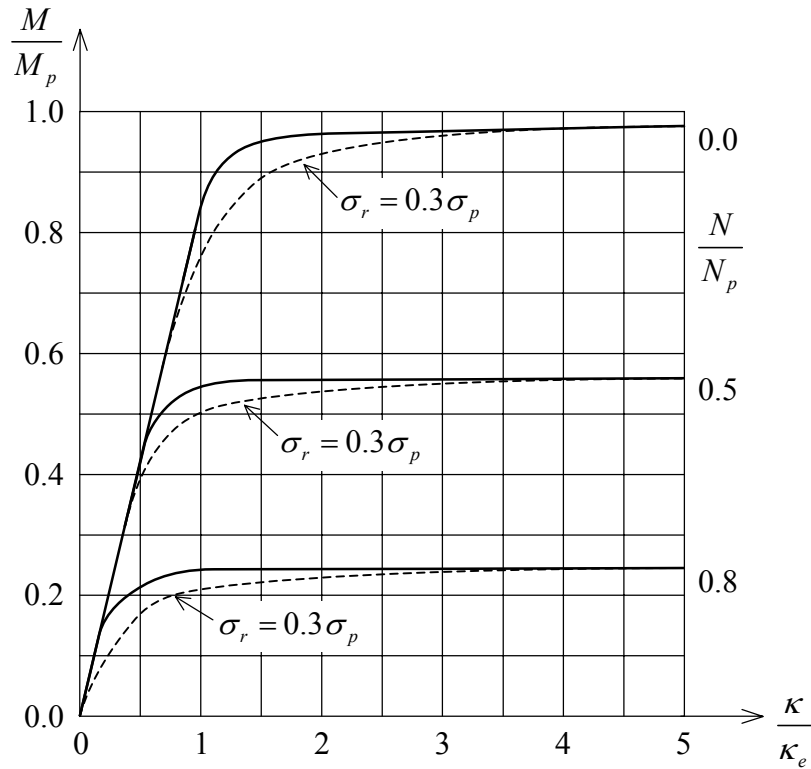


Fig. 7.16: I-shaped cross section.

7.3 Reinforced concrete cross-section

The reinforced concrete cross-section of Fig. 7.17 is considered. The beam has a width b , a height h and at the bottom side a reinforcement $A_s = \omega bh$. Both steel and concrete are considered ideal elastic-plastic. The steel yields at $+\sigma_p$ and $-\sigma_p$, the concrete has a

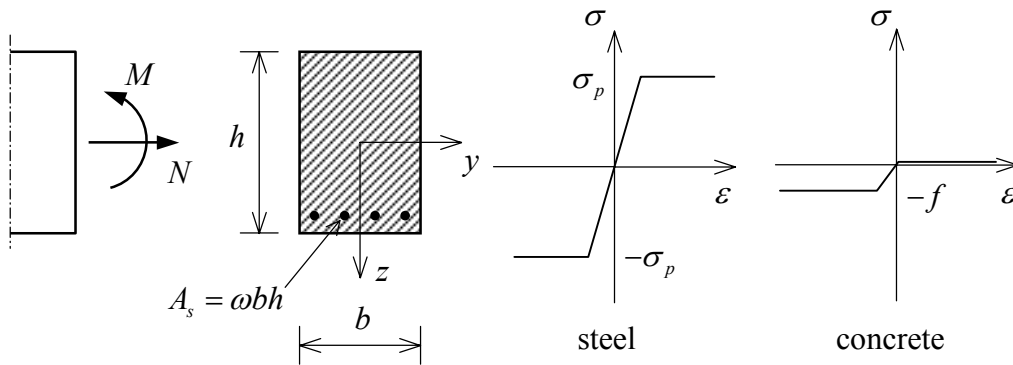


Fig. 7.17: Data reinforced concrete cross-section.

compressive yield strength of $-f$ and a tensile yield strength of zero. For the normal force N and the moment M the following definitions are used:

$$N = \iint \sigma_{xx} dydz \quad (7.18)$$

$$M = \iint z \sigma_{xx} dy dz \quad (7.19)$$

The y - z coordinate system is indicated too in Fig. 7.17. The origin of the system coincides with the geometrical centre of gravity of the cross-section, so it does not coincide with the elastic centre of gravity, usually used in the theory of elasticity. It is noted that the choice of a coordinate system in principle is arbitrary. However, one should take care during the comparison of results, that for normal forces $N \neq 0$, the moment is depending on the origin of the coordinate system.

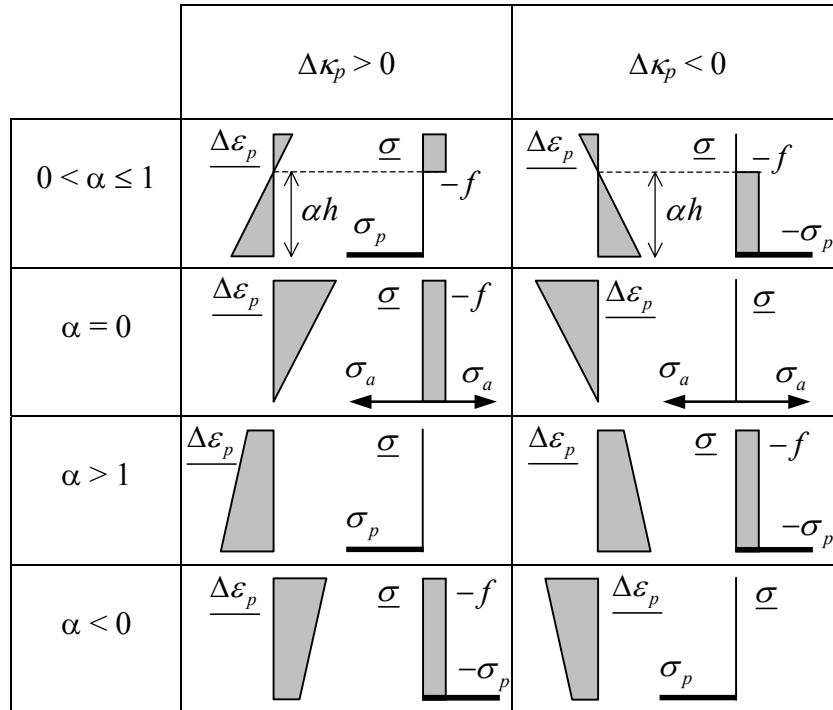


Fig.7.18: The stress and strain distributions that can be distinguished;
 $\Delta\kappa_p =$ plastic curvature; $\Delta\varepsilon_p =$ plastic strain of the centre fibre;
 $ah =$ distance between neutral line and bottom of beam.

In Fig. 7.18 a number of different cases of strain and stress distributions have been drawn. The first case will be worked out, with $\Delta\kappa_p > 0$ (positive curvature) and $0 \leq x \leq h$ (the neutral line is inside the cross-section, x is the distance from the neutral line to the top side of the beam). For the derivations of the formulae, the concrete cover on the reinforcement is neglected. Therefore, it is assumed that the reinforcement coincides with the concrete fibre at the bottom. For the mentioned case the following formulae are valid:

$$N = \omega b h \sigma_p - x b f \quad (7.20)$$

$$M = \omega b h \sigma_p \left(\frac{1}{2} h \right) - x b f \left(\frac{1}{2} h - \frac{1}{2} x \right) \quad (7.21)$$

For simplification of above relations it is defined:

$$N_p = \omega b h \sigma_p \quad (7.22)$$

$$c = \frac{A_s \sigma_p}{b h f} \quad (7.23)$$

where N_p is the yield force carried by the steel and c is the material reinforcement ratio as introduced in section 2.3. Substitution of these relations into (7.20), leads in combination with $A_s = \omega b h$ to:

$$\frac{N}{N_p} = 1 - \frac{x}{c h} \quad \text{or} \quad \frac{x}{h} = c \left(1 - \frac{N}{N_p} \right) \quad (7.24)$$

Now, x can be eliminated from (7.21), which provides:

$$M = \frac{h N_p}{2} + (N_p - N) \left(\frac{h}{2} \right) \left(1 - c + c \frac{N}{N_p} \right) = \frac{1}{2} h \left[(2 - c) N_p - (1 - 2c) N - c \frac{N^2}{N_p} \right]$$

The full-plastic moment M_p of chapter 2 shows up again (see (2.19)), being the ultimate positive moment that can be carried for $N = 0$:

$$M_p = \frac{1}{2} h (2 - c) N_p = \omega b h^2 \sigma_p \left(1 - \frac{1}{2} c \right) \quad (7.25)$$

Finally, for M it now follows:

$$\boxed{M = M_p - \frac{1}{2} h N \left(1 - 2c + c \frac{N}{N_p} \right)} \quad (7.26)$$

For the considered case ($0 \leq x \leq h$) the relation between the ultimate M and N is a top parabola as indicated in Fig. 7.19. For both ends of the curve it holds that $M = 0.5 h N_p = 0.5 \omega b h^2 \sigma_p = M_p / (2 - c)$. The maximum moment is reached halfway for:

$$N = N_p - \frac{1}{2} b h f = N_p \left(1 - \frac{1}{2c} \right) \quad \text{or for} \quad x = \frac{1}{2} h$$

The value of the maximum moment is:

$$M_{\max} = \omega b h^2 \sigma_p \left(1 + \frac{1}{4c} \right) = M_p \left(\frac{4c + 1}{4c(2 - c)} \right) \quad (7.27)$$

For $c = 0.1$ the maximum moment equals $1.8 M_p$. The fact that the moment reaches its maximum value for $x = h/2$ can be concluded directly on bases of normality. The tangent to the yield contour at the position of the maximum moment is horizontal, and therefore the

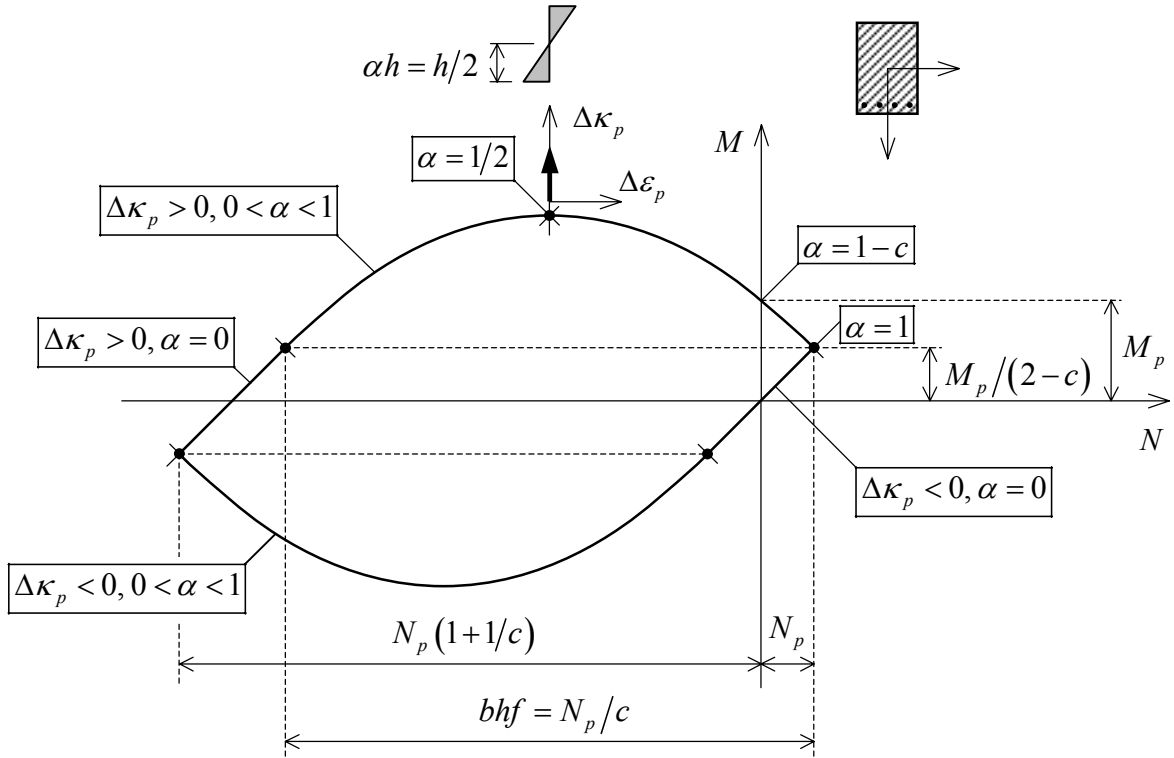


Fig. 7.19: Yield contour of a reinforced concrete cross-section with bottom reinforcement only.

deformation vector $(\Delta\kappa^p, \Delta\varepsilon^p)$ has to point in vertical direction. This means that $\Delta\varepsilon^p = 0$ and therefore $x = h/2$, as indicated in Fig. 7.19.

The second branch of the yield contour can be obtained by taking $x = h$, which means that the fibre with $\varepsilon = 0$ coincides exactly with the position of the reinforcement. The consequence of this is that the stress in the reinforcement is indeterminate and may vary between $-\sigma_p$ and $+\sigma_p$. The equation for this case are thus given by:

$$N = \omega b h \sigma_a - b h f \quad (7.28)$$

$$M = \frac{1}{2} \omega b h^2 \sigma_a \quad (7.29)$$

where $-\sigma_p < \sigma_a < +\sigma_p$. Elimination of the unknown steel stress σ_a leads to:

$$M = \frac{1}{2} N h + \frac{1}{2} b h^2 f = \frac{1}{2} h \left(N + \frac{N_p}{c} \right) \quad (7.30)$$

This straight branch is indicated too in Fig. 7.19. This exercise completes the yield contour for $\Delta\kappa_p > 0$ and $0 \leq x \leq h$. In Fig. 7.18 it easily can be seen that $x > h$ and $x < 0$ do not deliver any additional points. Since for $x < 0$ the same points on the yield contour are found as for $x = 0$. The points on the yield contour for $x > h$ directly follows from the yield contour for $x = h$ by substitution of $\sigma_a = \sigma_p$ in (7.28) and (7.29). For both ends of the yield contour the deformation vector $(\Delta\kappa^p, \Delta\varepsilon^p)$ is indeterminate, which also follows from the indeterminate character of the slope of the respective strain diagrams in Fig. 7.18.

Now, the derivation is continued for the case of a negative curvature. For $0 \leq x \leq h$ the normal force and moment are given by:

$$N = -\omega b h \sigma_p - \alpha b h f \quad (7.31)$$

$$M = -\omega b h \sigma_p \left(\frac{1}{2} h \right) - \alpha b h f \left(\frac{1}{2} h - \frac{1}{2} \alpha h \right) \quad (7.32)$$

Similarly to the derivation of (7.26), after elimination of α it follows:

$$\boxed{M = \frac{c M_p}{2 - c} + \frac{1}{2} h N \left(1 + 2c + c \frac{N}{N_p} \right)} \quad (7.33)$$

For $\Delta \kappa_p < 0$ and $\alpha = 0$ it finally holds:

$$N = -\omega b h \sigma_a \quad (7.34)$$

$$M = -\omega b h \sigma_a \frac{1}{2} h \quad (7.35)$$

or:

$$M = \frac{1}{2} N h \quad (7.36)$$

So, for $\Delta \kappa_p < 0$ a dip parabola and a straight line through the origin results, which can be seen in Fig. 7.19. If topside reinforcement is present the yield contour becomes slightly different, as can be seen from Fig. 7.20. For equal top and bottom reinforcement the yield contour is symmetrical with respect to the line $M = 0$. However, with respect to the line $N = 0$ the yield contour remains asymmetrical, because of the different properties of concrete in compression and tension.

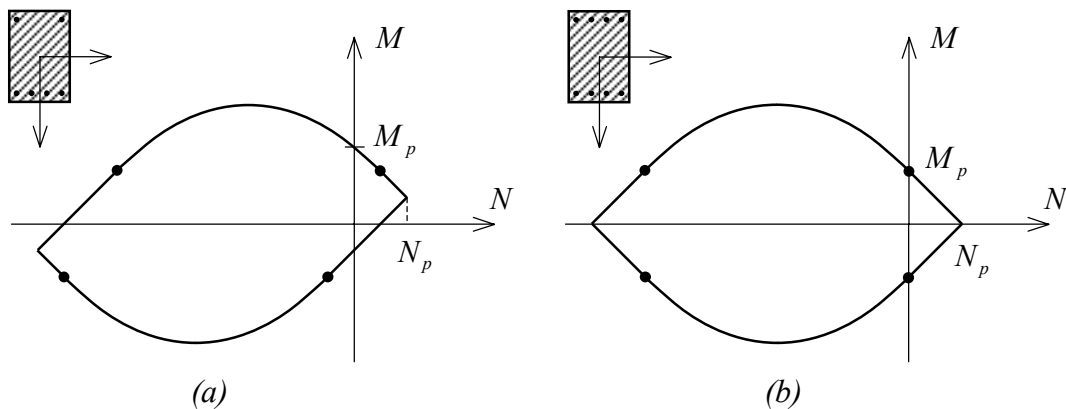


Fig. 7.20: Yield contours of reinforced concrete cross-sections with: different top and bottom reinforcements; identical top and bottom reinforcements.

7.4 Yield function and normality

The normality condition between loads and displacements of frames, as described in chapter 5, can also be demonstrated between the loads and deformations of a plastic hinge.

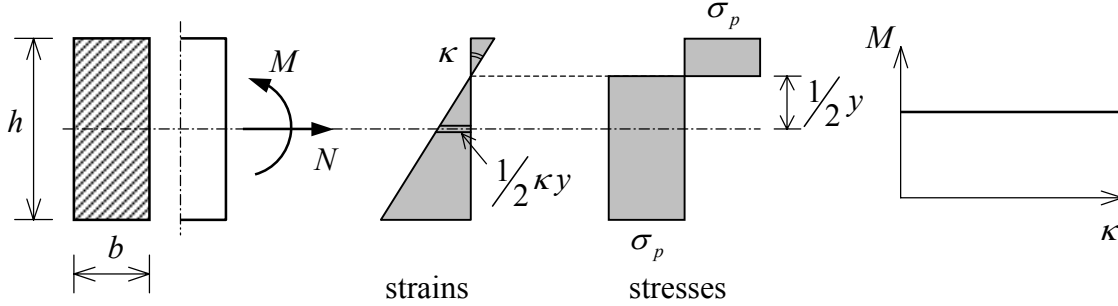


Fig. 7.21: Rectangular cross-section loaded by moment and normal force.

Fig. 7.21 shows a rectangular cross-section, loaded by a moment M and a normal force N . The strain and stress distributions are shown too, together with the M - κ diagram for given N (flat cross-sections remain flat). Starting from:

$$M = \frac{1}{4} \sigma_p b h^2 - \frac{1}{4} \sigma_p b y^2 \quad (7.37)$$

$$N = \sigma_p b y \quad (7.38)$$

For the yield function it can be derived:

$$\psi = M - \frac{1}{4} \sigma_p b h^2 + \frac{1}{4} \frac{N^2}{\sigma_p b} = 0 \quad (7.39)$$

$$\psi = \frac{M}{M_p} + \left(\frac{N}{N_p} \right)^2 - 1 = 0 \quad (7.40)$$

where $M_p = \sigma_p b h^2 / 4$ and $N_p = \sigma_p b h$.

The yield function is 2-dimensional and therefore it can be drawn as a yield contour (see Fig. 7.22). Because of symmetry only a quarter of the curve needs to be drawn ($M, N > 0$). The outward-pointing normal of the yield function can be obtained from the vector having the following components:

$$\frac{\partial \psi}{\partial M} = 1 \quad (7.41)$$

$$\frac{\partial \psi}{\partial N} = \frac{N}{2 \sigma_p b} = \frac{\sigma_p b y}{2 \sigma_p b} = \frac{y}{2} \quad (7.42)$$

From the strain diagram of Fig. 7.21 it turns out that the deformation vector, determined by the curvature κ and strain $\varepsilon = \kappa y / 2$, coincides with the outward-pointing normal on the yield contour. This proves the normality between load and deformation. Also in this case,

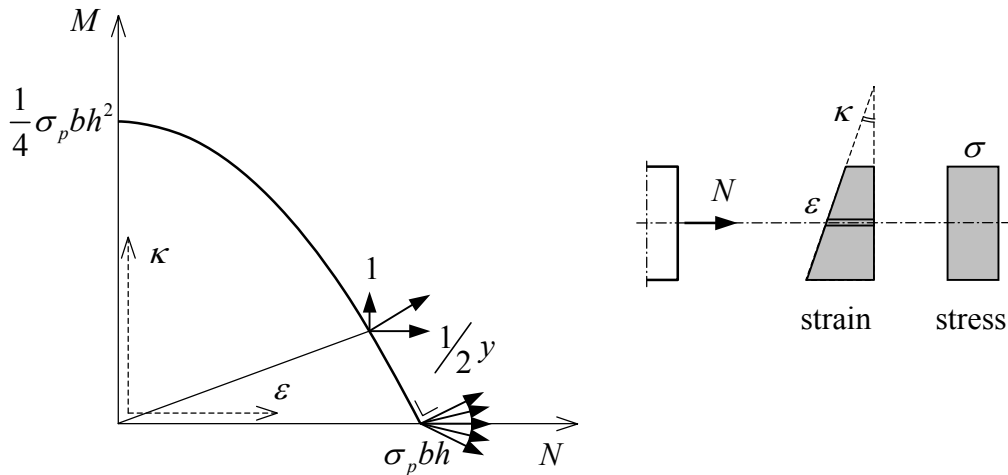


Fig. 7.22: Yield contour of rectangular cross-section.

it does not concern the absolute values of the plastic deformations but their relative increments (incremental deformations). For the case $N = 0$, the deformation vector is uniquely defined. This in contrast with the case $M = 0$, where the deformation vector can be obtained from a range of possibilities, bounded by the normal(s) on the yield contour(s) in that point ($\partial\psi/\partial M = \pm 1$, $\partial\psi/\partial N = h/2$). For $M > 0$ and $N < 0$ the yield contour can be obtained by reflection of the curve in Fig. 7.22 with respect to the line $N = 0$.

The normality condition can be extended to rotation and elongation in a plastic hinge. As mentioned before, the adoption of ideal-plastic material behaviour leads to the situation that plastic hinges are concentrated in one single cross-section. The beam parts rotate as rigid bodies about this cross-section. In Fig. 7.23 a plastic hinge has been drawn, which is subjected to both a moment M and a normal force N . During rotation M and N remain constant.

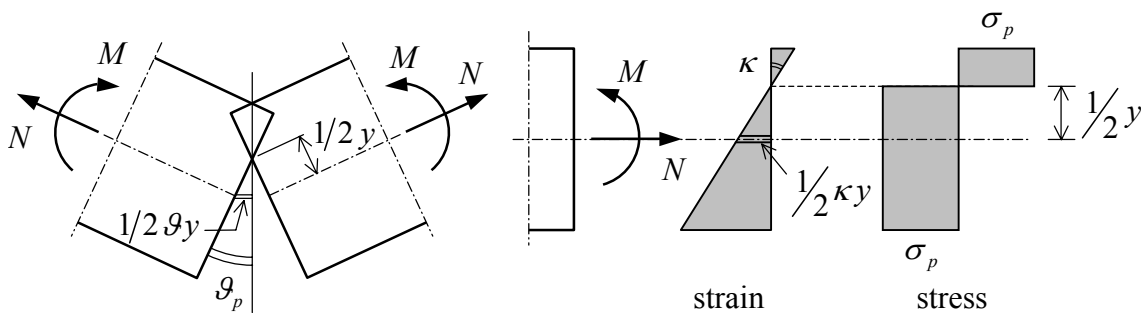


Fig. 7.23: Plastic hinge in rectangular cross-section.

For a given combination of M and N (situated on the yield contour), the energy dissipation E_d for a rotation ϑ equals:

$$E_d = M2\vartheta + N\vartheta y \tag{7.43}$$

For given M, N (which fixes y too) and ϑ , the dissipation E_d is constant, therefore:

$$dM2\vartheta + dN\vartheta y = 0 \tag{7.44}$$

From which it immediately follows that the deformation vector, determined by the components: rotation $2\mathcal{G}$ and elongation \mathcal{G}_y , is perpendicular to the yield surface. This result can be checked by using (7.41) and (7.42):

$$\frac{dM}{dN} = -\frac{\partial\psi}{\partial N} / \frac{\partial\psi}{\partial M} = -\frac{y}{2} \quad (7.45)$$

Equation (7.45) is identical to (7.44).

From the preceding text, under the assumptions of “cross-sections remain flat” and ideal-plastic material, it follows that the plastic deformations in a hinge can be described on basis of the normality condition. The normality property turns out to be important for problems, where the plastic strains in the plastic hinges play a role in the kinematical conditions. Some examples will be discussed.

Example 1: Frame structure with linear yield contour.

Consider a portal frame with two columns connected by hinges to the horizontal beam (see Fig. 7.24a). The cross-sections of the two columns are web-less I-sections, with a plastic M - N yield contour as displayed in Fig. 7.24a. The maximum allowable normal force is N_p and the maximum allowable moment is $M_p = N_p h / 2$. The frame is loaded by a horizontal force H and a vertical force V .

Firstly, an upper-bound solution will be given. Three mechanisms can be distinguished (Fig. 7.24b):

(1) A sway mechanism

$$Ha\mathcal{G} = 2M_p\mathcal{G} \rightarrow H = 2M_p/a$$

(2) A compression mechanism

$$Ve = N_p e \rightarrow V = N_p = 2M_p/h$$

(3) A combination mechanism

$$Ha\mathcal{G} + Ve = M_p\mathcal{G} + (M\mathcal{G} + Ne)$$

For the evaluation of this mechanism use is made of the linear M - N interaction formula:

$$M = M_p \left(1 - \frac{N}{N_p} \right)$$

and the simple normality relation $\mathcal{G}_m = \frac{1}{2} h\kappa$ or:

$$e = \frac{1}{2} h\mathcal{G}$$

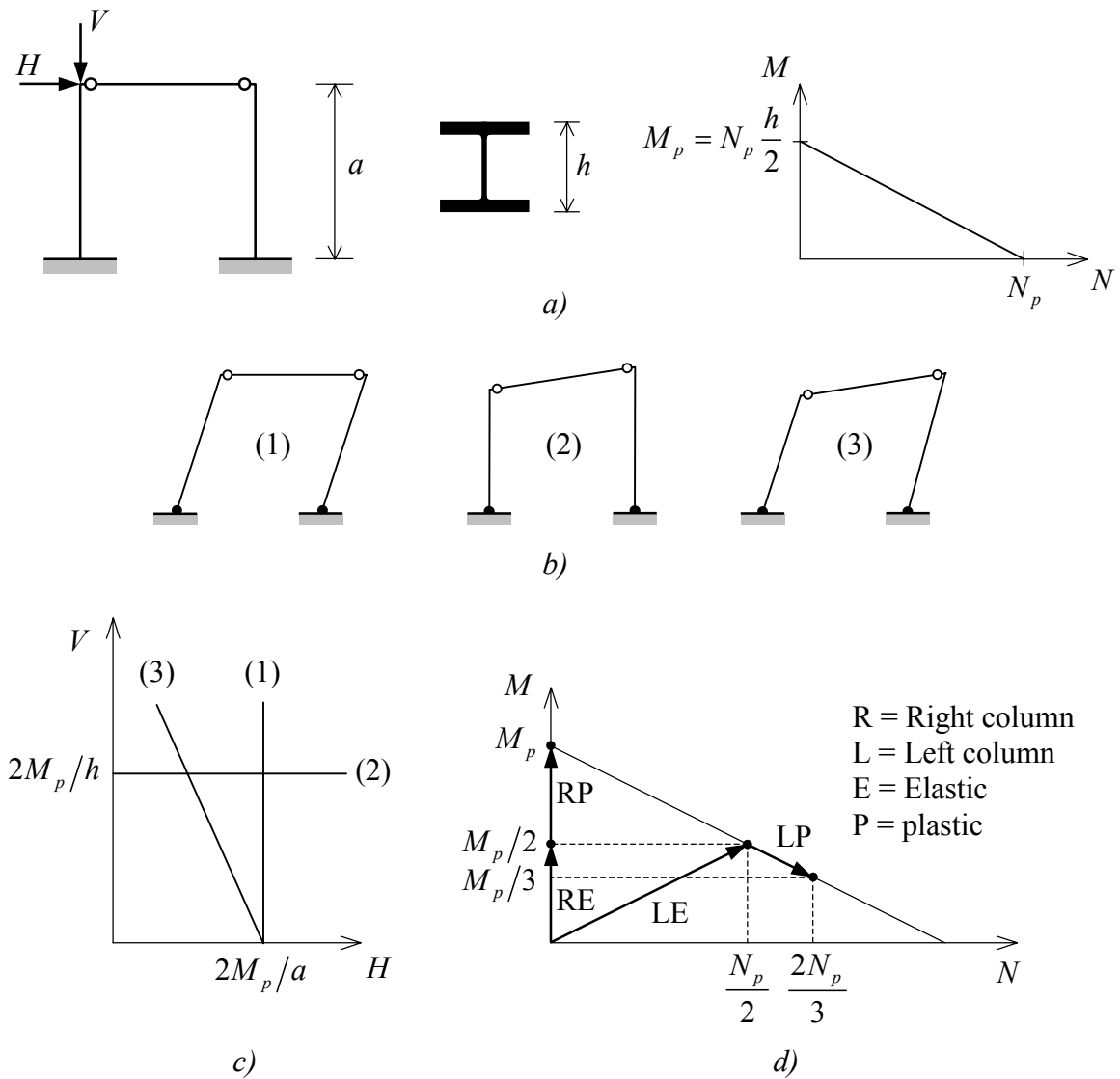


Fig. 7.24: Frame structure with linear yield contour.

Substitution provides:

$$Ha\vartheta + \frac{1}{2}hV\vartheta = M_p\vartheta + M_p\left(1 - \frac{N}{N_p}\right)\vartheta + N\frac{1}{2}h\vartheta$$

Division by ϑ and making use of $M_p = N_p h / 2$ leads to:

$$Ha + \frac{1}{2}hV = 2M_p$$

The three mechanisms are set out in Fig. 7.24c. It should be remarked that in practice normally a simpler procedure is followed: For each bar, the value of the normal failure force is estimated and on bases of that the full plastic moment determined. Then the failure

load is calculated. If the outcome is not satisfactory, the normal forces may be adapted and the calculation repeated.

Now, an elastic-plastic calculation is considered. A fixed ratio between H and V is chosen:

$$Ha = Vh$$

It is assumed that initially the structure is stress-free and without any deformation. When the load is slowly increased, the structure in first instance responds elastically. In this elastic phase it holds:

$$\begin{aligned} H_1 &= \text{transverse force in left column} &= H/2 \\ H_2 &= \text{transverse force in right column} &= H/2 \\ V &= \text{normal force in left column} \end{aligned}$$

In the left column the yield contour is reached if:

$$\frac{Ha}{2M_p} + \frac{V}{N_p} = 1$$

or if:

$$\frac{Ha}{2M_p} + \frac{Ha}{hN_p} = 1$$

With $N_p = 2M_p/h$ this condition becomes:

$$\frac{Ha}{2M_p} + \frac{Ha}{2M_p} = 1$$

For the external forces it then simply follows:

$$H = M_p/a \quad ; \quad V = M_p/h = N_p/2$$

In the right column:

$$\frac{Ha}{2M_p} + 0 = \frac{M_p}{2M_p} = \frac{1}{2} \leq 1$$

This column is not yielding yet. Fig. 7.24d shows which combinations of moment and normal force, are present in both columns.

For $h = M_p/a$, the load carrying capacity of the system has not been reached yet. The right column still can sustain a larger moment and the left column a larger normal force.

However, for the left column to carry a larger normal force it is required that the moment reduces. This is the elastic-plastic phase.

The external load increments ΔH_1 and ΔV of the left column have to satisfy:

$$\frac{\Delta H_1 a}{M_p} + \frac{\Delta V}{N_p} = 0$$

The increase of the transverse force ΔH_2 in the right column leads to plasticity if:

$$\frac{\Delta H_2 a}{M_p} + 0 = 1 - \frac{1}{2} = \frac{1}{2}$$

Further it holds:

$$\Delta H = \Delta H_1 + \Delta H_2$$

This brings the number of equations to three for the four unknowns ΔH , ΔH_1 , ΔH_2 and ΔV . Introduction of $\Delta V = a \Delta H / h$ then leads to:

$$\Delta H = \frac{M_p}{3a} \quad ; \quad \Delta V = \frac{M_p}{3h} = \frac{N_p}{6}$$

The total external load on the structure then equals:

$$H = \frac{M_p}{a} + \frac{M_p}{3a} = \frac{4}{3} \frac{M_p}{a} \quad ; \quad V = \frac{N_p}{2} + \frac{N_p}{6} = \frac{2}{3} N_p$$

For that situation the internal load in the left column is:

$$M = \frac{1}{3} M_p \quad ; \quad N = \frac{2}{3} N_p$$

and in the right column it is found:

$$M = M_p \quad ; \quad N = 0$$

In Fig. 7.24d these M - N combinations are drawn on the yield contour for both columns. It can easily be confirmed that this load indeed lies on the failure line, which also was found by the upper-bound analysis.

Example 2: Restrained beam, parabolic yield contour, geometrically non-linear

Fig. 7.25a shows a beam, which is restrained at both sides in such a manner that horizontal displacements are impossible. The relation between the force F and the displacement w of the middle of the beam has to be determined. The material is rigid plastic and the yield contour is as given in Fig. 7.22 (rectangular cross-section).

The problem is simple, as long as the analysis is geometrically linear. The beam does not deform until at $F = 8M_p/l$ failure occurs; the downward displacement w is indeterminate for

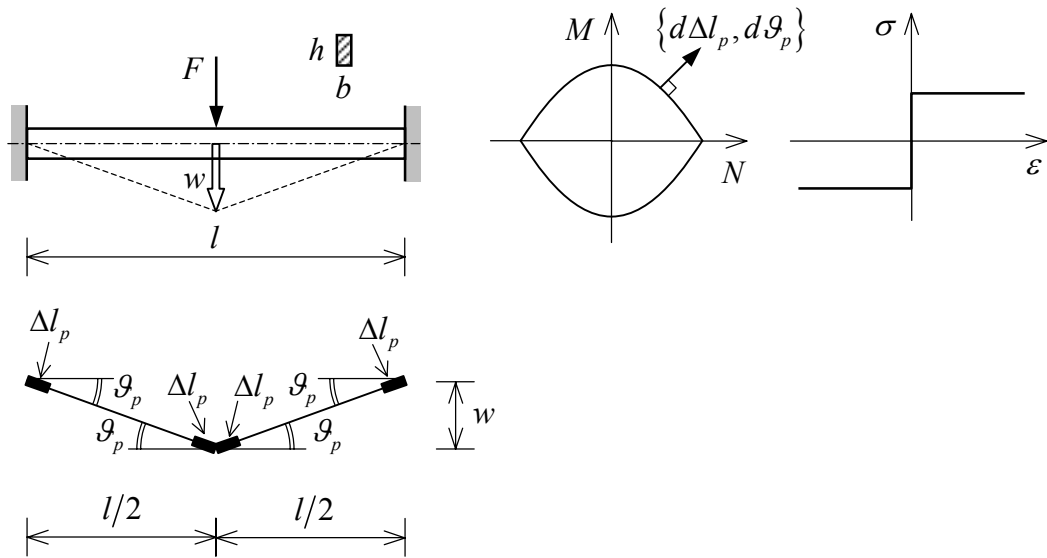


Fig. 7.25: Beam restrained at both ends.

the load (see Fig. 7.26). However, for large values of w the geometrical non-linear effects cannot be neglected anymore. Because the deflection w in combination with the given boundary conditions, cause the development of considerable plastic strains, generating normal forces. The way of how this happens including the influence of this on the total force transmission will be analysed below.

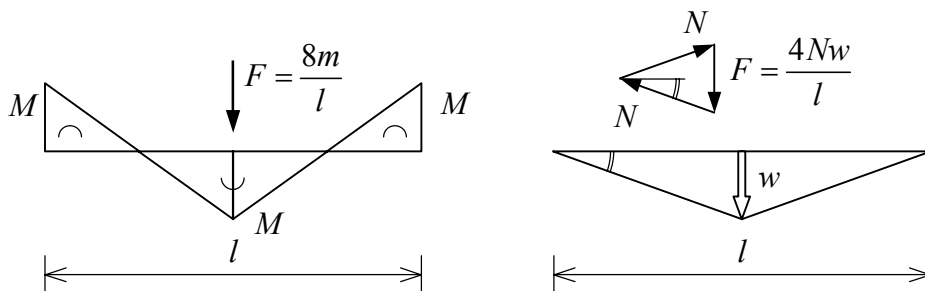


Fig. 7.26: Geometrical non-linear effects

On bases of the equilibrium equation, the normal force in the middle of the beam is equal to the normal forces at its restraints. If it is given that both middle and end cross-sections are yielding and the yield contour is symmetrical with respect to the N -axis, it can be concluded that the magnitudes of fixed-end and the field moments are equal. Finally, it can be shown (on basis of symmetry this is already very plausible, see Fig. 7.23) that the plastic elongation in the hinges at both fixed ends is equal to (ΔI_p) and in the middle of the beam is twice that amount $(2\Delta I_p)$. Using these assumptions, the equations will be composed, which are necessary for the solution of the problem.

1. Kinematical equations

Between the plastic angular displacement ϑ_p and the downward displacement w the following relation exists:

$$\vartheta_p = \frac{2w}{l} \quad (7.46)$$

The proposition of Pythagoras is used for the determination of the relation between the plastic elongation Δl_p and the downward displacement w :

$$\left(\frac{1}{2}l_p\right)^2 + w^2 = \left(\frac{1}{2}l_p + 2\Delta l_p\right)^2$$

Neglecting the quadratic terms in Δl_p leads to:

$$\Delta l_p = \frac{w^2}{2l} \quad (7.47)$$

2. Constitutive equations

The first constitutive equation is the yield condition. For the hinge in the field, it reads:

$$\psi = \frac{M}{M_p} + \left(\frac{N}{N_p}\right)^2 - 1 = 0 \quad (7.40)$$

The second constitutive equation follows from the normality condition (compare with (5.16)):

$$d\vartheta_p = \lambda \frac{\partial \psi}{\partial M} \quad ; \quad d(\Delta l_p) = \lambda \frac{\partial \psi}{\partial N}$$

Both equations are set up for infinitesimal increments. This is necessary because in this case, ϑ_p and Δl_p are continuously changing and normality only holds for displacement increments. Elimination of the unknown scale factor λ leads to:

$$\frac{d(\Delta l_p)}{d\vartheta_p} = \frac{\partial \psi / \partial N}{\partial \psi / \partial M} = \frac{2N/N_p^2}{1/M_p} = 2 \left(\frac{N}{N_p}\right) \left(\frac{M_p}{N_p}\right)$$

Through $M_p/N_p = h/4$ (rectangular cross-section), it finally follows:

$$\frac{d(\Delta l_p)}{d\vartheta_p} = \frac{h}{2} \left(\frac{N}{N_p}\right) \quad (7.48)$$

Note that the normality condition is not formulated in curvatures and strains, but in angular displacements and elongations. The reason is that it is useless to talk about strains and curvatures in relation to plastic hinges, because these quantities are infinite over an infinitesimal small length.

3. Equilibrium equation

The equilibrium equation reads (see Fig. 7.25b):

$$F = \frac{8M}{l} + \frac{4Nw}{l} \quad (7.49)$$

The first term is the geometrical linear bending contribution and the second term is the non-linear membrane action.

With the relations (7.46) up to (7.49) the considered problem is completely described. As first step in the solution procedure, the normality equation given by (7.48) is worked out further, by making use of the kinematical relations (7.46) and (7.47).

On basis of (7.46) it holds:

$$d\vartheta_p = \frac{2dw}{l}$$

On basis of (7.47) it holds:

$$d\Delta l_p = \frac{2wdw}{2l}$$

Substitution into (7.48) provides:

$$\frac{w}{2} = \frac{h}{2} \left(\frac{N}{N_p} \right) \quad \text{or} \quad \frac{N}{N_p} = \frac{w}{h} \quad (7.50)$$

The normal force appears to be proportional to the deflection. Naturally, the magnitude of N cannot exceed N_p . This means that the formula above is valid only for $0 \leq w \leq h$.

Now N is known as a function of w , the moment M can be determined too. Substitution of (7.50) into the yield condition (7.40) leads to:

$$\frac{M}{M_p} = 1 - \left(\frac{w}{h} \right)^2 \quad (7.51)$$

Combination of (7.50) and (7.51) with the equilibrium equation (7.49) provides the desired relation between F and w :

$$F = \frac{8M_p}{l} \left[1 - \left(\frac{w}{h} \right)^2 \right] + \frac{4N_p}{l} \frac{w^2}{h}$$

Through $M_p/N_p = h/4$ it finally follows:

$$F = \frac{8M_p}{l} \left[1 + \left(\frac{w}{h} \right)^2 \right] \quad ; \quad 0 \leq w \leq h \quad (7.52)$$

This relation is drawn in Fig. 7.27. Due to non-linear effects, the load carrying capacity for $w = h$ twice as big as for $w = 0$. So, during deformation, the force distribution is transferred from pure bending action ($M = M_p, N = 0$) into pure membrane action ($M = 0, N = N_p$).

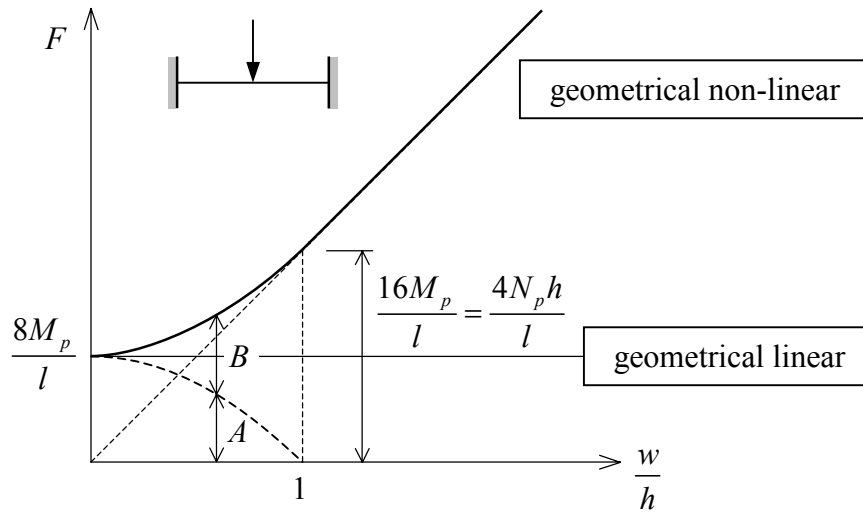


Fig. 7.27: Force-deflection curve for both geometrical linear and non-linear cases.

For $w > h$ the beam keeps taking up the load completely through membrane action. From (7.49) the relation between F and w can be derived to be:

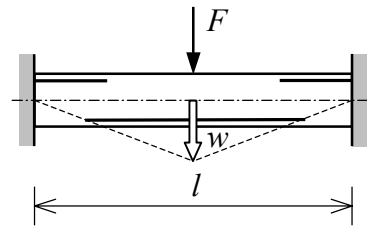
$$F = 0 + \frac{4N_p w}{l} = \frac{4N_p w}{l} \quad ; \quad w > h \quad (7.53)$$

This part of the load-displacement diagram is displayed in Fig. 7.27 too. The load carrying capacity of the beam seems to become infinite for infinite displacements. Naturally, this is not correct. In practice, the deformation capacity of the beam is already exceeded for several times the elementary failure load, which means that fracture will occur.

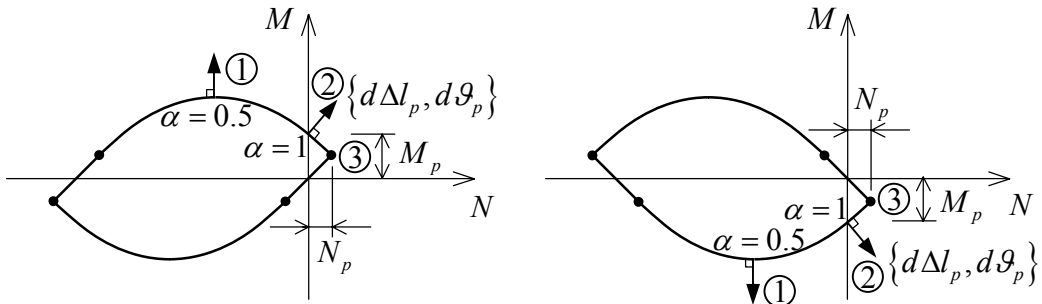
Example 3: Restrained reinforced concrete beam, geometrically non-linear

Consider the restrained concrete beam of Fig. 7.28a. In the middle cross-section only bottom reinforcement is present, and at the fixed ends only top reinforcement of the same amount. Therefore, for the middle cross-section the upper part of the yield contour of Fig. 7.19 is valid. The yield contour for the fixed ends can be found by reflection of the contour about the N -axis.

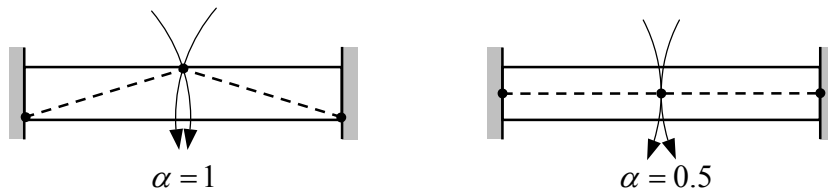
It is started with a geometrically linear consideration, as done for the previous problem. It seems to be obvious that the elementary failure load F_p , just as for the homogeneous beam is given by $8M_p/l$. However, for reinforced concrete beams this is not correct. Therefore, the yield contour for the middle cross-section is considered. At the point $N = 0, M = M_p$, the deformation vector $\{d\Delta l_p, d\vartheta_p\}$ has a horizontal component, which indicates a plastic elongation of the central fibre. Similarly it holds that for $N = 0, M = -M_p$ the central fibres of the fixed ends are changing length too. Because of the support conditions, the total length of the beam remains constant (no mechanism has developed yet). Therefore, for a kinematical admissible displacement field, it is required that the sum of the plastic elongations in the middle and the ends of the beam is equal to zero. In this symmetrical



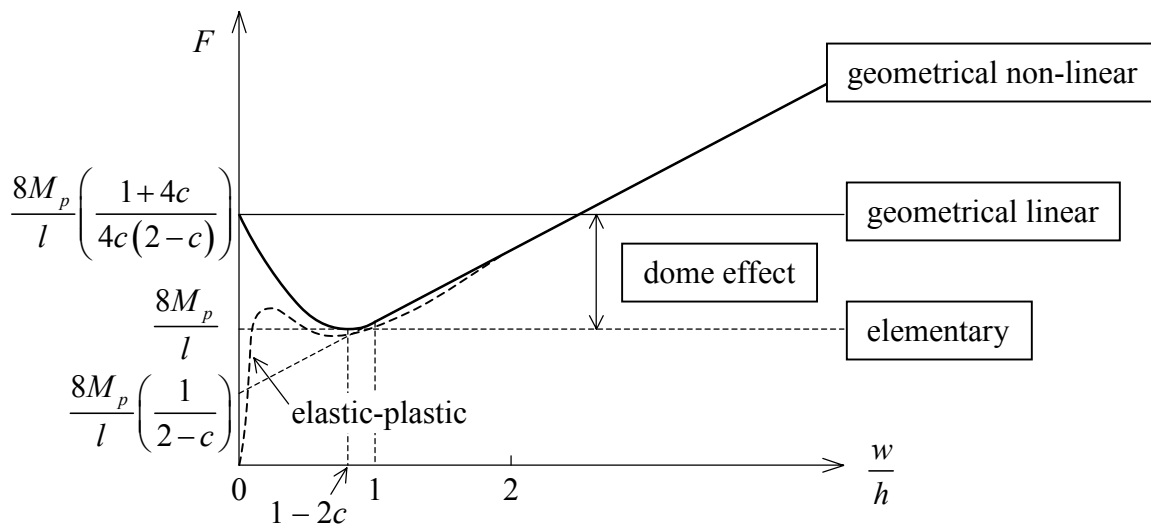
a) reinforced concrete beam



b) yield contours at the middle and ends of the beam for identical reinforcement percentages, respectively



c) geometrical explanation of the dome effect



d) load-deflection diagram

Fig. 7.28: Analysis of reinforced concrete beam.

case, this only can be achieved by making all separate elongations equal to zero. Thus, the deformation vector $\{d\Delta l_p, d\vartheta_p\}$ has to be vertical. Therefore, the moments have to be maximal and the failure load is given by:

$$F_p = \frac{8M_{\max}}{l} = \frac{8M_p}{l} \left(\frac{1 + \frac{1}{4c}}{2 - c} \right) \quad (7.54)$$

The difference with the elementary failure load $8M_p/l$, is originating from so-called retaining forces and is called the *dome effect*. Fig. 7.28c gives a geometric interpretation of this effect. For the stress distribution with $N = 0$ and $M = M_p$, the position of the neutral line in the beam middle is high and at the ends it is low. These stress zeros, also form the hinges of the mechanism. The Figure shows that during movement as a mechanism a normal force is created, which contradicts the assumption that $N = 0$. Therefore, a mechanism is possible only if all three hinges are situated at the same height, which in this case because of symmetry is in the geometric centre of gravity of the beam ($\alpha = 1/2$, Fig. 7.28c).

Now, the geometrical non-linear problem will be worked out. The kinematical relations and equilibrium equation remain the same as for the homogeneous beam. Naturally, the constitutive equations will change. The yield condition becomes:

$$\psi = M - M_p + \frac{1}{2}hN \left(1 - 2c + c \frac{N}{N_p} \right) = 0 \quad (7.55)$$

For the normality condition it follows:

$$\begin{aligned} d\vartheta_p = \lambda \quad ; \quad \frac{\partial \psi}{\partial M} = \lambda \\ d(\Delta l_p) = \lambda \quad ; \quad \frac{\partial \psi}{\partial N} = \frac{1}{2}h \left(1 - 2c + 2c \frac{N}{N_p} \right) \end{aligned}$$

Combination provides:

$$\frac{d(\Delta l_p)}{d\vartheta_p} = \frac{1}{2}h \left(1 - 2c + 2c \frac{N}{N_p} \right) \quad (7.56)$$

The derivation is similar to that of the homogeneous beam as discussed in one of the foregoing sections. It still holds that $d(\Delta l_p)/d\vartheta_p = w/2$, changing (7.56) into:

$$\frac{w}{2} = \frac{h}{2} \left(1 - 2c + 2c \frac{N}{N_p} \right) \rightarrow \frac{N}{N_p} = \frac{1}{2c} \left(\frac{w}{h} - 1 + 2c \right)$$

The moment M can be obtained after substitution into the yield criterion:

$$M = M_p - \frac{1}{2}hN_p \left(\frac{1}{4c} \right) \left(\frac{w}{h} - 1 + 2c \right) \left(2 - 4c + \frac{w}{h} - 1 + 2c \right) \rightarrow$$

$$M = M_p - \frac{1}{2}hN_p \left(\frac{1}{4c} \right) \left(\left(\frac{w}{h} \right)^2 - (1 - 2c)^2 \right)$$

From equilibrium it then follows:

$$F = \frac{8}{l} \left(M_p - \frac{hN_p}{8c} \left(\left(\frac{w}{h} \right)^2 - (1 - 2c)^2 \right) + \frac{1}{2}w \frac{N_p}{2c} \left(\frac{w}{h} - 1 + 2c \right) \right) \rightarrow$$

$$F = \frac{8}{l} \left(M_p + \frac{hN_p}{8c} (1 - 2c)^2 - \frac{1}{2}w \frac{N_p}{2c} (1 - 2c) + \frac{hN_p}{8c} \left(\frac{w}{h} \right)^2 \right)$$

With $M_p = hN_p(1 - c/2)$ (see (7.25)) this relation can be rewritten in a more organised way:

$$F = \frac{8M_p}{l} \frac{(4c + 1) - (2 - 4c) \left(\frac{w}{h} \right) + \left(\frac{w}{h} \right)^2}{4c(2 - c)} ; \quad 0 \leq w \leq h \quad (7.57)$$

Again, the relation between F and w is a parabola. The first term corresponds with the previously found dome effect from the geometrical linear calculation. The second term reduces F already for small values of w . This is the price that has to be paid for the large compressive force that actually creates the dome effect. The last term is quadratic in w and reflects the decrease of the normal force because of the bending deflection. With that, the F - w curve first reaches a minimum (see Fig. 7.28d), and then starts to rise as soon as the normal force becomes positive. The position of the minimum coincides with $N = 0$ and therefore exactly coincides with the elementary failure load $8M_p/l$. Formula (7.57) is valid up to $w = h$. At that deflection it holds $N = N_p$ and the point of the yield contour is reached. For $w > h$ the stress distribution remains the same. Therefore, it holds:

$$N = N_p ; \quad M = \frac{M_p}{2 - c}$$

Substitution in the equilibrium equation (7.49) in combination with (7.25) yields:

$$F = \frac{8}{l} \left(\frac{M_p}{2 - c} + \frac{1}{2}N_p w \right) = \frac{8M_p}{l} \left(\frac{1 + \frac{w}{h}}{2 - c} \right) ; \quad w > h \quad (7.58)$$

Just as for the homogeneous beam, this is a straight branch. However, the difference is that $M \neq 0$, which means that the line does not pass through the origin. Therefore, even for

large deflections a contribution by bending remains present and the displacement curve does not degenerate into a pure catenary curve.

Summarising:

- For $w = 0$ the stress distribution in the cross-section(s) corresponds to point 1 on the yield contour(s) ($N < 0$);
- For $0 < w/h \leq 1-2c$ under increasing deflection, the stress distribution in the cross-section(s) shifts on the yield contour(s) from point 1 to point 2 ($N = 0$);
- For $1-2c < w/h \leq 1$ under increasing deflection, the stress distribution in the cross-section(s) shifts on the yield contour(s) from point 2 to point 3 ($N = N_p$);
- For $w/h > 1$ under increasing deflection, the stress distribution in the cross-section(s) remains fixed at point 3 of the yield contour(s).

Finally, in Fig. 7.28d the elastic-plastic curve of F versus w/h is sketched too. It can be concluded that in that case the dome effect is less pronounced: only for sufficiently stiff constructions the dome effect can really be important, which is also confirmed by experiments. Anyway, in the design practice the dome effect is not taken into account. On the other hand, the increase of the load carrying capacity through membrane action is of great importance in case a concrete structure is exposed to fire.

8 The effect of shear forces on plastic frame behaviour

8.1 Steel cross-sections

Usually a plastic hinge has to transmit a transverse force too. This means that in the cross-section, in addition to normal stresses shear stresses are present. According to the lower-bound theorem the calculation then can be based on the following basic assumption:

“When in a cross-section in addition to normal stresses σ shear stresses τ are present, then these stresses can be distributed across the section in the most favourable manner.”

At those positions where both normal and shear stresses are present, the yield criterion of von Mises has to be satisfied:

$$\sigma_p = \sqrt{\sigma_x^2 + \sigma_y^2 - \sigma_x \sigma_y + 3\tau^2} \quad (8.1)$$

On basis of this relation the ultimate value of the shear stress τ in the absence of normal stresses becomes:

$$\tau_p = \frac{\sigma_p}{\sqrt{3}} = 0.58\sigma_p$$

It is called to mind, that shear stresses are linked to the difference $(\partial\sigma/\partial x)dx$ between the normal stresses in one fibre at both sides of a considered cross-sectional slice of the beam having thickness dx (see Fig. 8.1). When at both sides the yield stress σ_p is present, there is no difference in normal stress, which means that the shear stress is zero (see Fig. 8.2).

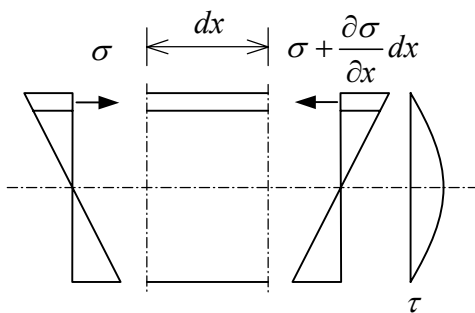


Fig. 8.1: Bending and shear elastic stage.

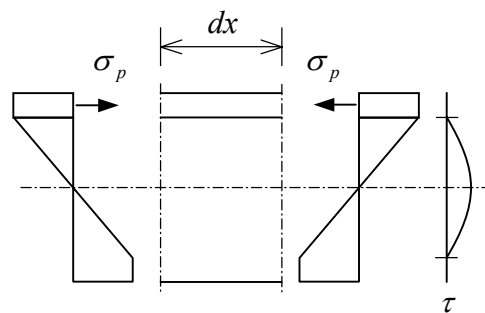


Fig. 8.2: Bending and shear elastic-plastic stage.

Therefore, shear stresses generated by the transverse force are present only in the part of the cross-section around the neutral line, which is the area where the bending stresses have not yet reached the value of σ_p .

8.1.1 Rectangular cross-sections

A cantilever beam is considered with a rectangular cross-section. The beam is loaded by a point load at the free end (Fig. 8.3). As discussed above, the stress distribution in the elastic part of the beam easily can be obtained from equilibrium. The normal stresses vary linearly across the height of the beam, the shear stresses are parabolic. It also was

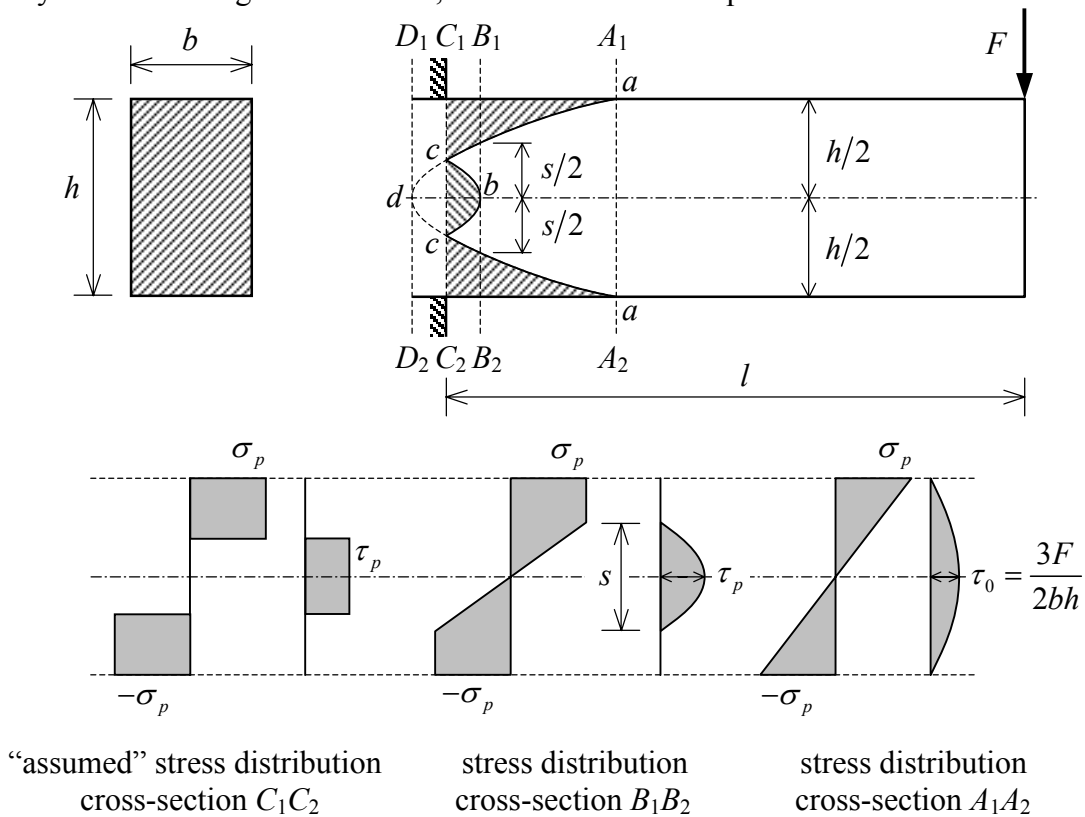


Fig. 8.3: Elastic-plastic stress distribution in a rectangular beam.

mentioned that, as soon as the extreme fibres start yielding due to bending action, the shear stresses will be concentrated in the centre of the beam around the neutral line where the normal stress distribution is still linear. The height of this area is indicated by s . The distribution of the shear stresses remains parabolic. If the height s becomes small enough, the maximum value of the shear stress reaches the yield shear stress. The magnitude of s for which this happens equals:

$$\tau = \frac{3T}{2bs} = \tau_p \quad \rightarrow \quad s = \frac{3T}{2b\tau_p}$$

where T is the transverse force in the beam, which is equal to F in this case. In the beam of Fig. 8.3 it is assumed that this state occurs in section B_1B_2 . At the left side of section B_1B_2 the shear yield area is spreading out. The state of failure is attained when this shear yield-area reaches the bending-yield area. In Fig. 8.3, this is the case in section C_1C_2 . It does not turn out to be easy to find the correct stress distribution in this cross-section. A very simple and most obvious assumption is a distribution of rectangular stress fields, as indicated in Fig. 8.4a. For this stress distribution the interaction formula for T and M are derived.

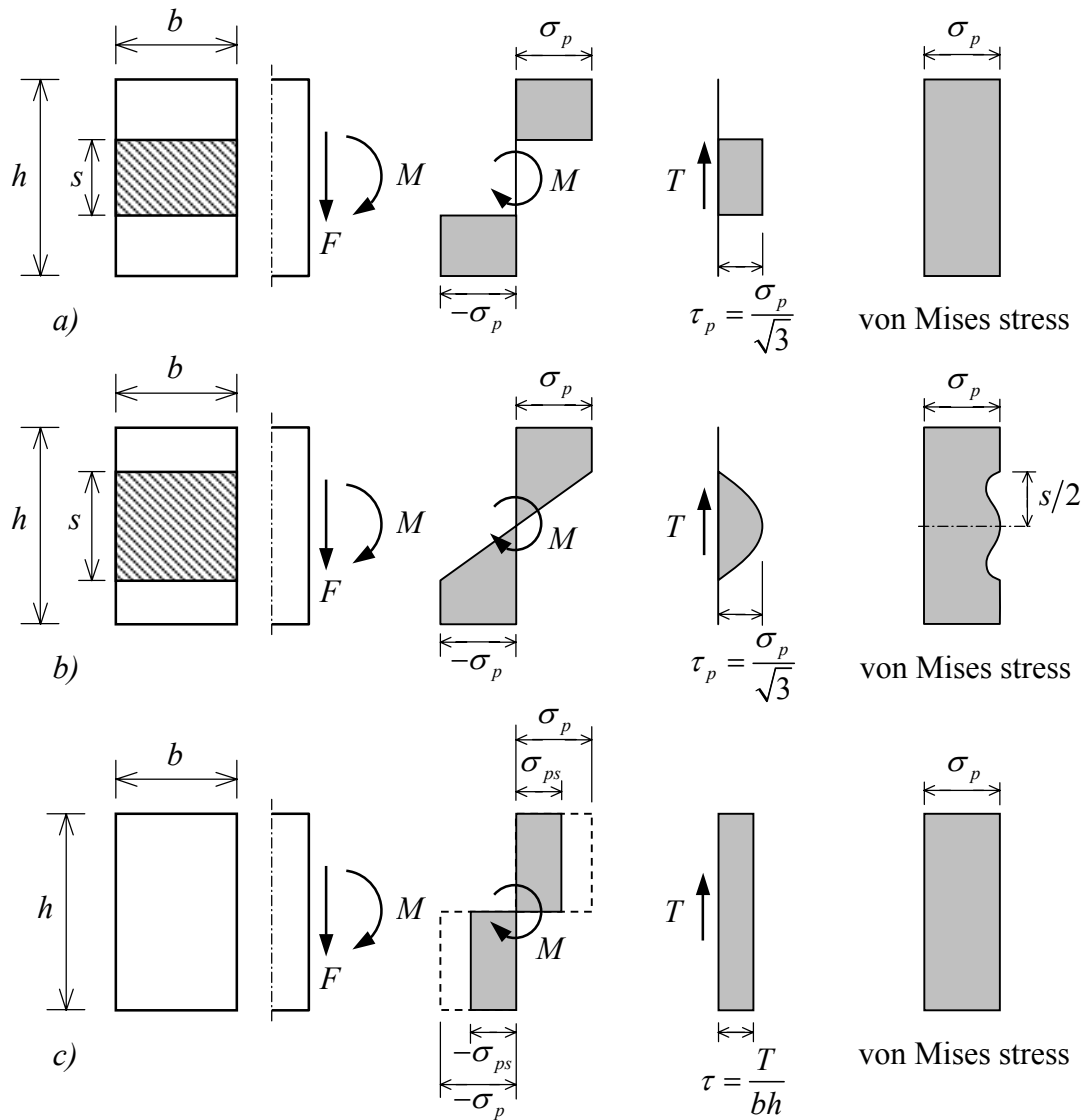


Fig. 8.4: Three possible stress distributions in the end-cross-section.

$$\left. \begin{aligned} T &= \frac{\sigma_p}{\sqrt{3}} bs \\ T_p &= \frac{\sigma_p}{\sqrt{3}} bh \end{aligned} \right\} \rightarrow \frac{T}{T_p} = \left(\frac{s}{h} \right) \quad \text{(a)}$$

$$\left. \begin{aligned} M &= \frac{1}{4} bh^2 \sigma_p - \frac{1}{4} bs^2 \sigma_p \\ M_p &= \frac{1}{4} bh^2 \sigma_p \end{aligned} \right\} \rightarrow \frac{M}{M_p} = 1 - \left(\frac{s}{h} \right)^2 \quad \text{(b)}$$

combination of (a) and (b) delivers:

$$\frac{M}{M_p} + \left(\frac{T}{T_p} \right)^2 = 1 \quad (8.2)$$

It is interesting to investigate what interaction formula is obtained for the stress distribution present in section B_1B_2 of Fig. 8.3 (also see Fig. 8.4b):

$$\left. \begin{aligned} T &= \frac{2}{3} \frac{\sigma_p}{\sqrt{3}} bs \\ T_p &= \frac{\sigma_p}{\sqrt{3}} bh \end{aligned} \right\} \rightarrow \frac{T}{T_p} = \frac{2}{3} \left(\frac{s}{h} \right) \quad (c)$$

$$\left. \begin{aligned} M &= \frac{1}{4} bh^2 \sigma_p - \frac{1}{12} bs^2 \sigma_p \\ M_p &= \frac{1}{4} bh^2 \sigma_p \end{aligned} \right\} \rightarrow \frac{M}{M_p} = 1 - \frac{1}{3} \left(\frac{s}{h} \right)^2 \quad (d)$$

combination of (c) and (d) delivers:

$$\frac{M}{M_p} + \frac{3}{4} \left(\frac{T}{T_p} \right)^2 = 1 \quad ; \quad \frac{T}{T_p} \leq \frac{2}{3} \quad (8.3)$$

It is remarkable that (8.2) provides larger values than (8.3).

A third possibility is to distribute the shear stress uniformly across the entire cross-section (computational model of Heyman and Dutton, see Fig. 8.4c). Doing so, the normal stresses are lowered to a reduced yield stress σ_{ps} , which follows from the applied yield criterion:

$$\sigma_{ps} = \sigma_p \sqrt{1 - \frac{3\tau^2}{\sigma_p^2}}$$

On basis of this stress distribution, it is quite simple to derive:

$$\left. \begin{aligned} T &= \tau bh \\ T_p &= \tau_p bh \end{aligned} \right\} \rightarrow \frac{T}{T_p} = \frac{\tau}{\tau_p} \quad (e)$$

$$\left. \begin{aligned} M &= \frac{1}{4} bh^2 \sigma_{ps} \\ M_p &= \frac{1}{4} bh^2 \sigma_p \end{aligned} \right\} \rightarrow \frac{M}{M_p} = \frac{\sigma_{ps}}{\sigma_p} = \sqrt{1 - \frac{3\tau^2}{\sigma_p^2}} \quad (f)$$

Combination of (e) and (f) gives:

$$\frac{M}{M_p} = \sqrt{1 - \left(\frac{T}{T_p}\right)^2} \rightarrow \left(\frac{M}{M_p}\right)^2 + \left(\frac{T}{T_p}\right)^2 = 1 \quad (8.4)$$

Anyway, the “lower-bound solutions” provided by (8.2) up to (8.4) are no real lower-bound solutions. For this solution it is required that, the equilibrium is investigated of the 2-dimensional stress state in the rectangle $A_1C_1C_2A_2$ (see Fig. 8.3). This exercise has been done by Drucker, who found the following result:

$$\frac{M}{M_p} + \left(\frac{T}{T_p}\right)^4 = 1 \quad (8.5)$$

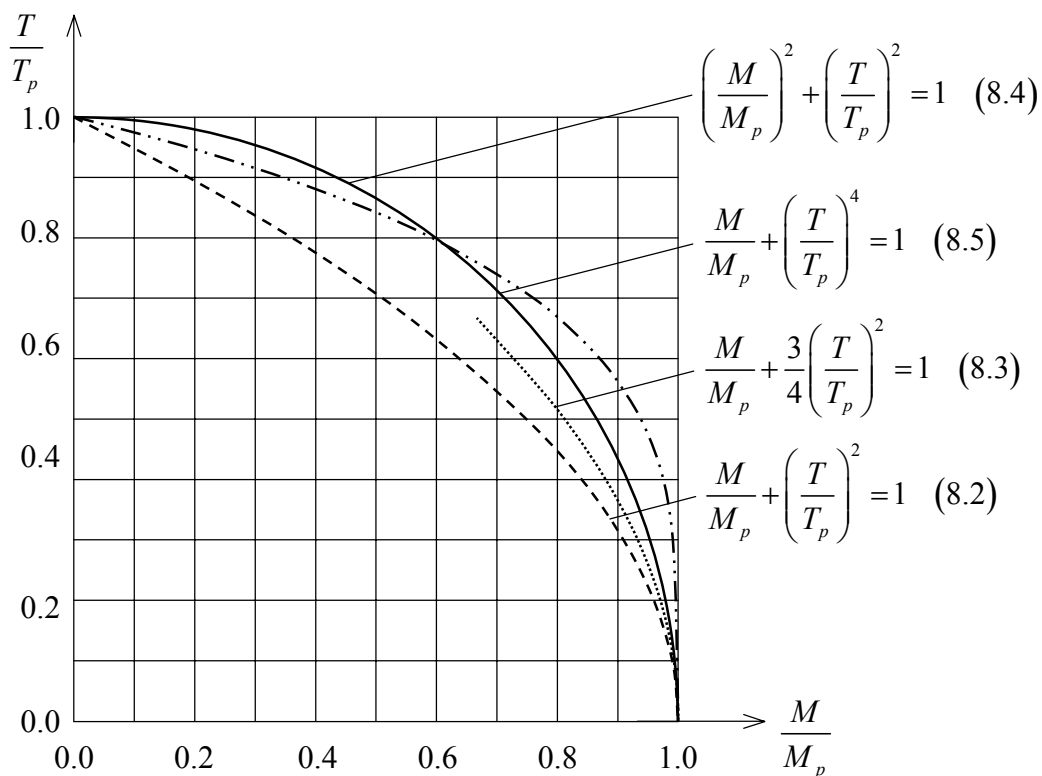


Fig. 8.5: Various results for bending shear interaction for rectangular beams.

In Fig. 8.5 the interaction formulae are displayed in graphical form. It can be observed that (8.2) and (8.3) are good lower bounds. However, solution (8.4) is too optimistic for large values of T .

Example: Simply supported beam with point load in the middle

This example is an illustration of the importance of the reduction of the full-plastic moment by a transverse force. Fig. 8.6 shows a statically determined beam with rectangular cross-section, loaded by a point load in the middle of the beam. The transverse force is equal to:

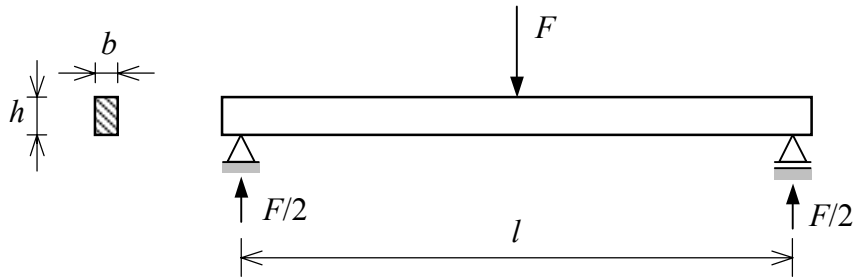


Fig.8.6: Simply supported beam with point load in the middle.

$$T = \frac{F}{2} = \frac{2M}{l} = \frac{M}{M_p} * \frac{2M_p}{l}$$

Through $M_p = \sigma_p b h^2 / 4$ and $T_p = \sigma_p b h / \sqrt{3}$ it follows:

$$\frac{T}{T_p} = \frac{M}{M_p} * \frac{2M_p}{T_p} = \frac{M}{M_p} \left(\frac{h\sqrt{3}}{2l} \right)$$

Combination with (8.3) provides:

$$\left(\frac{M}{M_p} \right)^2 + \left(\frac{M}{M_p} \right)^2 \left(\frac{h\sqrt{3}}{2l} \right)^2 = 1 \rightarrow \left(\frac{M}{M_p} \right)^2 \left(1 + \frac{3h^2}{4l^2} \right) = 1$$

$$\text{For } \frac{h}{l} = \frac{1}{10} \text{ it follows: } \left(\frac{M}{M_p} \right)^2 = \left(1 + \frac{3}{4} * \frac{1}{100} \right) = 1 \rightarrow M = 0.996 M_p$$

$$\text{For } \frac{h}{l} = \frac{1}{5} \text{ it follows: } \left(\frac{M}{M_p} \right)^2 = \left(1 + \frac{3}{4} * \frac{1}{25} \right) = 1 \rightarrow M = 0.985 M_p$$

$$\text{For } \frac{h}{l} = \frac{1}{2} \text{ it follows: } \left(\frac{M}{M_p} \right)^2 = \left(1 + \frac{3}{4} * \frac{1}{4} \right) = 1 \rightarrow M = 0.918 M_p$$

It can be concluded that only for very short high beams ($h = l/2$) the influence of the shear force becomes significant.

8.1.2 I-sections

For I-sections (see Fig. 8.7), it is assumed that the transverse force is carried by the web. For simplicity, a uniform shear stress distribution is adopted, comparable with the model of Heyman and Dutton (Fig. 8.4c). For calculation of the moment in the web the reduced yield stress σ_{ps} has to be applied (because of the shear stress) and in the flanges, the yield stress σ_p . It follows:

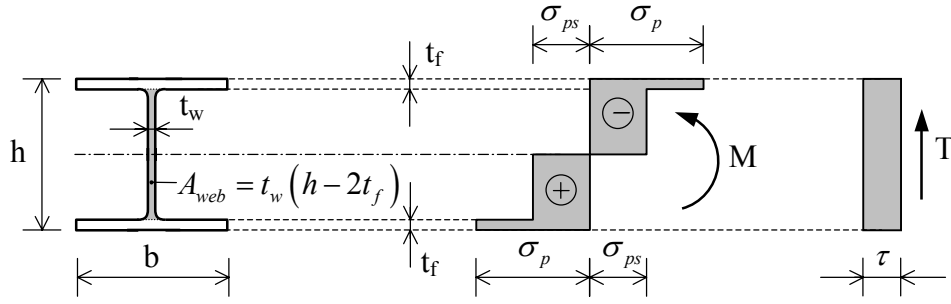


Fig. 8.7: I-beam.

$$\left. \begin{aligned} T &= A_{web} \tau \\ T_p &= A_{web} \frac{\sigma_p}{\sqrt{3}} \end{aligned} \right\} \rightarrow \frac{T}{T_p} = \frac{\tau \sqrt{3}}{\sigma_p} \neq$$

$$\sigma_{ps} = \sigma_p \sqrt{1 - \frac{3\tau^2}{\sigma_p^2}}$$

So:

$$\sigma_{ps} = \sigma_p \sqrt{1 - \left(\frac{T}{T_p} \right)^2} \quad (a)$$

$$M = M_p - M_{p,web} \left(1 - \frac{\sigma_{ps}}{\sigma_p} \right) \rightarrow \frac{M}{M_p} = 1 - \frac{M_{p,web}}{M_p} \left(1 - \frac{\sigma_{ps}}{\sigma_p} \right) \quad (b)$$

Or:

$$\frac{M_{p,web}}{M_p} = \frac{A_{web} \frac{h}{4}}{A_{flange} h + A_{web} \frac{h}{4}} = \frac{A_{web}}{4A_{flange} + A_{web}} = \frac{A_{web}}{2A - A_{web}} \quad (c)$$

Combination of (a), (b) and (c) yields:

$$\frac{M}{M_p} = 1 - \left(1 - \sqrt{1 - \left(\frac{T}{T_p} \right)^2} \right) \frac{A_{web}}{2A - A_{web}} \quad (8.6)$$

Fig. 8.8 show the range of all interaction curves obtained by (8.6), for the broad-flanged HE series and IPE series, respectively. For comparison, the interaction curve for rectangular cross-sections according (8.4) can be found as well. For I-beams, the reduction is even less then for rectangular cross sections.

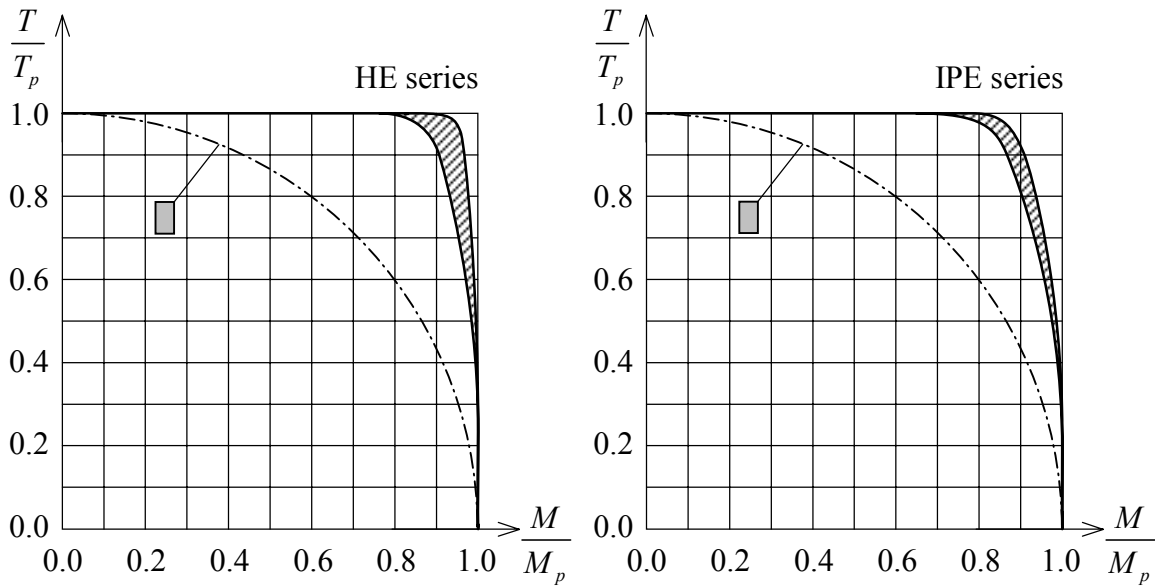


Fig. 8.8: Bending-shear interaction for HE and IPE sections..

8.2 Reinforced concrete cross-sections

8.2.1 Introduction

As mentioned in section 8.1, the influence of the transverse force on the ultimate load carrying capacity is quite limited. However, for concrete beams this may be quite different. This is caused by the low tensile strength of concrete, as a result of which the carrying of shear stresses quickly becomes a problem. Therefore, the transverse force indeed is important for concrete structures. The first extra possibility to transmit a transverse force is through the dome effect. Use is made of the fact that normally the load is applied on the top of the beam, while the supports are situated at the bottom. It is only effective for short high beams. If the dome effect is not sufficient, reinforcement to take up the transverse force has to be applied. This can be done by bended bars, but normally stirrups are used.

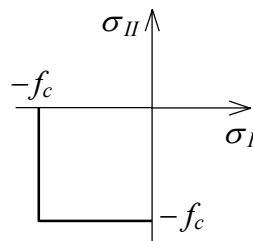


Fig. 8.9: Material model for concrete without tensile strength.

In these lecture notes, the analysis of the transverse bearing capacity by the dome effect and stirrups is based on a material model for concrete without any tensile strength and compressive strength f_c (Fig. 8.9). This means that in practice the bearing capacity generally will be higher.

8.2.2 Yield lines

To gain understanding in the transverse bearing capacity of concrete beams, just like for steel structures upper- and lower-bound calculations are utilised. For the upper-bound calculation, yield lines are used. A yield line is a material zone with length L , small thickness Δ and a width b equal to the width of the beam, in which plastic deformations occur (see Fig. 8.10). The thickness Δ only has been introduced for convenience. Actually, just like the plastic hinge, the yield line is not expected to have a thickness. The material at both sides of the yield line is considered to behave elastic or rigid, which means all plastic deformations are concentrated in the yield line.

A right-handed rectangular coordinate system is attached to the yield line, with axes s

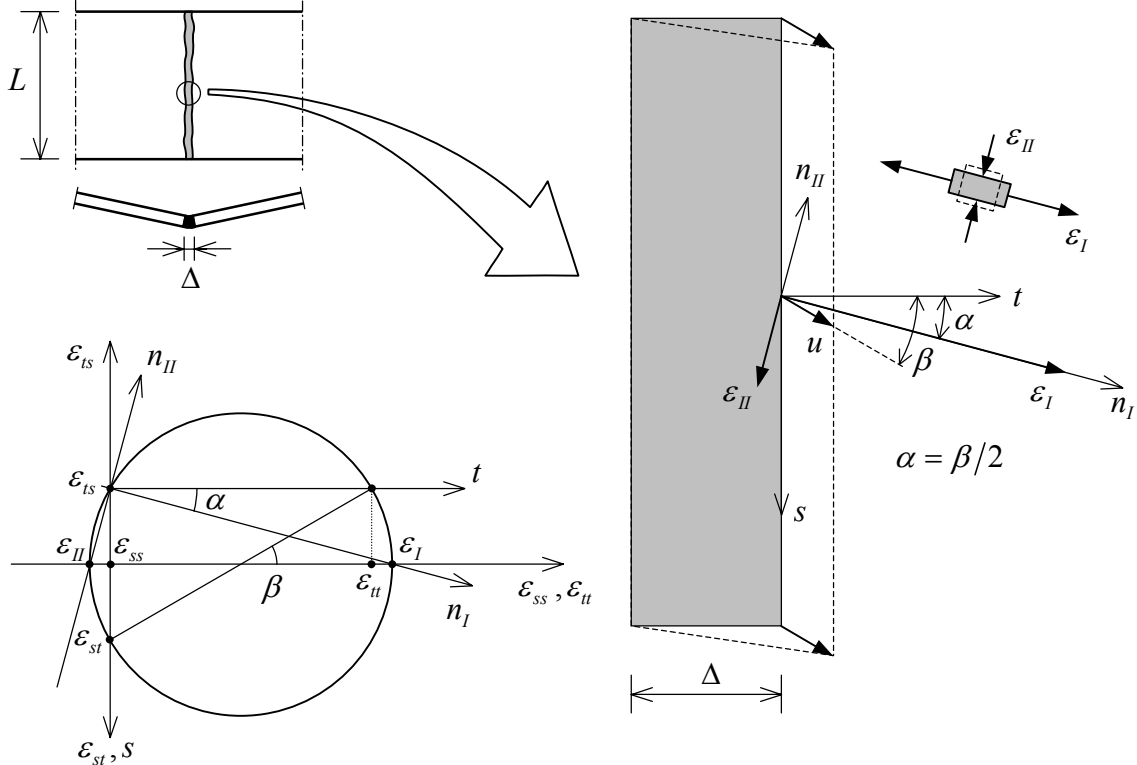


Fig. 8.10: Deformation of a yield line.

(longitudinally) and t (transversely). It is assumed that the beam parts at both sides of the yield line experience a mutual displacement. Suppose the left part of the beam is fixed and the right part displaces over a distance u . For the yield line this means that the left edge is fixed too and the right edge displaces over the same distance u (see Fig. 8.10).

Given the displacement u under an angle β with the normal on the yield line, the deformations in the yield line can be determined to be:

$$\begin{aligned}
 \varepsilon_{ss} &= 0 \\
 \varepsilon_{tt} &= u \cos \beta / \Delta \\
 \varepsilon_{st} = \varepsilon_{ts} &= \frac{1}{2} u \sin \beta / \Delta
 \end{aligned} \tag{8.7}$$

These are the longitudinal, transverse and shear strains, respectively. For calculation of the energy dissipation in the yield line, it is handy to know the principal strains:

$$\begin{aligned}\varepsilon_I &= \frac{1}{2} \frac{u}{\Delta} \cos \beta + \frac{1}{2} \frac{u}{\Delta} = \frac{1}{2} \frac{u}{\Delta} (\cos \beta + 1) \\ \varepsilon_{II} &= \frac{1}{2} \frac{u}{\Delta} \cos \beta - \frac{1}{2} \frac{u}{\Delta} = \frac{1}{2} \frac{u}{\Delta} (\cos \beta - 1)\end{aligned}\quad (8.8)$$

where the principal direction α is equal to half of β (see Fig. 8.10):

$$\text{Principal direction: } \alpha = \frac{1}{2} \beta \quad (8.9)$$

The internal work done over the length L is then given by:

$$A_i = (\varepsilon_I \sigma_I + \varepsilon_{II} \sigma_{II}) \Delta L b \quad (8.10)$$

Mohr's circle shows that one of the two principal strains is always negative. Because the tensile strength of concrete was set to zero, this means that only the principal compressive stress σ_{II} delivers a contribution to the internal work. Therefore, relation (8.10) reduces to:

$$A_i = \varepsilon_{II} \sigma_{II} \Delta L b$$

Substitution of $\sigma_{II} = -f_c$ and ε_{II} given by (8.8) delivers:

$$A_i = \frac{1}{2} \frac{u}{\Delta} (1 - \cos \beta) (-f_c) \Delta L b = \frac{1}{2} f_c u L (1 - \cos \beta) \quad (8.11)$$

This determines the expression for the energy dissipation of a yield line, which can be used in an upper-bound calculation. Note that the arbitrarily chosen thickness Δ of the yield line does not play any role in the final formula.

It should be remarked that there are two types of yield lines: lines with increasing Δ and lines with decreasing Δ . In the first case (see Fig. 8.10) β is smaller than 90° and the largest principal strain lies more or less in the direction of the normal on the yield line. The upsetting direction is then more or less along the yield line. For the second type, β is larger than 90° , the upsetting direction for which coincides more or less with the normal on the yield line.

Example

Consider the cantilever beam of Fig. 8.11. The free end of the beam is loaded by a uniformly distributed compressive load σ_c . A yield line is considered under an arbitrarily chosen angle γ . If again a displacement u is assumed under an angle β with the yield line, equating the internal work to the external work of the load σ_c delivers:

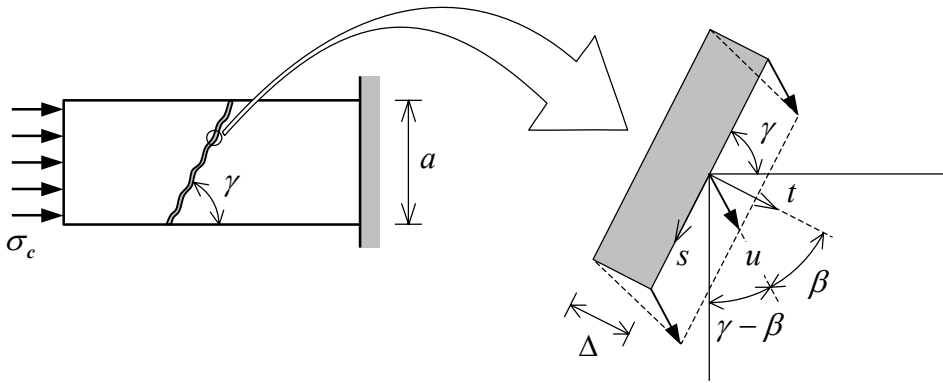


Fig. 8.11: Beam under compression.

$$\frac{1}{2} f_c u (a / \sin \gamma) (1 - \cos \beta) = \sigma_c a u \sin(\gamma - \beta) \rightarrow \sigma_c = f_c \frac{1 - \cos \beta}{2 \sin(\gamma - \beta) \sin \gamma}$$

The lowest load follows from minimisation with respect to the angle γ .

$$\frac{\partial \sigma_c}{\partial \gamma} = 0 \rightarrow \cos(\beta - \gamma) \sin \gamma = \sin(\beta - \gamma) \cos \gamma \rightarrow \tan(\beta - \gamma) = \tan \gamma$$

It follows:

$$\beta - \gamma = \gamma \rightarrow \gamma = \frac{\beta}{2}$$

For the lowest load, the angle β has to be twice the angle of the yield line. Substitution of this result in the relation for σ_c delivers:

$$\sigma_c = f_c \frac{1 - \cos \beta}{2 \sin(\beta/2) \sin(\beta/2)} = f_c \frac{1 - (1 - 2 \sin^2(\beta/2))}{2 \sin^2(\beta/2)} = f_c$$

In fact, the choice of β and γ is not important, since the load carrying capacity is always the same. The only important fact is that β is equal to 2γ .

Two special cases will be considered, a perpendicular yield line and one under an angle of 45° (see Fig. 8.12). In the table below, the results are summarised.

γ	90°	45°
β	180°	90°
ε_I	0	$u/2\Delta$
ε_{II}	$-u/\Delta$	$-u/2\Delta$
σ_I	0	0
σ_{II}	$-f_c$	$-f_c$

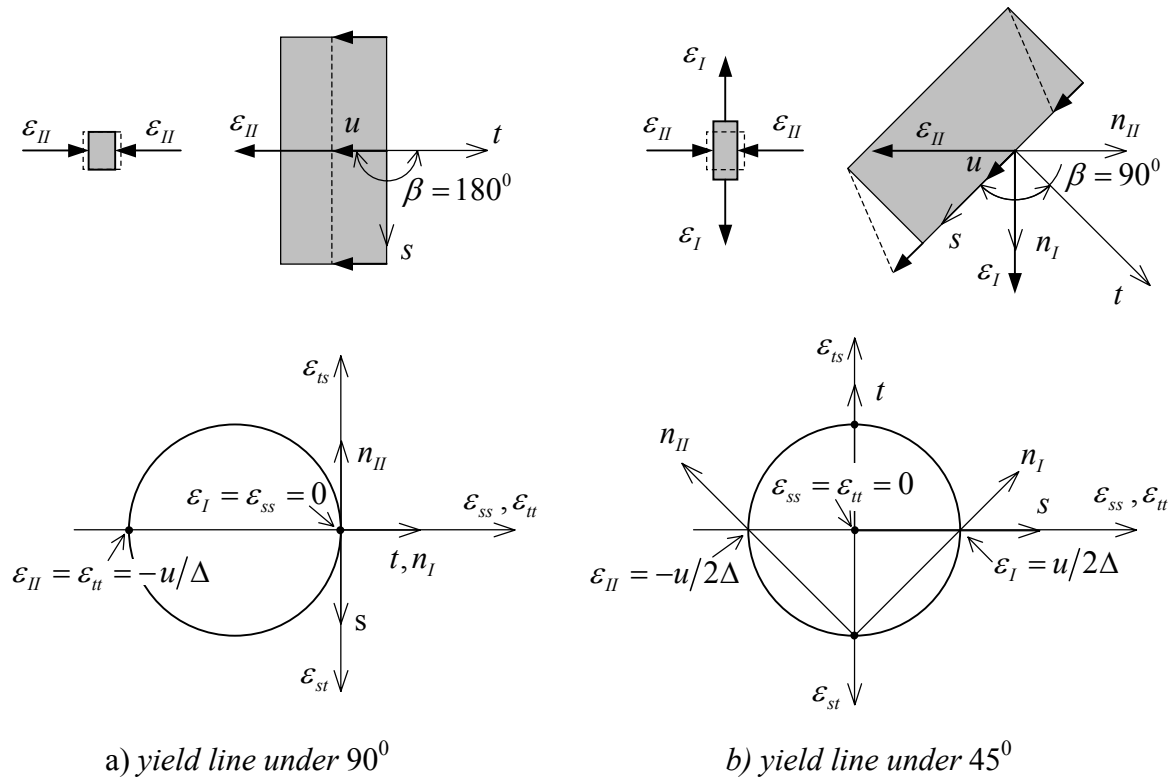


Fig. 8.12: Yield lines under different angles.

The principal strains are different, but the stresses for both cases are identical. One principal stress is always horizontal and equal to $-f_c$, while the other is vertical and equal to zero.

8.2.3 Beam with stirrup reinforcement / upper-bound calculation

Consider a beam loaded by a transverse force and a moment (see Fig. 8.13). The beam has both stirrup and bottom reinforcement. It is assumed that the concrete cannot sustain tensile loads. The used nomenclature is:

- V = transverse force
- M = bending moment
- H = lever, effective beam height
- B = beam width
- d_s = stirrup distance
- a = distance point load to support
- f_c = compressive strength concrete
- f_y = yield strength steel of reinforcements
- σ_s = tensile stress in stirrups
- σ_0 = tensile stress in bottom reinforcement
- A_s = total stirrup area
- A_0 = total area bottom reinforcement

The considered mechanism is displayed in Fig. 8.13 as well. The part at the right side of the yield line experiences a downward displacement u . It is assumed that both the stirrup reinforcement and the concrete are yielding; the bottom reinforcement is not yielding. The

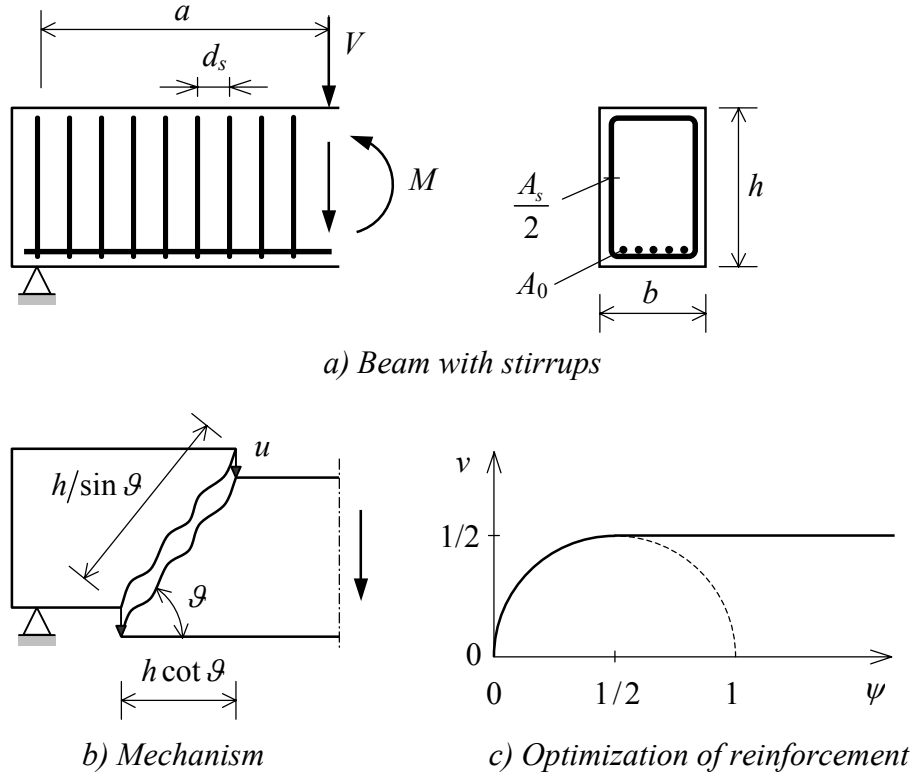


Fig. 8.13: Beam with stirrup reinforcement / upper-bound calculation.

work performed by the external load equals $V * u$. The internal work consists out of two parts, being contribution of the yield line (as discussed in 8.2.2) and the contribution of the stirrups in the yield line. Equating the internal to the external work yields:

$$\frac{1}{2} b f_c u (h / \sin \vartheta) (1 - \cos \vartheta) + A_s f_y u (h \cot \vartheta / d_s) = V u \quad (8.12)$$

where relation (8.11) has been used with $L = h / \sin \beta$ and $\beta = \vartheta$. For the transverse failure force, it then follows:

$$V = s_y b h \cot \vartheta + \frac{1}{2} f_c b h \left(\frac{1}{\sin \vartheta} - \cot \vartheta \right) \quad (8.13)$$

The effective yield stress in the steel has been introduced defined by $s_y = A_s f_y / b d_s$. Division by $f_c b h$ provides:

$$v = \frac{\tau}{f_c} = \frac{1}{2} \left(\sqrt{1 + \cot^2 \vartheta} - (1 - 2\Psi) \cot \vartheta \right) \quad (8.14)$$

where:

$$\tau = \frac{V}{b h} \quad (\text{average shear stress}) \quad (8.15)$$

$$\psi = \frac{s_y}{f_c} = \frac{A_s f_y}{b d_s f_c} \quad (\text{material reinforcement fraction for the stirrups}) \quad (8.16)$$

The lowest upper-bound solution can be found by optimising the angle of the yield line. Through $\partial\tau/\partial\vartheta = 0$ and some arithmetic manipulations it is found:

$$\cot \vartheta = \frac{1 - 2\psi}{2\sqrt{\psi(1-\psi)}} \quad (8.17)$$

Substitution into (8.14) delivers:

$$v = \frac{\tau}{f_c} = \sqrt{\psi(1-\psi)} \quad (8.18)$$

This is half a circle as shown in Fig. 8.13c. For $\psi = 0$ (no stirrup reinforcement) the load carrying capacity is zero. When stirrup reinforcement is added, the load carrying capacity increases rapidly. For $\psi > 0.5$, the load carrying capacity seems to reduce. This is not correct of course. In this area, the amount of steel is so large that no yielding of the steel occurs. The model does not account for this phenomenon correctly ($\cot \vartheta$ becomes smaller than 0 and ϑ larger than 90°). Naturally, for larger stirrup reinforcement, the load carrying capacity τ/f_c remains at a constant value equal to 0.5.

For very low values of ψ the formula is not completely correct as well. Then the inclination of the yield line decreases. A physical constraint occurs for $\cot \vartheta = a/h$. When this value is substituted instead of (8.17), the failure load becomes:

$$v = \frac{\tau}{f_c} = \frac{1}{2} \sqrt{\left(\frac{a}{h}\right)^2 + 1} - \frac{1}{2} \frac{a}{h} (1 - 2\psi) \quad (8.19)$$

with $\psi = 0$, it then follows:

$$v = \frac{\tau}{f_c} = \frac{1}{2} \sqrt{\left(\frac{a}{h}\right)^2 + 1} - \frac{1}{2} \frac{a}{h} \approx \frac{1}{4} \frac{a}{h} \quad (8.20)$$

So, for $\psi = 0$, the load carrying capacity is not equal to zero. Anyway, for slender beams the load carrying capacity is small. For example for $a/h = 0.25$ it holds that $v = 0.06$, compared with $v = 0.5$ for $\psi = 0.5$ this is small of course.

The phenomenon that a high beam still has load carrying capacity, which is possible because the angle of the yield line is limited, is called “dome action”. During the discussion of the lower-bound solution, this phenomenon will be considered again.

Finally, the equation is also useful for finding approximations of v for concrete without reinforcement. The value of τ is about 0.4 times the tensile strength, which in its turn is 5 to 10 percent of the compressive strength. This leads to values of v ranging from 0.02 to 0.04.

8.2.4 Beam with stirrup reinforcement / lower-bound calculation

The lower-bound calculation is based on an equilibrium system, which is based on (see Fig. 8.14):

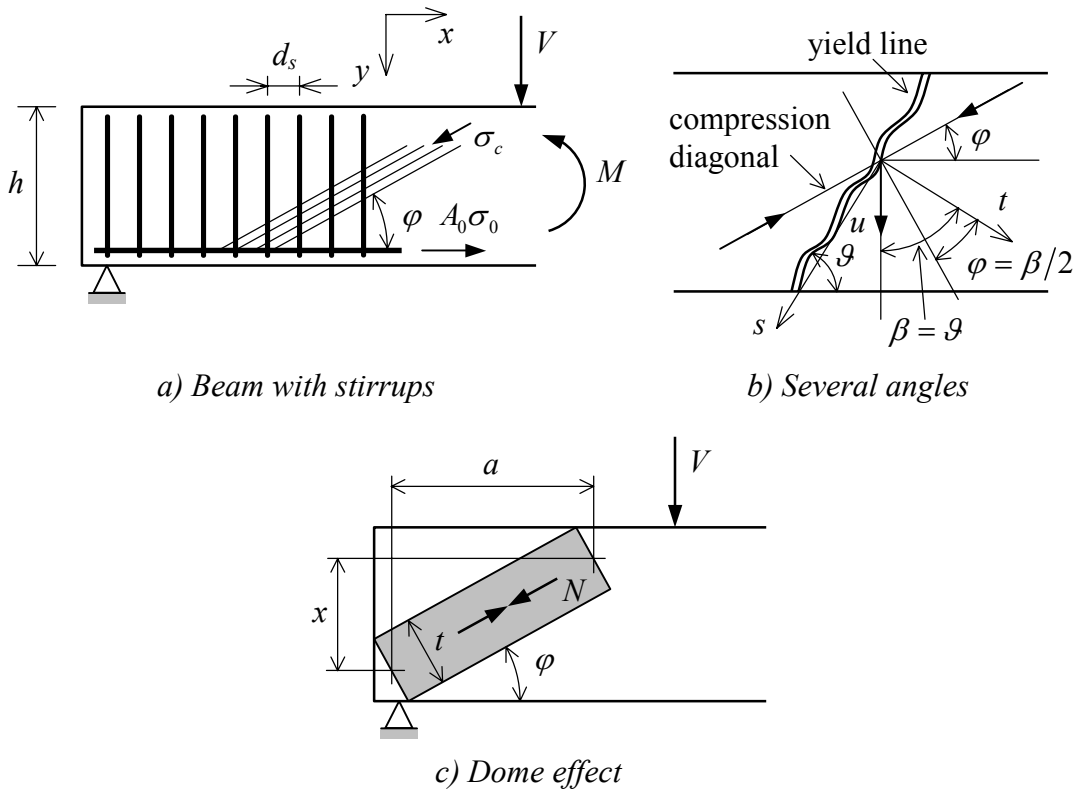


Fig. 8.14: Beam with stirrup reinforcement / lower-bound calculation.

- a vertical distributed vertical tensile stress s due to the stirrups;
- a unidirectional stress σ_c in the concrete under an angle φ (compression diagonals);
- a stress in the bottom reinforcement equal to σ_0 .

The angle φ is a degree of freedom that can be optimised. In terms of σ_{xx} , σ_{yy} and σ_{xy} the stresses can be summarized as follows:

$$\begin{aligned} \sigma_{xx} &= -\sigma_c \cos^2 \varphi \\ \sigma_{xx} &= -\sigma_c \sin^2 \varphi + s \quad ; \quad s = \frac{A_s \sigma_s}{b d_s} \\ \sigma_{xy} &= -\sigma_c \cos \varphi \sin \varphi \end{aligned} \quad (8.21)$$

The equilibrium relations between these stresses and the transverse force V and bending moment M are given by:

$$V = \int \sigma_{xy} dA = bh \sigma_{xy} = bh \sigma_c \sin \varphi \cos \varphi \quad (8.22)$$

$$M = Va = \int \sigma_{xx} y dA = -\frac{1}{2} h^2 b \sigma_c \cos^2 \varphi + h A_0 \sigma_0 \quad (8.23)$$

The last equation provides the moment equilibrium about the upper fibre. Further, it follows from $\sigma_{yy} = 0$ that:

$$s = \sigma_c \sin^2 \varphi \quad (8.24)$$

The yield conditions are respectively:

$$\sigma_c < f_c \quad ; \quad s < s_y = \frac{A_s f_y}{b d_s} \quad ; \quad \sigma_0 < f_y \quad (8.25)$$

Assuming the bottom reinforcement is over dimensioned so that only the concrete and stirrups are yielding, it holds:

$$\sigma_c = f_c \quad ; \quad s = s_y \quad (8.26)$$

In that case, it follows:

$$s_y = f_c \sin^2 \varphi \quad (8.27)$$

$$V = bhf_b \cos \varphi \sin \varphi = bh\sqrt{s_y (f_c - s_y)} \quad (8.28)$$

Division by bhf_b provides:

$$v = \frac{\tau}{f_c} = \sqrt{\left(\frac{s_y}{f_c}\right)\left(1 - \frac{s_y}{f_c}\right)} = \sqrt{\psi(1-\psi)} \quad (8.29)$$

Comparison with (8.18) shows that for both the lower- and upper-bound calculation the same result is found. This means that an exact solution has been found, however within the limitations of the model. Particularly, the details of the force entry around the load and supports have not been considered.

It is also interesting to look into the found angles for the compression diagonals of the lower-bound solution and the yield lines of the upper-bound solution. For the lower-bound solution it has been found that the optimum value of φ corresponds with $\sin^2 \varphi = \psi$, or expressed in the cotangent:

$$\cot \varphi = \sqrt{\frac{1-\psi}{\psi}} \quad (8.30)$$

For the optimum slope of the yield line it was found:

$$\cot \vartheta = \frac{1-2\psi}{2\sqrt{\psi(1-\psi)}} \quad (8.31)$$

Through the formula for the double angle, it can be derived:

$$\cot 2\varphi = \frac{\cot^2 \varphi - 1}{2 \cot \varphi} = \frac{\frac{1-\psi}{\psi} - 1}{2\sqrt{\frac{1-\psi}{\psi}}} = \frac{1-2\psi}{2\sqrt{\psi(1-\psi)}} = \cot \vartheta \rightarrow \varphi = \frac{\vartheta}{2} \quad (8.32)$$

From Fig. 8.14b it is clear that this is exactly in agreement with the theory of section 8.2.3, where it has been shown that the angle α of the principal stress equals half the angle β between the yield line and the direction of the relative displacement between the beam parts.

Naturally for completeness, the bottom reinforcement has to be checked as well. The following equation has to be satisfied:

$$A_0 f_y > \frac{M}{h} + \frac{1}{2} V \cot \varphi \quad (8.33)$$

To investigate the effect of dome action for the lower-bound calculation, in first instance a beam is considered without stirrup reinforcement (see Fig. 8.14c). In addition, it is assumed that sufficient bottom reinforcement is present. The compressive force in the slanting compression diagonal under an angle φ equals:

$$N = t b f_c \quad (8.34)$$

where t is the thickness of the imaginary compression bar. This thickness will be determined later. The transverse force V is equal to the vertical component of N , i.e:

$$V = N \sin \varphi \quad (8.35)$$

The following geometrical relations are important:

$$\left. \begin{array}{l} t \cos \varphi + x = h \\ \frac{x}{h} = \tan \varphi \end{array} \right\} \rightarrow t = \frac{h - a \tan \varphi}{\cos \varphi} \quad (8.36)$$

Substitution of t in N and subsequently of N in V leads to:

$$V = b f_c \sin \varphi \frac{h - a \tan \varphi}{\cos \varphi} \quad (8.37)$$

Division by $b h f_c$ yields:

$$v = \frac{V}{b h f_c} = \tan \varphi \left(1 - \frac{a}{h} \tan \varphi \right) \quad (8.38)$$

The thickness t still has to be optimised. Of course, it is much handier to optimise the value of $\tan \varphi$. This delivers $\tan \varphi = h / 2a$. The lower-bound value for V then becomes:

$$v = \frac{V}{bhf_c} = \frac{h}{2a} \left(1 - \frac{a}{h} \frac{h}{2a} \right) = \frac{1}{4} \frac{h}{a} \quad (8.39)$$

This result is almost identical to the upper-bound solution without stirrup reinforcement (see (8.20)). For this case, it also holds that no attention has been paid to the details of the force entry and the location of the reinforcements. Therefore, it is out of the question that the real lower-bound solution has been found. Experiments show that the above-derived results in most cases are 20 to 30 percent too high, in spite of the fact that zero tensile strength for concrete was assumed. For finding more realistic failure loads, it is better to generate so-called “*strut and tie*” solutions. Fig. 8.15 shows some examples. Naturally, these calculations are also subjected to several model inaccuracies. Of course, concrete is no plastic material, but a material subjected to cracking, displaying a complicated post-

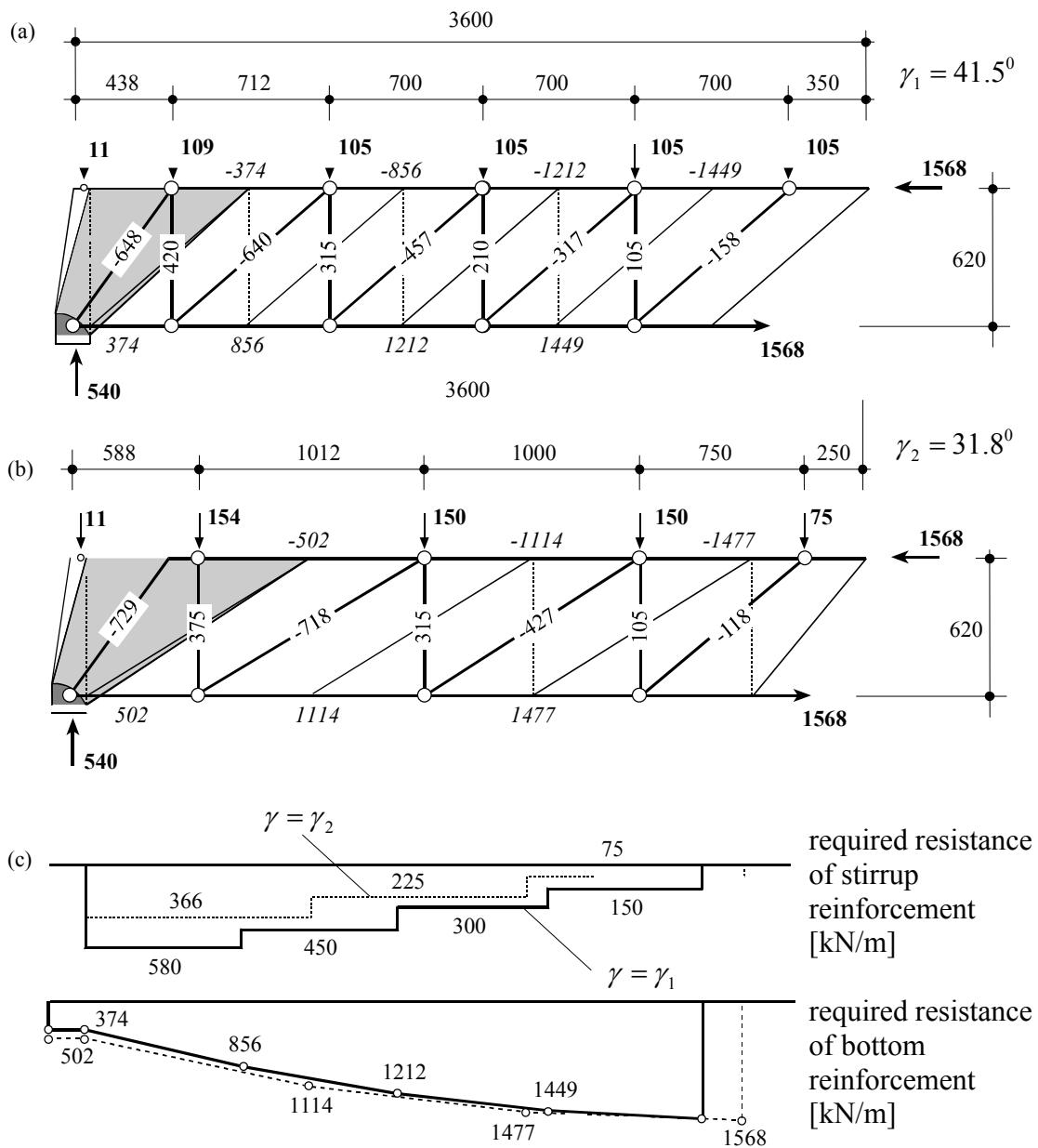


Fig. 8.15: Strut and tie solutions.

cracking behaviour. In addition, the interaction between concrete and steel is very complicated. A sound analysis can only be made by heavy non-linear computer programmes. Even then, in numerous cases the results do not show the desired agreement with experimental tests. For the daily practice, these computer programmes are not suitable. In most cases, the design practice relies on the design formulae given in the standardisation codes, which often have a strong empirical character.

Reading list

- Neal, B.G., *The Plastic Methods of Structural Analysis*, Chapman & Hall Ltd, London (1963)
- Kollbrunner, C.F., Hajdin, N., *Dünnwandige Stäbe band 2*, Springer-Verlag, Berlin/Heidelberg (1975)
- Krausz, A.S., Krausz, K., *Unified constitutive laws of plastic deformation*, Academic Press, San diego (1996)
- Moy, S.S.J., *Plastic methods for steel and concrete structures*, Macmillan, London (1981)
- Nielsen, M. P., Braestrup, M.W., Jensen, B.C., *Concrete plasticity*, “Beam Shear, Shear in Joints, Punching Shear”, Special publication, Technical University of Denmark, Copenhagen (1978)
- Jin-Ping Zhang, *Strength of cracked concrete pt. 1*, “Shear Strength of Conventional Reinforced Concrete Beams, Deep Beams, Corbels, and Prestressed Reinforced Concrete Beams without Shear Reinforcement”, Technical University of Denmark, Department of Structural Engineering, Lyngby, Series R No. 311 (1994)
- Jin-Ping Zhang, *Strength of cracked concrete pt. 2*, “Micromechanical Modelling of Shear Failure in Cement Paste and in Concrete”, Technical University of Denmark, Department of Structural Engineering and Materials, Lyngby, Series R No. 17 (1997)
- Jin-Ping Zhang, *Strength of cracked concrete pt. 3*, “Load Carrying Capacity of Panels Subjected to In-plane Stresses”, Technical University of Denmark, Department of Structural Engineering and Materials, Lyngby, Series R No. 18 (1997)
- Linh Cao Hoang, *Yield Conditions for Cracked Reinforced Concrete Disks*, Technical University of Denmark, Department of Structural Engineering and Materials, Lyngby, Series R No. 66 (2000)
- Mitchell, D., ASCE, M., Cook, W. D., “Preventing Progressive Collapse of Slab Structures”, *Journal of Structural Engineering*, Vol. 110, No. 7, July(1984)
- Bigaj, A. J., *proefschrift: Structural dependence of rotation capacity of plastic hinges in RC beams and slabs*, Diss., Delft (1999)